MICROCOPY RESOLUTION TEST CHART

NATIONAL BUREAU OF STANDARDS 1963-A

GA-A18140

AD-A161 987

VARIABLE BAND GAP MATERIALS FOR THERMOPHOTOVOLTAIC GENERATORS

FINAL TECHNICAL REPORT
FOR THE PERIOD
AUGUST 15, 1984 TO AUGUST 15, 1985

by
L. D. WOOLF, J. C. BASS, and N. B. ELSNER

DTIC
ELECTE
DEC 6 1985

SEPTEMBER 1985

85 12-6 079

GA Technologies

GA-A18140

VARIABLE BAND GAP MATERIALS FOR THERMOPHOTOVOLTAIC GENERATORS

FINAL TECHNICAL REPORT
FOR THE PERIOD
AUGUST 15, 1984 TO AUGUST 15, 1985

by
L. D. WOOLF, J. C. BASS, and N. B. ELSNER

GA PROJECT 3768
SEPTEMBER 1985

REPORT DOCUMENTATION PAGE

1a. REPORT SECURITY CLASSIFICATION Unclassified	1b. RESTRICTIVE MARKINGS None
2a. SECURITY CLASSIFICATION AUTHORITY	3. DISTRIBUTION/AVAILABILITY OF REPORT
2b. DECLASSIFICATION/DOWNGRADING SCHEDULE	~~copies~~ Approved for publi... distribution...

4. PERFORMING ORGANIZATION REPORT NUMBER(S) GA-A18140	5. MONITORING ORGANIZATION REPORT NUMBER(S) AFOSR

6a. NAME OF PERFORMING ORGANIZATION GA Technologies Inc.	6b. OFFICE SYMBOL (If applicable) GA	7a. NAME OF MONITORING ORGANIZATION AFOSR /$\eta\rho$

6c. ADDRESS (City, State, and ZIP Code) P.O. Box 85608 San Diego, CA 92138	7b. ADDRESS (City, State, and ZIP Code) Bolling AFB, DC 20332-6448

8a. NAME OF FUNDING/SPONSORING ORGANIZATION AFOSR	8b. OFFICE SYMBOL (If applicable) $\eta\rho$	9. PROCUREMENT INSTRUMENT IDENTIFICATION NUMBER F49620-84-C-0105

8c. ADDRESS (City, State, and ZIP Code) Bolling AFB, DC 20332-6448	10. SOURCE OF FUNDING NUMBERS

PROGRAM ELEMENT NO.	PROJECT NO.	TASK NO.	WORK UNIT ACCESSION NO
61102F	2301	A7	

11. TITLE (include Security Classification)

Variable Band Gap Materials for Thermophotovoltaic Generators

12. PERSONAL AUTHOR(S)

Woolf, Lawrence D.; Bass, John C.; Elsner, Norbert B.

13a. TYPE OF REPORT Final	13b. TIME COVERED FROM 8/15/84 TO 8/15/85	14. DATE OF REPORT (Year, Month, Day) September 1985	15 PAGE COUNT 131

16. SUPPLEMENTARY NOTATION

17. COSATI CODES			18. SUBJECT TERMS (Continue on reverse if necessary and identify by block number)
FIELD	GROUP	SUB-GROUP	Thermophotovoltaic energy conversion; high-temperature photovoltaic properties; InGaAs, Si; nuclear-thermophotovoltaic energy conversion; theoretical model of thermophotovoltaics; TPV; space power system. GaAs

19. ABSTRACT (Continue on reverse if necessary and identify by block number)

Thermophotovoltaic (TPV) properties of InGaAs cells with band gaps of either 1.15 or 1.2 eV, GaAs cells, and Si cells were investigated. In particular, dark and illuminated current vs voltage characteristics were obtained for a number of these concentrator cells at cell temperatures ranging from 300 to 550 K and currents varying from 10^{-8} to 10 A. Based on these data, the temperature dependence of the TPV efficiency for each of these cells was inferred for a fixed value of the parasitic absorption of the below-band-gap energy photons. For a given weighted parasitic absorption of 5%, the InGaAs cells have a significantly higher TPV efficiency than the GaAs or Si cells. TPV efficiencies approaching 40% at 300 K and 26% at 500 K appear feasible for the InGaAs cells. Based on these data, it was calculated that the specific mass of a space-based nuclear-TPV energy conversion system would be 10 kg/kW if InGaAs cells with 5% weighted parasitic absorption were used. In addition, a theoretical model was developed for determining the optimum efficiency of single and multiple band gap cells in TPV energy conversion.

20. DISTRIBUTION/AVAILABILITY OF ABSTRACT ☐ UNCLASSIFIED/UNLIMITED ☒ SAME AS RPT ☐ DTIC USERS	21. ABSTRACT SECURITY CLASSIFICATION Unclassified
22a. NAME OF RESPONSIBLE INDIVIDUAL Bruce Smith	22b. TELEPHONE (Include Area Code) (202) 767-...	22c. OFFICE SYMBOL

DD FORM 1473, 84 MAR 83 APR edition may be used until exhausted
All other editions are obsolete

ABSTRACT

Thermophotovoltaic (TPV) properties of InGaAs cells with band gaps of either 1.15 or 1.2 eV, GaAs cells, and Si cells were investigated. In particular, dark and illuminated current vs voltage characteristics were obtained for a number of these concentrator cells at cell temperatures ranging from 300 to 550 K and currents varying from 10^{-8} to 10 A. Based on these data, the temperature dependence of the TPV efficiency for each of these cells was inferred for a fixed value of the parasitic absorption of the below-band-gap energy photons. For a given weighted parasitic absorption of 5%, the InGaAs cells have a significantly higher TPV efficiency than the GaAs or Si cells. TPV efficiencies approaching 40% at 300 K and 26% at 500 K appear feasible for the InGaAs cells. Based on these data, it was calculated that the specific mass of a space-based nuclear-TPV energy conversion system would be 10 kg/kW if InGaAs cells with 5% weighted parasitic absorption were used. In addition, a theoretical model was developed for determining the optimum efficiency of single and multiple band gap cells in TPV energy conversion.

CONTENTS

FIGURES

FIGURES (Continued)

FIGURES (Continued)

TABLES

TABLES (Continued)

1. INTRODUCTION AND RESEARCH OBJECTIVES

Thermophotovoltaic (TPV) energy converters use a heat source to raise the temperature of an emitter material so that it emits photons. When absorbed in a photovoltaic cell, these photons cause electron-hole pairs to be created and an electric current to flow. The heat source for this process can be a nuclear reactor, a radioactive isotope generator, concentrated solar energy, or a fossil-fuel burner.

To optimize the efficiency of TPV cells, the thermal emitter should operate at a temperature such that the maximum number of photons emitted have an energy closely matched to the band gap energy of the cell photovoltaic material. For typical cell temperatures of 300 to 600 K and emitter temperatures of 1500 to 2300 K, the maximum conversion efficiency occurs for cells with band gaps in the range of 0.7 to 1.2 eV. For a given cell and emitter temperature (and weighted parasitic absorption, see Section 3), there is an optimum band gap which maximizes the TPV efficiency. The solid solution alloys of InAs-GaAs are quite attractive in that the band gap is direct in these materials and can be varied from 0.35 to 1.4 eV by changing the relative proportion of InAs to GaAs. Significant improvements in the efficiency of TPV energy conversion can be achieved if parasitic photon absorption is minimized so that the below-band-gap photons are not absorbed in the cell but are reflected back to the thermal emitter to help keep it hot.

TPV cell material for space power applications must be able to operate at a relatively high temperature in order to minimize the mass of the radiator used to transfer waste heat. Lower radiator mass leads to lower specific mass (kg/kW), a major goal in space power applications.

In 1982, GA Technologies Inc. (GA) completed a study for NASA-Lewis Laboratories (Ref. 1-1) which indicated that TPV energy conversion has great potential for space power applications. For a 100-kW space nuclear power system, this study indicated that the specific mass for a TPV-based system was 7 to 15 kg/kW. By comparison, the specific mass for comparable thermionic- and thermoelectric-based nuclear space power systems is ~30 kg/kW.

The primary purpose of the present program was to measure TPV properties of variable direct band gap InGaAs cells and estimate their efficiency and performance for actual TPV operating conditions expected for a space power environment. To achieve these goals, an apparatus was designed and fabricated for measuring some TPV properties of cells at elevated cell temperatures. Data were obtained for InGaAs, GaAs, and Si cells and were extensively analyzed. These results were used to estimate efficiencies at variable cell and emitter temperatures, assuming a low value for the parasitic absorption that should be attainable. Finally, the specific mass of a TPV-based space power system was calculated using these data. In addition, micrometallurgical analyses were conducted on various cells to verify the composition and the homogeneity of the alloys. This task was accomplished using scanning electron microscopy (SEM) and energy dispersive analysis of X-rays (EDAX). The problems and techniques for fabricating 1-cm^2 and larger cells were also evaluated.

During the program, it became clear that a more thorough analysis of the optimum band gap for maximum TPV efficiency than that presented in a previous report (Ref. 1-1) was required. In that report, the basic assumptions were not clearly presented and the detailed dependence of the TPV efficiency on numerous parameters was not discussed. Therefore, an extensive analysis of the optimum TPV efficiency and associated band gap as a function of emitter temperature, cell temperature, parasitic absorption, and other factors was performed.

Another route to achieving high conversion efficiencies in solar photovoltaics is through the use of multiple band gap cells. Since multiple band gap cells should also have higher conversion efficiencies in a TPV system compared with single band gap cells, a generalized theory of multiple band gap TPV cells was developed for the first time. For the particular case of a two band gap cell, the optimum TPV efficiency and associated band gaps were calculated using the same input parameter spectrum previously taken for the one band gap cell.

2. TEST MATERIALS AND LARGE-AREA-CELL FABRICATION FEASIBILITY

The materials tested during this program included GaAs, Si, $In_{0.25}Ga_{0.75}As$ (E_g = 1.15 eV), and $In_{0.20}Ga_{0.80}As$ (E_g = 1.20 eV) research concentrator solar cells that were able to conduct current densities of ~10 A/cm^2 with no appreciable series resistance losses. Those cells were not fabricated to achieve high TPV efficiencies; i.e., they were expected to exhibit significant free carrier absorption and low back surface reflectivity. The InGaAs cells studied did exhibit this expected parasitic absorption. These cells are discussed in more detail in Section 6.

Variable direct band gap InGaAs cells have been fabricated and studied at Varian Associates, Inc. for solar applications (Refs. 2-1, 2-2, 2-3). InGaAs cells were obtained from Dr. Jan Werthen of Varian, and GaAs and Si cells were received from Dr. Peter Isles of Applied Solar Energy Corporation. Si TPV cells were obtained from Professor Richard Swanson of Stanford University.

The InGaAs cells were fabricated using the technique of metalorganic chemical vapor deposition (MOCVD) and had areas of 0.49 cm^2. It appears that fabricating 1-cm^2 and larger cells presents no great technological challenge since high-quality GaAs cells (Ref. 2-4) of 4-cm^2 area with 18.7% efficiency (1 sun, AMO) have been fabricated using the same technique of MOCVD. The only major difference in construction of the InGaAs and the GaAs cells is that a grading layer is required in the InGaAs cell to account for the difference in lattice parameter between the GaAs substrate and the InGaAs base layer. Thus, the techniques for fabricating large-area InGaAs cells are within the scope of the present state of the art.

3. OPTIMUM EFFICIENCY OF SINGLE AND MULTIPLE BAND GAP CELLS IN TPV ENERGY CONVERSION

3.1. INTRODUCTION

Numerous investigations have examined the maximum theoretical performance obtainable from single and multiple band gap photovoltaic cells (Refs. 3-1 through 3-6). These studies have determined the maximum efficiency of such cells under 1 sun as well as concentrated sunlight conditions and also as a function of the temperature of the cell. Although various approaches have been used, all the results are in fairly close agreement. These analyses have provided useful guidance in the design of single and multiple band gap cells for high-efficiency photovoltaic systems.

Another route to high efficiencies is through TPV energy conversion (Ref. 3-7). In TPV systems, a source of energy such as concentrated sunlight, nuclear material, fossil fuel, or a radioisotope heat source is used to heat an intermediate thermal emitter to a temperature of 1500 to 2500 K. The emitter then radiates photons which are incident on the TPV cells.

Two factors contribute to the high efficiency of a TPV conversion system relative to solar photovoltaic systems (Refs. 3-8 through 3-11). First, the emitter is at a lower temperature than the sun, resulting in less energy being radiated at short wavelengths where the cell is inefficient. Second, the long-wavelength (below-band-gap energy) photons are reflected back to the emitter, keeping it hot, so their energy is not wasted.

Potential semiconductor materials for TPV cells have been investigated both experimentally and theoretically. In particular, Swanson

(Refs. 3-8 through 3-13) studied the performance of Si cells that were optimized for high TPV efficiency. Vera et al. (Refs. 3-14, 3-15) have explored the theoretical efficiency of both Ge and tandem Si/Ge cells in TPV energy conversion. Although others have considered the maximum efficiency in TPV energy conversion (Refs. 3-16 through 3-19), there have been no detailed studies of the band gaps required for maximizing the conversion efficiency of single and multiple band gap TPV cells.

This section describes a general theory for the efficiency of multiple band gap TPV cells that is a generalization of the approach used by Swanson for a single band gap cell (Refs. 3-8 through 3-10). Then calculations are presented for the band gap(s) and corresponding efficiencies that maximize the TPV performance of one and two band gap cells as a function of cell temperature, emitter temperature, and parasitic absorption.

3.2. THEORY OF MULTIPLE BAND GAP TPV CELLS

In this theory, the general approach and terminology follow those developed by Swanson for single band gap TPV cells (Refs. 3-8 through 3-10). We assume that the radiation incident on the cell is blackbody in nature. The TPV cell is fabricated such that the radiation is first incident on the highest band gap cell with band gap E_{g1}. We assume that all the light with energy $\hbar\omega > E_{g1}$ is absorbed in cell No. 1 and that it transmits all the light with energy $\hbar\omega < E_{g1}$ to the remaining cells. Cell No. 2 then absorbs all the light with energy $E_{g2} < \hbar\omega < E_{g1}$, and so on for the rest of the cells. There are assumed to be n cells.

The TPV conversion efficiency is given by

$$\eta_{TPV} = \frac{P_{out}}{P_{abs}} \quad , \tag{3-1}$$

where P_{out} is the power output per unit area and P_{abs} is the power absorbed per unit area. The output power per unit area at the maximum power point is

$$P_{out} = \sum_{i=1}^{n} J_{mpi} V_{mpi} \quad , \tag{3-2}$$

where J_{mpi} is the current per unit area and V_{mpi} is the voltage at the maximum power point for cell i. Following Swanson, we define an electrical efficiency factor η_{eleci} as

$$\eta_{eleci} = \frac{J_{mpi} V_{mpi}}{J_{phi} V_{gi}} \quad , \tag{3-3}$$

where J_{phi} is the total photogenerated current per unit area from cell i and $V_{gi} = E_{gi}/q$, with q being the magnitude of the charge of the electron. Then the maximum power output per unit area becomes

$$P_{out} = \sum_{i=1}^{n} J_{phi} V_{gi} \eta_{eleci} \quad . \tag{3-4}$$

For calculating the power absorbed, we assume that the spectral intensity of the incident radiation is that of a blackbody. Then the power incident on the TPV cell per unit area and angular frequency ω is

$$P(\omega) = \frac{\omega^2}{4\pi^2 c^2} \frac{\hbar\omega}{e^{\hbar\omega/k_B T_E} - 1} \quad , \tag{3-5}$$

where T_E is the temperature of the blackbody emitter. The total power incident per unit area is then

$$P_{inc} = \int_{0}^{\infty} P(\omega) d\omega = \sigma T_E^4 \quad , \tag{3-6}$$

3-3

where σ is Stefan's constant. Now the power per unit area absorbed by the TPV cell is

$$P_{abs} = \int_0^\infty \left(\sum_{i=1}^n A_i(\omega) P_i(\omega) \right) d\omega \quad , \tag{3-7}$$

where $A_i(\omega)$ is the spectral absorptance of cell i and $P_i(\omega)$ is the spectral intensity incident on cell i. For $\hbar\omega > E_{gi}$, the desired absorption mechanism is the photogeneration of electron-hole pairs. However, for $\hbar\omega < E_{gi}$, other absorption mechanisms dominate and contribute to parasitic losses in efficiency. Therefore, for each cell, the spectral absorptance can be written

$$A_i(\omega) = A_{phi}(\omega) + A_{pari}(\omega) \quad , \tag{3-8}$$

where $A_{phi}(\omega)$ is the spectral absorptance resulting in photogeneration and A_{pari} is the parasitic absorptance.

For simplicity of analysis, we now invoke the following assumptions. First, we take

$$\left.\begin{array}{ll} A_{phi}(\omega) = 1 & \text{for} \quad E_{gi} < \hbar\omega < E_{gi-1} \\[2mm] A_{phi}(\omega) = 0 & \text{for} \quad \hbar\omega < E_{gi} \end{array}\right\} . \tag{3-9}$$

This requires that the thickness of cell i be larger than the absorption length of the incident light in the energy range $E_{gi} < \hbar\omega < E_{gi-1}$ and that cell i have a quantum efficiency of 1. Secondly, we define

$$A_{par}(\omega) = \sum_{i=1}^n A_{pari}(\omega) \quad . \tag{3-10}$$

3-4

Then Eq. 3-7 becomes

$$P_{abs} = \int_0^{\omega_{gn}} A_{par}(\omega)P(\omega)d\omega + \int_{\omega_{gn}}^{\infty} P(\omega)d\omega \quad , \qquad (3-11)$$

where $\omega_{gi} = E_{gi}/\hbar$. Also, the number of photons of energy $\hbar\omega$ incident on the TPV cell per unit area and time is $P(\omega)/\hbar\omega$, so

$$\left.\begin{array}{l} J_{ph1} = q \displaystyle\int_{\omega_{g1}}^{\infty} \dfrac{P(\omega)}{\hbar\omega} \, d\omega \\[20pt] J_{ph2} = q \displaystyle\int_{\omega_{g2}}^{\omega_{g1}} \dfrac{P(\omega)}{\hbar\omega} \, d\omega \\[12pt] \cdot \\ \cdot \\ \cdot \\[12pt] J_{phn} = q \displaystyle\int_{\omega_{gn}}^{\omega_{gn-1}} \dfrac{P(\omega)}{\hbar\omega} \, d\omega \end{array}\right\} \qquad . \qquad (3-12)$$

From the previous equations, the TPV efficiency can be rewritten as

$$\eta_{TPV} = \frac{\displaystyle\sum_{i=1}^{n} J_{phi}V_{gi}\eta_{eleci}}{\displaystyle\int_0^{\omega_{gn}} A_{par}(\omega)P(\omega)d\omega + \int_{\omega_{gn}}^{\infty} P(\omega)d\omega} \quad , \qquad (3-13)$$

or

$$\eta_{TPV} = \sum_{i=1}^{n} \frac{\eta_{usei}\eta_{eleci}}{1 + \dfrac{\overline{A}_{par}}{\overline{A}_{ph}}} = \sum_{i=1}^{n} \eta_{TPVi} \quad , \qquad (3-14)$$

where

$$\eta_{usei} = \frac{J_{phi}V_{gi}}{\int_{\omega_{gn}}^{\infty} P(\omega)d\omega} \quad , \tag{3-15}$$

$$\overline{A}_{par} = \frac{\int_{0}^{\omega_{gn}} A_{par}(\omega)P(\omega)d\omega}{\int_{0}^{\infty} P(\omega)d\omega} \quad , \tag{3-16}$$

$$\overline{A}_{ph} = \frac{\int_{\omega_{gn}}^{\infty} P(\omega)d\omega}{\int_{0}^{\infty} P(\omega)d\omega} \quad . \tag{3-17}$$

In this equation, $\overline{A}_{par}$ is the *weighted parasitic absorption* and $\overline{A}_{ph}$ is the *weighted photoproduction absorption*. For high TPV efficiencies, it is necessary that the ratio of $\overline{A}_{par}/\overline{A}_{ph}$ be small. For a single band gap TPV cell, $(1 - \eta_{use})$ represents the excess kinetic energy lost owing to the absorption of photons with energy greater than E_g. For multiple band gap TPV cells, the total use factor may be defined as

$$\sum_{i=1}^{n} \eta_{usei} = \frac{V_{g1} \int_{\omega_{g1}}^{\infty} \frac{P(\omega)}{\hbar\omega} d\omega + V_{g2} \int_{\omega_{g2}}^{\omega_{g1}} \frac{P(\omega)}{\hbar\omega} d\omega + \ldots + V_{gn} \int_{\omega_{gn}}^{\omega_{gn-1}} \frac{P(\omega)}{\hbar\omega} d\omega}{\int_{\omega_{gn}}^{\infty} P(\omega)d\omega} \quad . \tag{3-18}$$

Since

$$1 - \sum_{i=1}^{n} \eta_{usei} < 1 - \frac{V_{gn} \int_{\omega_{gn}}^{\infty} \frac{P(\omega)}{\hbar\omega} d\omega}{\int_{\omega_{gn}}^{\infty} P(\omega)d\omega} \quad , \tag{3-19}$$

3-6

the kinetic energy lost owing to absorption of photons with energy in excess of the band gap is lower for a multiple band gap TPV cell than for a single band gap TPV cell with band gap equal to the lowest band gap of the multiple band gap cell. As for a single band gap cell, the electrical efficiency factor n_{eleci} represents the inherent fill factor, series resistance, shunt resistance, etc., losses inherent in the ith cell.

3.3. SINGLE BAND GAP TPV CELL

It is useful to calculate explicit expressions for the various terms in the TPV efficiency equation before discussing optimization routines. This section presents the theory previously developed by Swanson (Refs. 3-8 through 3-10). For a cell with a single band gap energy E_g, illuminated by a blackbody at temperature T_E, the use factor η_{use} becomes

$$\eta_{use} = \frac{V_g \int_{\omega_g}^{\infty} \frac{P(\omega)}{\hbar\omega} \, d\omega}{\int_{\omega_g}^{\infty} P(\omega) d\omega} \quad . \tag{3-20}$$

From Eq. 3-5, this expression becomes

$$\eta_{use} = \frac{\int_{\beta}^{\infty} \frac{u^2 du}{e^u - 1}}{\int_{\beta}^{\infty} \frac{u^3 du}{e^u - 1}} \quad , \tag{3-21}$$

where $u = \hbar\omega/(k_B T_E)$ and $\beta = E_g/(k_B T_E)$. For the range of T_E and E_g to be considered, typically $\beta > 5$. Therefore, in the above integrals, the approximation $e^u - 1 \rightarrow e^u$ is used. The use factor can then be explicitly written as

$$\eta_{use} = \frac{\beta^3 + 2\beta^2 + 2\beta}{\beta^3 + 3\beta^2 + 6\beta + 6} \quad . \tag{3-22}$$

In a similar manner, it can be shown that

$$\overline{A}_{ph} = \frac{e^{-\beta}(\beta^3 + 3\beta^2 + 6\beta + 6)}{\pi^4/15} \quad , \tag{3-23}$$

and

$$J_{ph} = \frac{q}{4\pi^2 c^2} \left(\frac{k_B T_E}{\hbar}\right)^3 [e^{-\beta}(\beta^2 + 2\beta + 2)] \quad , \tag{3-24}$$

$$= 1.011 \times 10^{-8} T_E^3 [e^{-\beta}(\beta^2 + 2\beta + 2)]$$

where J_{ph} has units of A/cm^2 and T_E is in degrees K.

Then for a single band gap cell, the TPV efficiency is given by

$$\eta_{TPV} = \frac{\eta_{use}\eta_{elec}}{1 + \frac{\overline{A}_{par}}{\overline{A}_{ph}}} \quad , \tag{3-25}$$

where

$$\eta_{elec} = \frac{J_{mp}V_{mp}}{J_{ph}V_g} \quad . \tag{3-26}$$

The I vs V characteristics of the TPV cell are taken to obey the standard diode equation

3-8

$$J = J_{ph} - J_o \left[\exp \left(\frac{qV}{k_B T_C} \right) - 1 \right] \quad , \tag{3-27}$$

where

$$J_o = B_o \exp \left(\frac{-E_g}{k_B T_C} \right) \quad . \tag{3-28}$$

Here, T_C is the cell temperature, V is the terminal voltage, and, following Bennett and Olsen (Ref. 3-2), B_o is assumed to equal 10^6 A/cm^2. The electrical power output per unit area is

$$P_{out} = JV \quad . \tag{3-29}$$

The values of $J(V)$ and V which maximize the power output are J_{mp} and V_{mp}.

3.4. TWO BAND GAP TPV CELL

Following the methodology and assumptions outlined above, the TPV efficiency for a two band gap TPV cell is found to be

$$\eta_{TPV} = \frac{\eta_{use1} \eta_{elec1}}{1 + \dfrac{\overline{A}_{par}}{\overline{A}_{ph}}} + \frac{\eta_{use2} \eta_{elec2}}{1 + \dfrac{\overline{A}_{par}}{\overline{A}_{ph}}} \quad , \tag{3-30}$$

where

$$\eta_{use1} = \frac{e^{-\beta_1} \left(\beta_1^3 + 2\beta_1^2 + 2\beta_1 \right)}{e^{-\beta_2} \left(\beta_2^3 + 3\beta_2^2 + 6\beta_2 + 6 \right)} \quad , \tag{3-31}$$

$$\eta_{use2} = \frac{\beta\left[e^{-\beta_2}\left(\beta_2{}^2 + 2\beta_2 + 2\right) - e^{-\beta_1}\left(\beta_1{}^2 + 2\beta_1 + 2\right)\right]}{e^{-\beta_2}\left(\beta_2{}^3 + 3\beta_2{}^2 + 6\beta_2 + 6\right)} \quad , \quad (3\text{-}32)$$

$$\eta_{elec1} = \frac{J_{mp1}V_{mp1}}{J_{ph1}V_{g1}} \quad , \quad\quad\quad (3\text{-}33)$$

$$\eta_{elec2} = \frac{J_{mp2}V_{mp2}}{J_{ph2}V_{g2}} \quad , \quad\quad\quad (3\text{-}34)$$

$$J_{ph1} = \frac{q}{4\pi^2 c^2}\left(\frac{k_B T_E}{\hbar}\right)^3 \left[e^{-\beta_1}\left(\beta_1^2 + 2\beta_1 + 2\right)\right] \quad , \quad (3\text{-}35)$$

$$J_{ph2} = \frac{q}{4\pi^2 c^2}\left(\frac{k_B T_E}{\hbar}\right)^3 \left[e^{-\beta_2}\left(\beta_2{}^2 + 2\beta_2 + 2\right) - e^{-\beta_1}\left(\beta_1{}^2 + 2\beta_1 + 2\right)\right] \quad ,$$
$$(3\text{-}36)$$

and

$$\overline{A}_{ph} = \frac{e^{-\beta_2}\left(\beta_2{}^3 + 3\beta_2{}^2 + 6\beta_2 + 6\right)}{\pi^4/15} \quad . \quad (3\text{-}37)$$

In the above equations, $\beta_1 = E_{g1}/(k_B T_E)$ and $\beta_2 = E_{g2}/(k_B T_E)$.

As for the single band gap cell, the I vs V characteristics for each cell are given by

$$J_1 = J_{ph1} - J_{o1}\left[\exp\left(\frac{qV}{k_B T_C}\right) - 1\right] \quad , \quad (3\text{-}38)$$

$$J_{o1} = B_o \exp\left(\frac{-E_{g1}}{k_B T_C}\right) \quad , \qquad\qquad (3\text{-}39)$$

$$J_2 = J_{ph2} - J_{o2} \left[\exp\left(\frac{qV}{k_B T_C}\right) - 1\right] \quad ,$$

$$J_{o2} = B_o \exp\left(\frac{-E_{g2}}{k_B T_C}\right) \quad . \qquad\qquad (3\text{-}40)$$

Again, the value of B_o is taken to be equal to 10^6 A/cm^2 in the following calculations.

3.5. OPTIMUM EFFICIENCY OF SINGLE BAND GAP TPV CELL

To compute the maximum TPV efficiency of a single band gap cell, a computer program was developed based on the equations derived in Section 3.3. Since the cell temperature, emitter temperature, and weighted parasitic absorption are strongly dependent on the cell construction and environment, these three variables were input parameters to the computer program. For each value of emitter temperature, cell temperature, and weighted parasitic absorption, the band gap which led to the largest TPV efficiency was calculated. For weighted parasitic absorption values of 0.05 and 0.10, the optimum band gap and associated TPV efficiency for selected emitter temperatures and cell temperatures are presented in Table 3-1 and displayed in Fig. 3-1.

A number of trends are apparent from this analysis. With increasing emitter temperature, the optimum band gap and corresponding TPV efficiency both increase. With increasing cell temperature, the optimum band gap increases, while the associated TPV efficiency decreases. For increasing weighted parasitic absorption, both the optimum band gap and the TPV efficiency decrease.

TABLE 3-1
OPTIMUM TPV EFFICIENCY AND ASSOCIATED SINGLE BAND GAP
FOR SELECTED VALUES OF EMITTER TEMPERATURE T_E,
CELL TEMPERATURE T_C, AND WEIGHTED PARASITIC
ABSORPTION $\overline{A}_{par}$

T_E (K)	T_C (K)	$\overline{A}_{par} = 0.05$		$\overline{A}_{par} = 0.1$	
		E_g (eV)	η_{TPV}	E_g (eV)	η_{TPV}
1500	300	0.78	0.2802	0.71	0.2267
	400	0.84	0.1936	0.78	0.1497
	500	0.91	0.1235	0.85	0.0902
	600	0.98	0.0702	0.93	0.0480
1700	300	0.85	0.3213	0.77	0.2645
	400	0.91	0.2400	0.84	0.1907
	500	0.97	0.1707	0.90	0.1301
	600	1.04	0.1137	0.98	0.0824
1900	300	0.93	0.3551	0.84	0.2960
	400	0.98	0.2793	0.90	0.2263
	500	1.04	0.2128	0.96	0.1669
	600	1.10	0.1556	1.03	0.1174
2100	300	1.00	0.3833	0.90	0.3225
	400	1.06	0.3127	0.96	0.2570
	500	1.11	0.2496	1.02	0.1998
	600	1.17	0.1938	1.08	0.1505
2300	300	1.08	0.4071	0.97	0.3449
	400	1.13	0.3413	1.02	0.2835
	500	1.18	0.2817	1.08	0.2289
	600	1.24	0.2281	1.14	0.1808
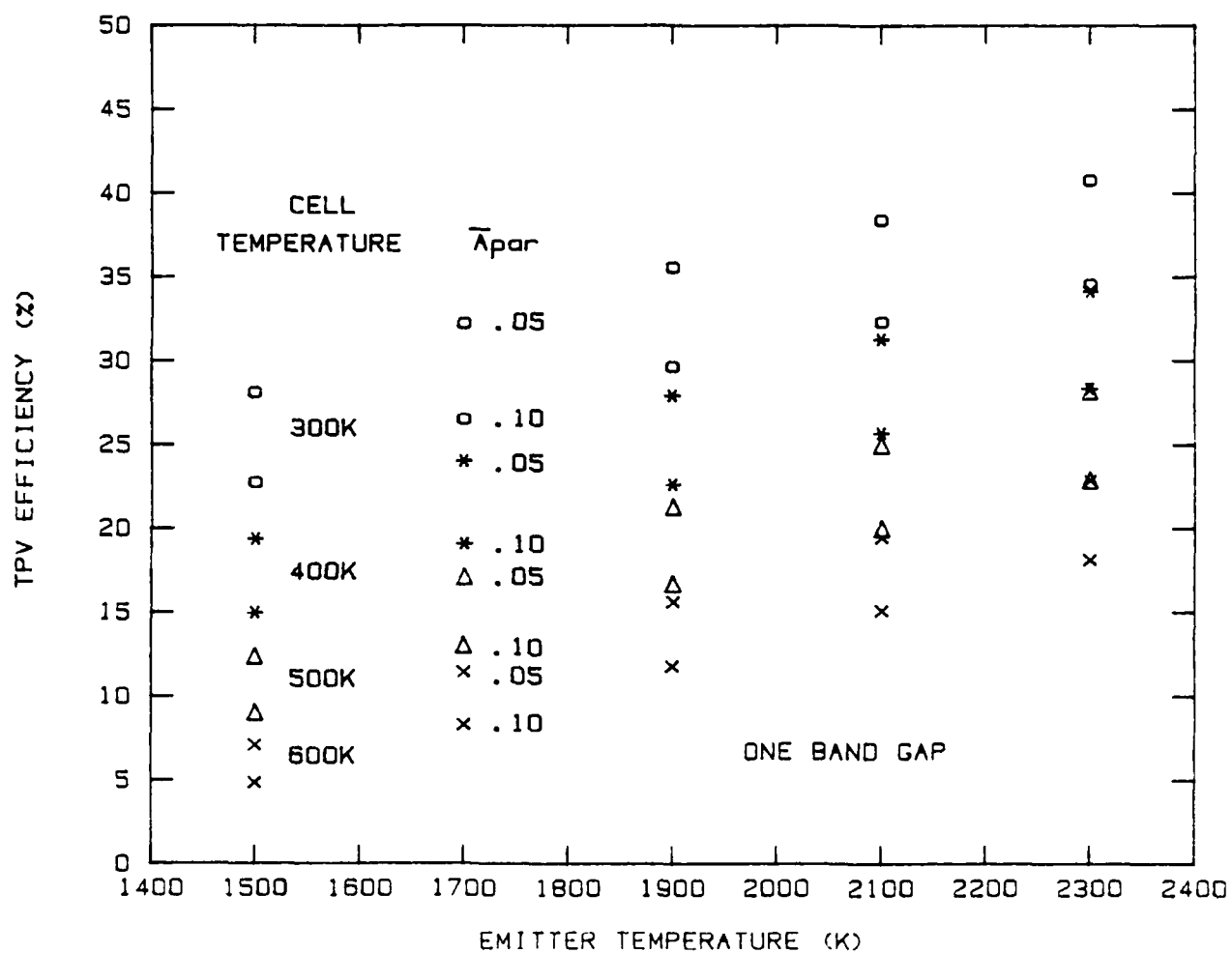
Fig. 3-1. Maximum TPV efficiency of a single band gap cell as a function
of emitter temperature for selected values of cell temperature
and weighted parasitic absorption $\bar{A}_{par}$

The values of the input parameters chosen are those that probably correspond to actual requirements of a realistic TPV system. The TPV cells would be heated to a fairly high temperature (since the blackbody emitter is a fairly intense source of radiation) which would depend on the amount of passive or active cooling applied to them. A 600 K temperature is a realistic upper limit of operation for present-day photovoltaic cells. A maximum emitter temperature of 2300 K was chosen since at higher temperature, significant vaporization of emitter material (such as tungsten, graphite, etc.) and its subsequent deposition on the TPV cells would block the incoming radiation and adversely affect the photogenerated current. Weighted parasitic absorption of Si p-i-n TPV cells as low as 0.05 has been achieved by Swanson (Refs. 3-9, 3-13) and so was taken as a lower limit. For weighted parasitic absorption greater than 0.10, the TPV efficiency becomes comparable to photovoltaic systems and so was chosen as an upper limit. We note that for an emitter temperature of 2300 K, a cell temperature of 300 K, and weighted parasitic absorption of 0.05, a TPV efficiency of 40.7% is calculated.

To more clearly elucidate the extreme importance of low parasitic absorption for achieving high TPV efficiency, the TPV efficiency as a function of band gap energy is plotted in Fig. 3-2 for selected values of weighted parasitic absorption $(\overline{A}_{par})$. These curves were calculated assuming an emitter temperature of 2100 K and a cell temperature of 300 K. For $\overline{A}_{par} = 0$, the TPV efficiency increases monotonically with band gap since both η_{use} and η_{elec} increase with increasing band gap. For finite values of $\overline{A}_{par}$, η_{TPV} has a rather flat maximum. This indicates that if the parasitic absorption of the TPV cell is known, then the band gap energy which maximizes η_{TPV} may vary by as much as ± 0.1 eV without significant loss of efficiency.

The results of another calculation which illuminates the relationship between η_{TPV} and $\overline{A}_{par}$ are presented in Fig. 3-3. Here both the maximum η_{TPV} and associated band gap are plotted as a function $\overline{A}_{par}$. Both η_{TPV} and the related band gap are strongly decreasing functions of increasing parasitic absorption, particularly for values of $\overline{A}_{par} \leq 0.2$.
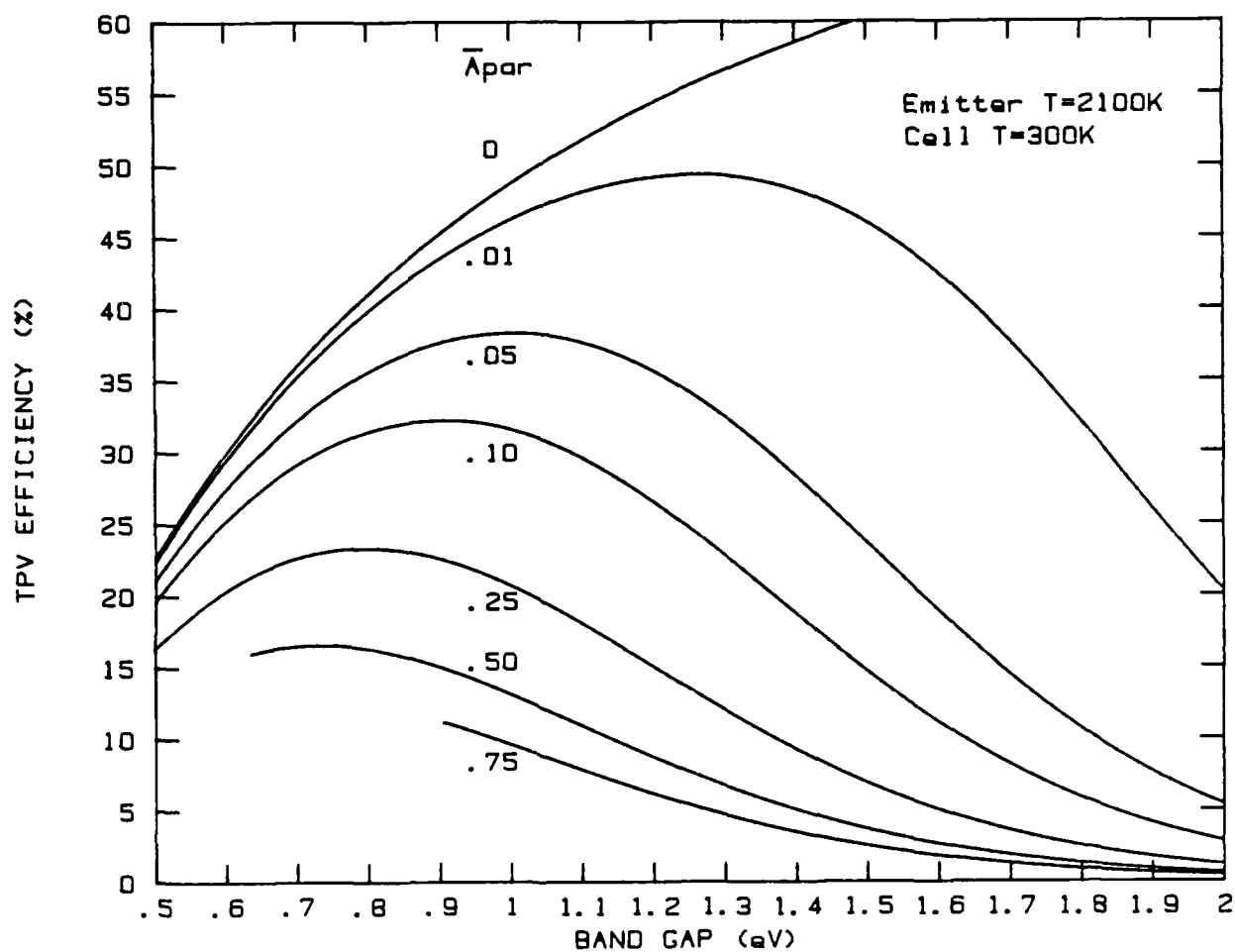
Fig. 3-2. TPV efficiency versus band gap for selected values of weighted parasitic absorption $\overline{A}_{par}$ at an emitter temperature of 2100 K and a cell temperature of 300 K
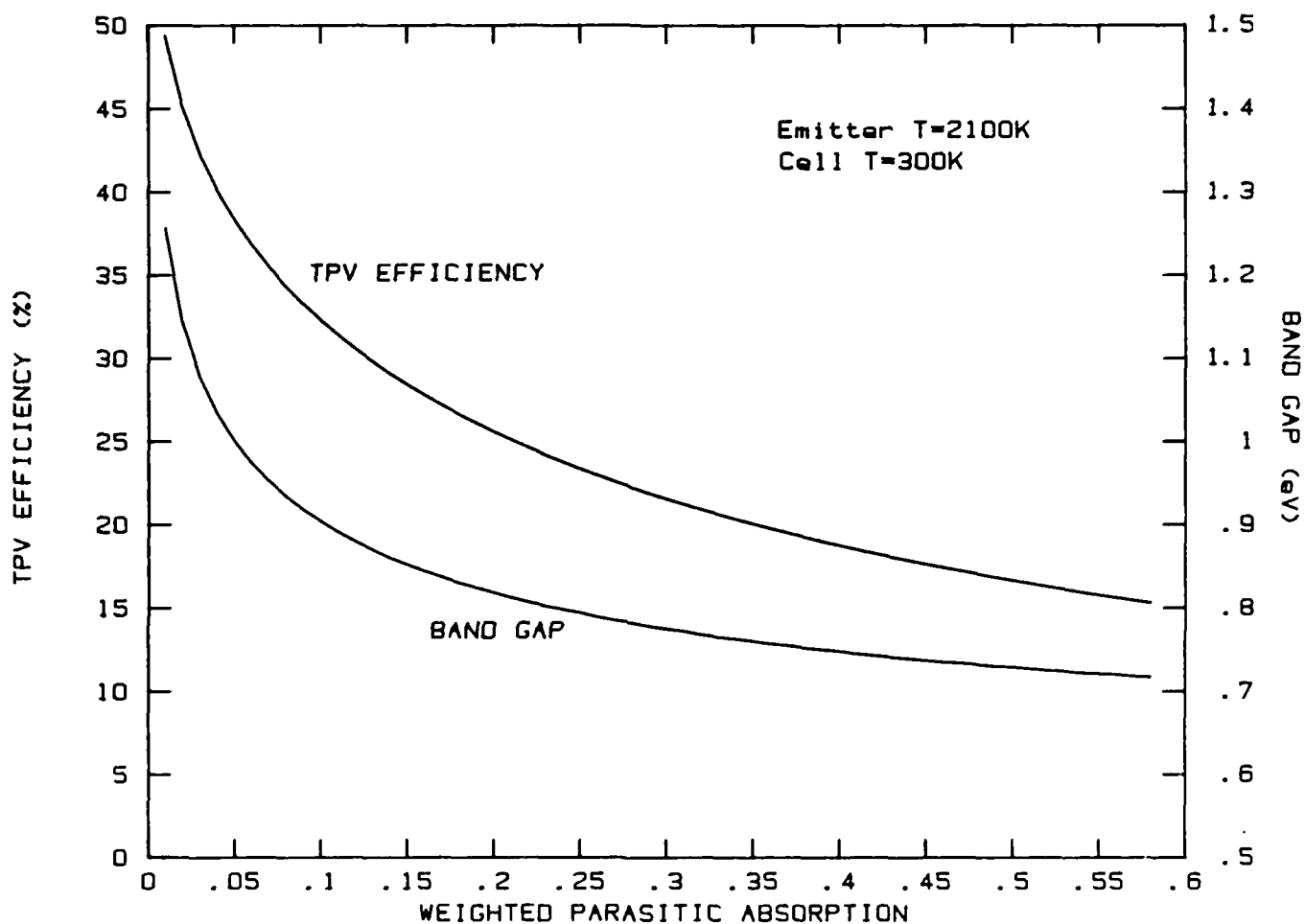
Fig. 3-3. Optimum TPV efficiency and associated band gap versus
weighted parasitic absorption $\overline{A}_{par}$ for an emitter
temperature of 2100 K and a cell temperature of
300 K

This again emphasizes the need for low parasitic absorption TPV cells for maximizing TPV efficiency. It also demonstrates that in order to fabricate TPV cells of optimum efficiency, the emitter temperature, cell temperature, and parasitic absorption must all be considered.

For finite values of $\overline{A}_{par}$, the curve of η_{TPV} versus band gap energy has a maximum because $\overline{A}_{ph}$ decreases with increasing band gap. This is more clearly shown in Fig. 3-4, where the factors $\overline{A}_{ph}$, η_{elec}, η_{use}, $\eta_{elec} \cdot \eta_{use}$, $1/(1 + \overline{A}_{par}/\overline{A}_{ph})$, and η_{TPV}, which equals the product of the previous two factors, are plotted versus band gap energy. Whereas $\eta_{elec} \cdot \eta_{use}$ gradually increases with band gap, the factor $1/(1 + \overline{A}_{par}/\overline{A}_{ph})$ rapidly decreases with increasing band gap, leading to the maximum in the η_{TPV} versus band gap curve.

The interrelationship between η_{TPV}, $\overline{A}_{par}$, and band gap is also illustrated in Fig. 3-5, where η_{TPV} is plotted versus weighted parasitic absorption for band gap fixed values of 0.7, 1.1, 1.4, and 1.8 eV. These curves illustrate that the higher band gap cells have a greater η_{TPV} for low values of $\overline{A}_{par}$, whereas the lower band gap cells are more efficient for high values of $\overline{A}_{par}$ owing to their larger values of $\overline{A}_{ph}$.

Finally, we consider the case of maximum weighted parasitic absorption where none of the below-band-gap energy photons are reflected back to the emitter; instead they are all absorbed by the TPV cell. Then the value of $\overline{A}_{par}$ is as large as it can be in the above theory, namely $\overline{A}_{par} = 1 - \overline{A}_{ph}$, where $\overline{A}_{ph}$ is determined from Eq. 3-23. For selected values of T_E and T_C, the band gap which led to the largest TPV efficiency was calculated subject to the constraint of $\overline{A}_{par} = 1 - \overline{A}_{ph}$. These results are presented in Table 3-2 along with the values of $\overline{A}_{par}$ associated with the parameters T_E, T_C, and E_g. The magnitudes of both E_g and η_{TPV} are significantly lower than those calculated under the conditions of $\overline{A}_{par} = 0.05$ and $\overline{A}_{par} = 0.10$ as shown in Table 3-1. The TPV efficiency decreases considerably faster with increasing cell temperature for the maximum $\overline{A}_{par}$ condition compared with low values of $\overline{A}_{par}$. For example, at $T_E = 2100$ K, η_{TPV} decreases by 71% between 300 and 600 K

3-17
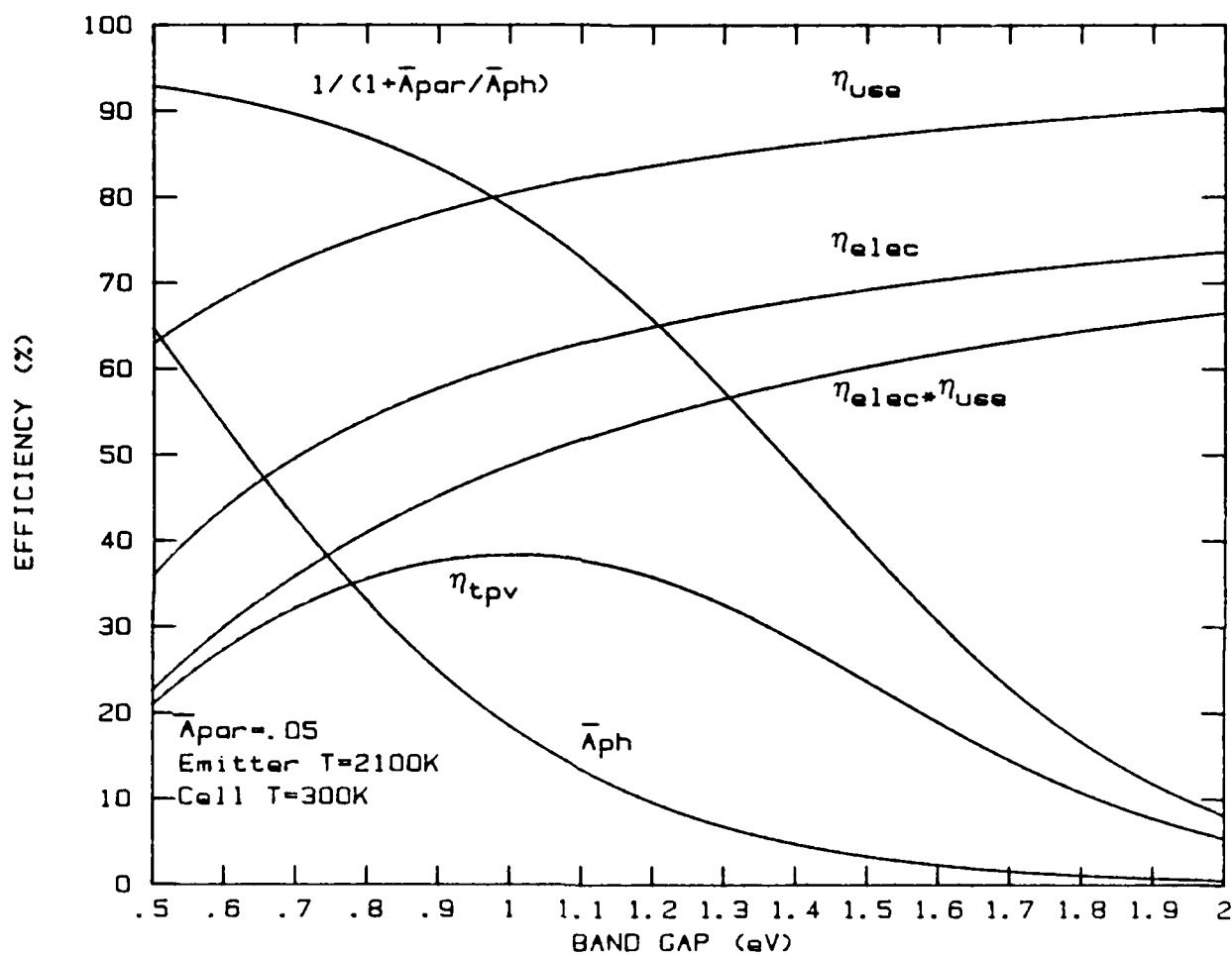
Fig. 3-4. TPV efficiency factors η_{TPV}, η_{use}, η_{elec}, $\eta_{elec} \cdot \eta_{use}$, $\overline{A}_{ph}$, and $1/(1 + \overline{A}_{par}/\overline{A}_{ph})$ versus band gap energy for an emitter temperature of 2100 K, a cell temperature of 300 K, and a weighted parasitic absorption of $\overline{A}_{par} = 0.05$

Fig. 3-5. TPV efficiency versus weighted parasitic absorption $\bar{A}_{par}$ for
fixed band gaps of 0.7, 1.1, 1.4, and 1.8 eV, an emitter
temperature of 2100 K, and a cell temperature of 300 K.
Shown in the inset is the TPV efficiency versus $\bar{A}_{par}$ for
low values of $\bar{A}_{par}$.

TABLE 3-2

OPTIMUM TPV EFFICIENCY AND ASSOCIATED SINGLE
BAND GAP FOR SELECTED VALUES OF EMITTER
TEMPERTURE T_E AND CELL TEMPERATURE T_C
UNDER THE CONDITION $\overline{A}_{par} = 1 - \overline{A}_{ph}$

T_E (K)	T_C (K)	E_g (eV)	η_{TPV}	$\overline{A}_{par}$
1500	300	0.52	0.0885	0.604
	400	0.62	0.0456	0.728
	500	0.72	0.0214	0.821
	600	0.82	0.0090	0.886
1700	300	0.55	0.1145	0.554
	400	0.64	0.0674	0.663
	500	0.73	0.0371	0.753
	600	0.82	0.0190	0.824
1900	300	0.58	0.1383	0.513
	400	0.66	0.0892	0.605
	500	0.74	0.0549	0.687
	600	0.83	0.0321	0.764
2100	300	0.61	0.1597	0.478
	400	0.68	0.1102	0.555
	500	0.76	0.0734	0.635
	600	0.85	0.0471	0.714
2300	300	0.64	0.1788	0.449
	400	0.71	0.1298	0.521
	500	0.79	0.0918	0.597
	600	0.86	0.0630	0.658

when $\overline{A}_{par} = 1 - \overline{A}_{ph}$, yet it decreases by only 49% when $\overline{A}_{par} = 0.05$. It is interesting to note that even under these "worst case" conditions, a TPV conversion efficiency as high as 18% is calculated for $T_E = 2300$ K and $T_C = 300$ K.

3.6. OPTIMUM EFFICIENCY OF TWO BAND GAP TPV CELLS

Based on the explicit equations presented in Section 3.4, a computer program was developed to calculate the maximum TPV efficiency for two different band gaps. In this case, the input parameters were again the emitter temperature, the cell temperature, and the weighted parasitic absorption. As previously shown by others (Refs. 3-2, 3-3), as a first approximation for determining the efficiency of two band gap photovoltaic cells, it is reasonable to assume matching short circuit currents from each band gap. Calculation of the maximum TPV efficiency for two band gaps proceeded by determining, for each upper band gap, the lower band gap where the short circuit currents from each band gap are equal.

The upper band gap is varied for each value of cell temperature, emitter temperature, and parasitic absorption; the lower band gap where equality of short circuit current occurs is calculated; and the band gaps which give the maximum TPV efficiency are determined. Whereas the short circuit currents from each band gap are equal, the values of J_{mp1} and J_{mp2}, the current densities from each band gap at the respective maximum power points, are not identical. Results for the input parameter spectrum previously used for the one band gap case are tabulated for the two band gap case in Table 3-3 and presented graphically in Fig. 3-6.

As for the single band gap case, with increasing emitter temperature, both the higher and lower band gaps as well as n_{TPV} increase in magnitude. With increasing cell temperature, both band gaps increase,

3-21

TABLE 3-3
OPTIMUM TPV EFFICIENCY AND ASSOCIATED TWO BAND GAPS FOR SELECTED
VALUES OF EMITTER TEMPERATURE T_E, CELL TEMPERATURE T_C, AND
WEIGHTED PARASITIC ABSORPTION $\overline{A}_{par}$

T_E (K)	T_C (K)	$\overline{A}_{par} = 0.05$			$\overline{A}_{par} = 0.1$		
		E_{g1} (eV)	E_{g2} (eV)	η_{TPV}	E_{g1} (eV)	E_{g2} (eV)	η_{TPV}
1500	300	0.87	0.75	0.3130	0.80	0.67	0.2591
	400	0.93	0.81	0.2164	0.87	0.75	0.1712
	500	1.00	0.88	0.1382	0.94	0.82	0.1034
	600	1.07	0.96	0.0786	1.02	0.90	0.0551
1700	300	0.95	0.81	0.3586	0.87	0.72	0.3020
	400	1.01	0.87	0.2678	0.94	0.80	0.2178
	500	1.08	0.95	0.1906	1.01	0.87	0.1487
	600	1.14	1.01	0.1269	1.08	0.95	0.0942
1900	300	1.03	0.87	0.3963	0.95	0.79	0.3378
	400	1.09	0.93	0.3114	1.01	0.85	0.2581
	500	1.16	1.01	0.2372	1.07	0.91	0.1903
	600	1.22	1.07	0.1734	1.14	0.99	0.1339
2100	300	1.12	0.94	0.4277	1.02	0.84	0.3679
	400	1.18	1.01	0.3486	1.08	0.90	0.2929
	500	1.24	1.07	0.2781	1.14	0.96	0.2276
	600	1.30	1.13	0.2158	1.21	1.04	0.1714
2300	300	1.20	1.00	0.4542	1.10	0.90	0.3935
	400	1.26	1.07	0.3804	1.16	0.96	0.3231
	500	1.32	1.13	0.3137	1.22	1.03	0.2607
	600	1.38	1.19	0.2537	1.28	1.09	0.2057
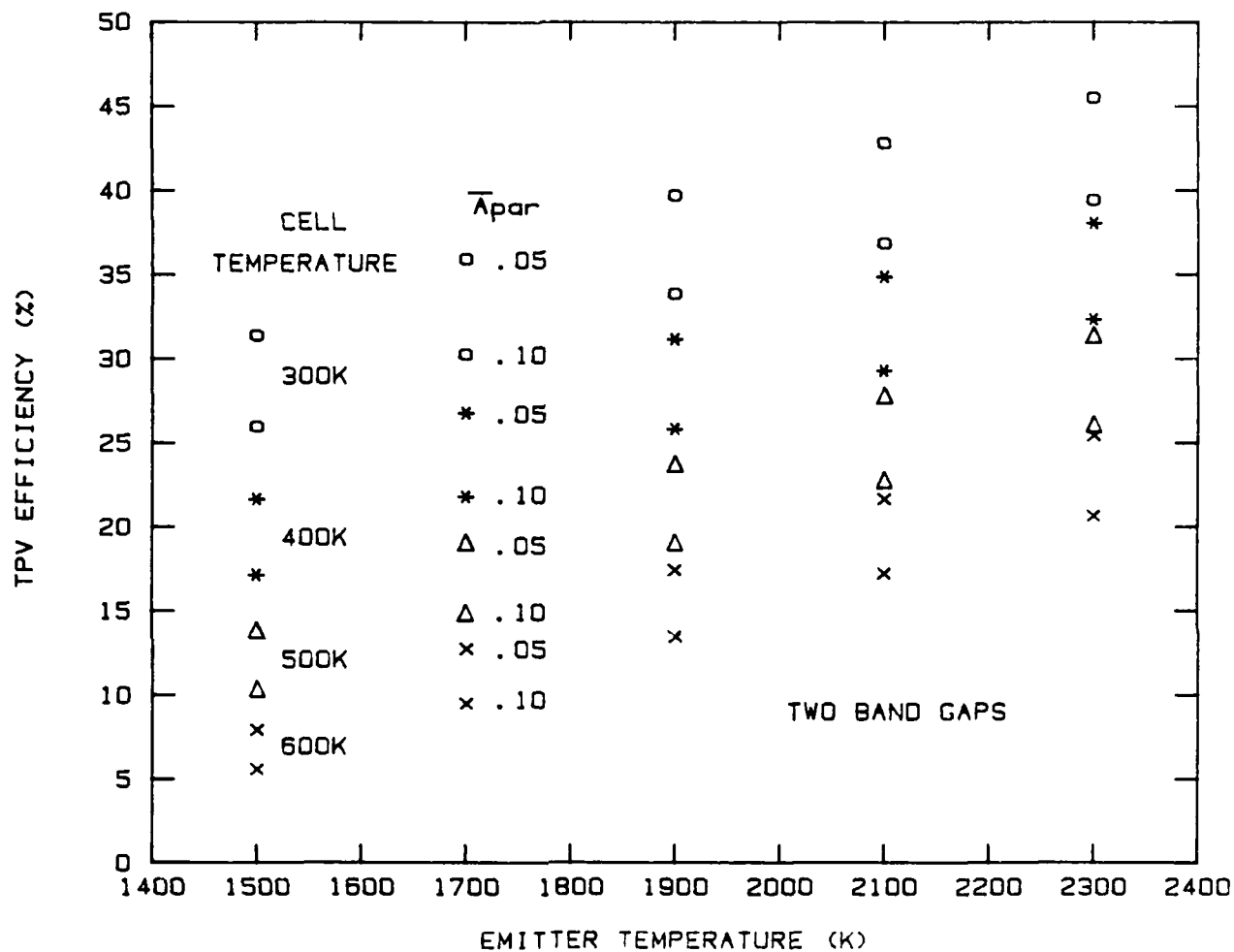
Fig. 3-6. Maximum TPV efficiency for two band gaps as a function of emitter temperature for selected values of cell temperature and weighted parasitic absorption $\overline{A}_{par}$

while n_{TPV} decreases. For increasing values of $\overline{A}_{par}$, both of the band gaps and n_{TPV} decrease. In comparison with the single band gap TPV efficiency at a given value of cell and emitter temperature and $\overline{A}_{par}$, the two band gap TPV efficiency is only about 10% higher. For example, at T_C = 300 K and T_E = 2100 K for $\overline{A}_{par}$ = 0.05, n_{TPV} = 0.3833 for a single band gap, while n_{TPV} = 0.4277 for two band gaps, an increase of 11%.

As is apparent from Eq. 3-14, n_{TPV} can be considered to be a sum of the individual TPV efficiencies n_{TPVi} arising from each band gap. Again assuming that the short circuit currents from each band gap match, n_{TPV}, n_{TPV1}, and n_{TPV2} and the lower band gap have been calculated as a function of the higher band gap cell No. 1. These curves are plotted in Fig. 3-7 for the parameters T_E = 2100 K, T_C = 300 K, and $\overline{A}_{par}$ = 0.05. For increasing values of the higher band gap, the maximum of n_{TPV1}, then n_{TPV}, and finally n_{TPV2} is attained. Also apparent from the calculation is that n_{TPV1} lies above n_{TPV2}. Lastly, we note that the value of the lower band gap increases almost linearly with higher band gap energy.

To determine the sensitivity of the TPV efficiency to the short circuit current matching condition, we have calculated the TPV efficiency for a fixed lower band gap of E_{g2} = 0.94 eV as a function of the higher band gap for T_E = 2100 K, T_C = 300 K, and selected values of $\overline{A}_{par}$. These results are shown in Fig. 3-8. Comparing n_{TPV} for equal short circuit currents shown in Fig. 3-6 and Table 3-2 for $\overline{A}_{par}$ = 0.05 (where E_{g2} = 0.94 eV and η = 42.77%) with the curve shown in Fig. 3-8 for $\overline{A}_{par}$ = 0.05 indicates that optimum efficiency of 43.13% for E_{g2} = 0.94 eV occurs at an upper band gap of 1.20 eV, close to the equal short circuit current upper band gap of 1.12 eV. Indeed, the efficiencies at these two points differ by only 1%.

We have also calculated the optimum two band gap configuration without any constraints for the conditions of $\overline{A}_{par}$ = 0.05, T_E = 2100 K,
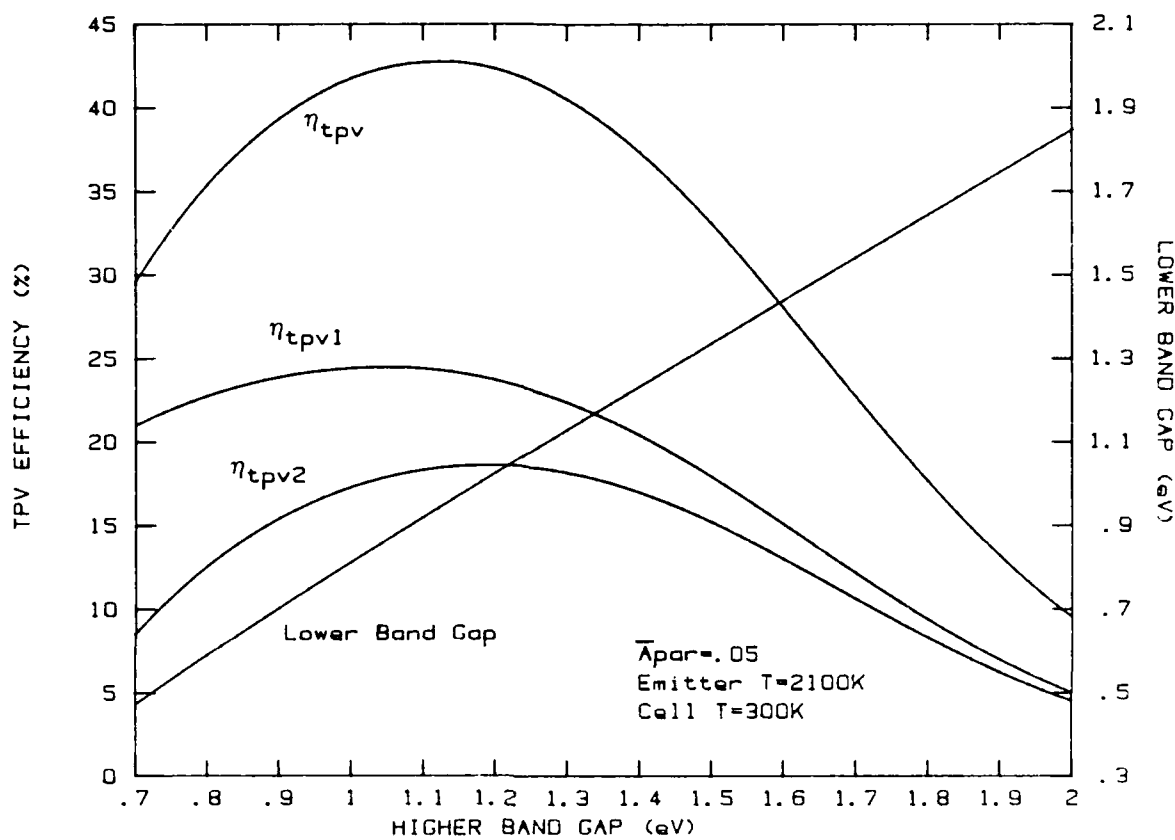
Fig. 3-7. TPV efficiency factors η_{TPV}, η_{TPV1}, and η_{TPV2} and lower band gap versus higher band gap energy for an emitter temperature of 2100 K, a cell temperature of 300 K, and a weighted parasitic absorption of $\overline{A}_{par} = 0.05$
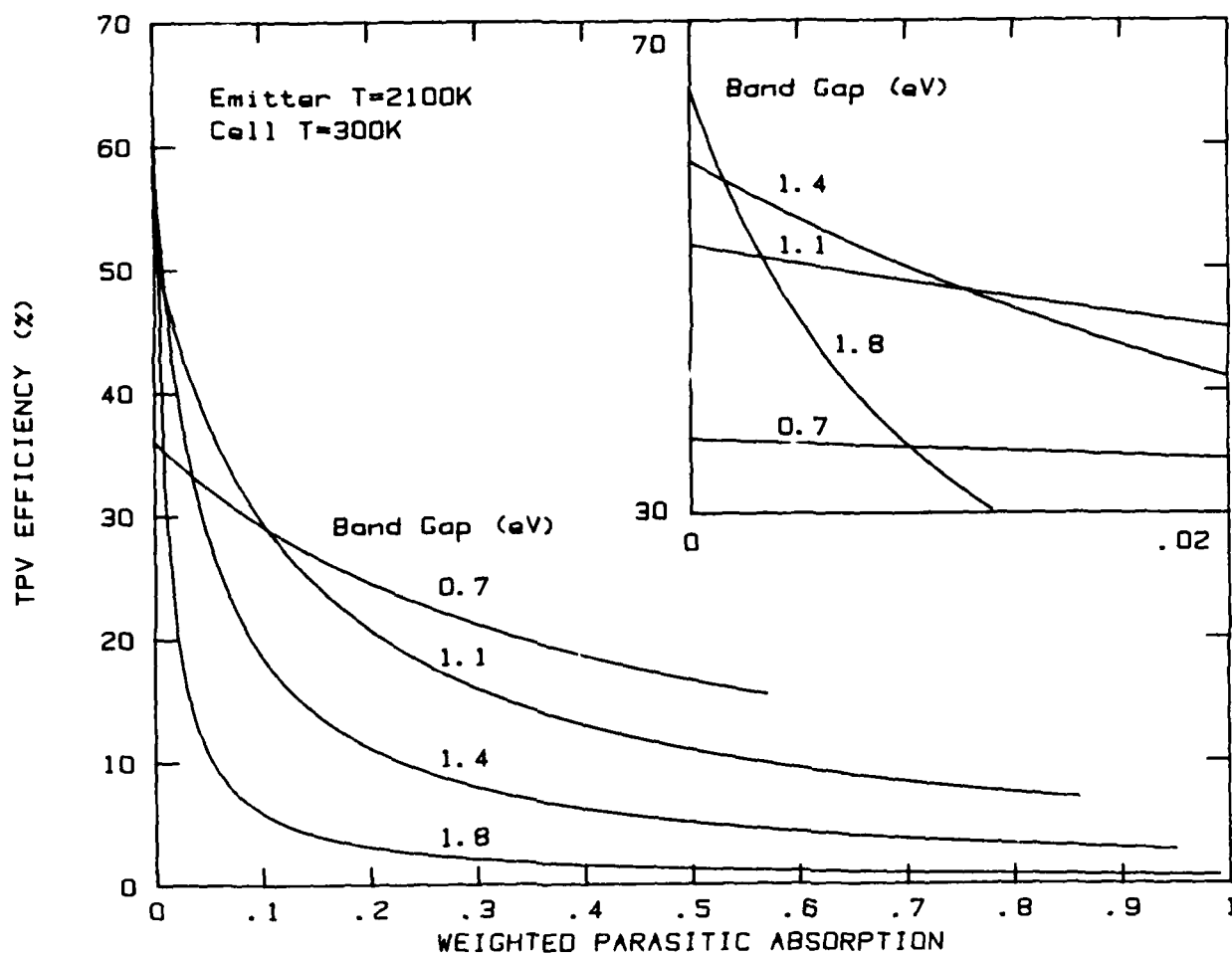
3-25
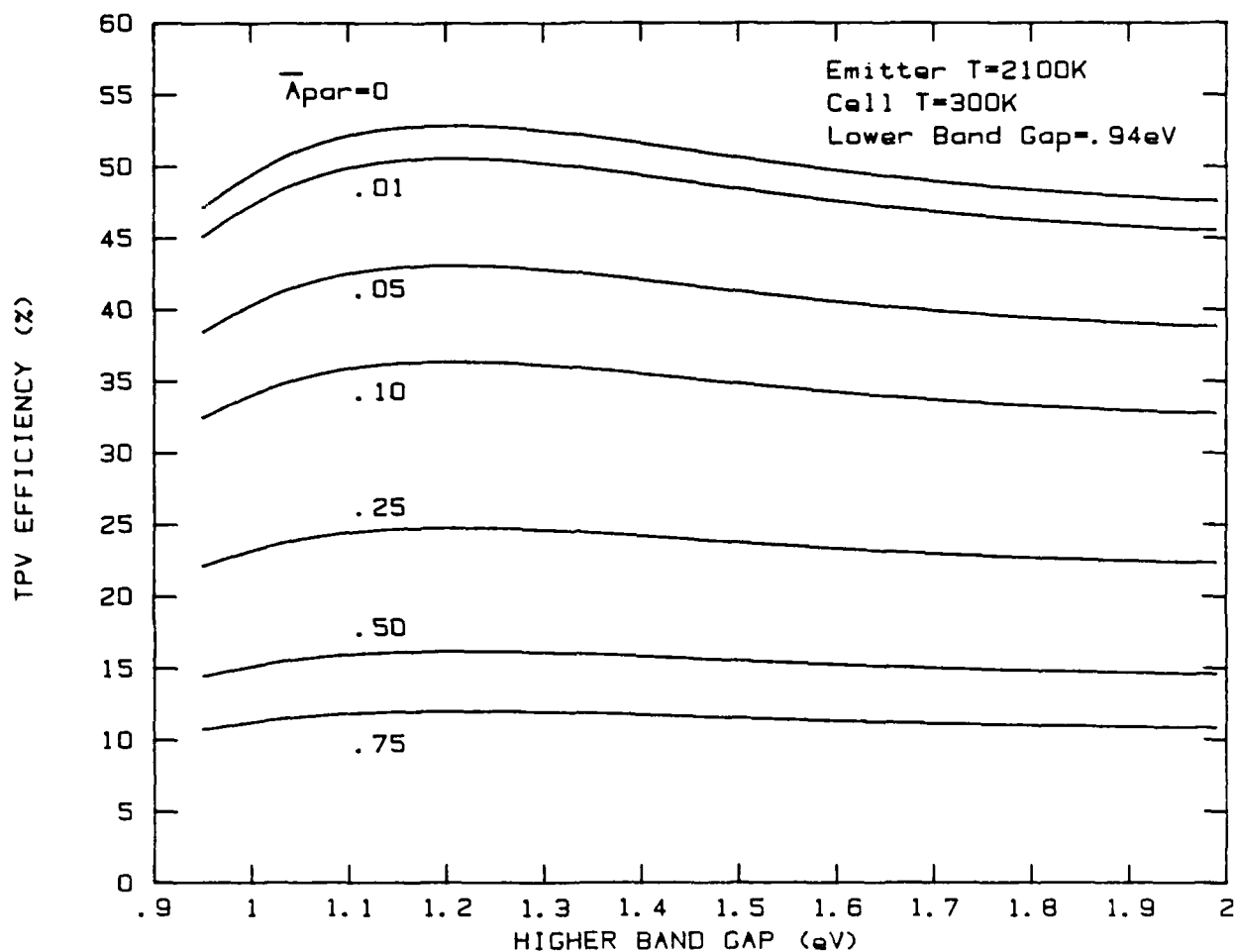
Fig. 3-8. TPV efficiency versus higher band gap energy for various values of weighted parasitic absorption $\overline{A}_{par}$ and fixed values of emitter temperature of 2100 K, cell temperature of 300 K, and lower band gap of 0.94 eV

and T_C = 300 K. In this case, η_{TPV} = 0.4313, E_{g1} = 1.20 eV, and E_{g2} = 0.94 eV, precisely the same values found above. Thus, for these conditions the optimum TPV efficiencies both with and without short circuit current matching constraints are found at the same value of the lower band gap energy and differ by less than 1%. Unlike the current matching TPV efficiency, for no constraints, η_{TPV1} = 0.191 is less than η_{TPV2} = 0.240. In addition, at the maximum power point J_{mp1} = 7.08 A/cm^2, while J_{mp2} = 12.56 A/cm^2 is significantly larger.

To again indicate the requirement of low parasitic absorption for high TPV efficiency, we have calculated the maximum η_{TPV} and the corresponding values of E_{g1} and E_{g2} as a function of weighted parasitic absorption, assuming equal short circuit currents from each band gap. These results are displayed in Fig. 3-9.

As for the single band gap case, we have also calculated the optimum TPV efficiency and associated two band gaps, assuming equal short circuit currents, under the condition of maximum weighted parasitic absorption of $\overline{A}_{par}$ = 1 − $\overline{A}_{ph}$. For selected values of T_E and T_C, the results are displayed in Table 3-4 along with the corresponding value of $\overline{A}_{par}$. Again, the magnitudes of E_g and η_{TPV} are significantly lower than those calculated under the conditions of $\overline{A}_{par}$ = 0.05 and $\overline{A}_{par}$ = 0.10 as shown in Table 3-3. The TPV conversion efficiency does reach a fairly high value of 24% for T_E = 2300 K and T_C = 300 K. With increasing cell temperature, η_{TPV} decreases significantly faster for $\overline{A}_{par}$ = 1 − $\overline{A}_{ph}$ compared with $\overline{A}_{par}$ = 0.05 and 0.1, as previously noted for the single band gap case. Under the condition $\overline{A}_{par}$ = 1 − $\overline{A}_{ph}$, η_{TPV} for the two band gap case is approximately 33% higher than η_{TPV} for a single band gap. This is a significantly larger improvement than the ~10% increase in η_{TPV} found when $\overline{A}_{par}$ = 0.05 and 0.1. Thus, for a TPV energy conversion system which does not recycle the below band gap energy photons back to the emitter, the use of multiple band gaps offers an attractive route for boosting the efficiency.
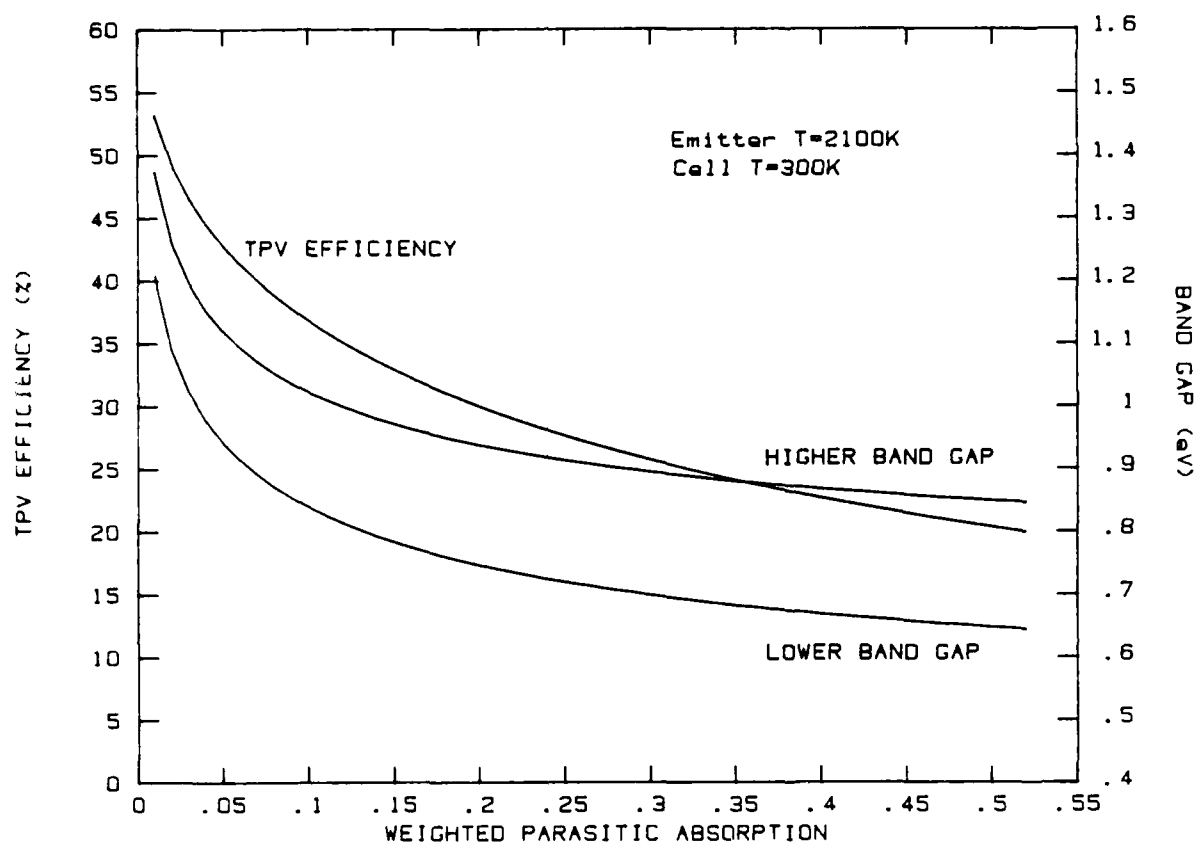
Fig. 3-9. Optimum TPV efficiency and asociated lower and higher band gaps versus weighted parasitic absorption $\bar{A}_{par}$ for an emitter temperature of 2100 K and cell temperature of 300 K

TABLE 3-4

OPTIMUM TPV EFFICIENCY AND ASSOCIATED TWO BAND GAPS
FOR SELECTED VALUES OF EMITTER TEMPERATURE T_E
AND CELL TEMPERATURE T_C UNDER THE
CONDITION $\overline{A}_{par} = 1 - \overline{A}_{ph}$

T_E (K)	T_C (K)	E_{g1} (eV)	E_{g2} (eV)	n_{TPV}	$\overline{A}_{par}$
1500	300	0.60	0.46	0.1189	0.509
	400	0.68	0.54	0.0605	0.637
	500	0.78	0.65	0.0279	0.761
	600	0.87	0.75	0.0116	0.841
1700	300	0.64	0.47	0.1544	0.446
	400	0.72	0.56	0.0899	0.568
	500	0.80	0.65	0.0489	0.673
	600	0.89	0.75	0.0247	0.767
1900	300	0.68	0.48	0.1870	0.393
	400	0.76	0.58	0.1196	0.509
	500	0.83	0.66	0.0728	0.600
	600	0.91	0.74	0.0421	0.689
2100	300	0.73	0.51	0.2164	0.363
	400	0.80	0.59	0.1482	0.458
	500	0.87	0.67	0.0979	0.546
	600	0.94	0.75	0.0622	0.624
2300	300	0.78	0.53	0.2425	0.339
	400	0.84	0.61	0.1750	0.414
	500	0.90	0.68	0.1228	0.486
	600	0.98	0.77	0.0836	0.575

3.7. CONCLUSIONS

A theory has been developed to calculate the TPV energy conversion efficiency of multiple band gap cells that is based on the single band gap theory previously used by Swanson (Refs. 3-8 through 3-10). Explicit equations have been derived for determining the TPV efficiency of both one and two band gap cells. For the single band gap cell, the optimum efficiency and associated band gap have been calculated for various values of emitter temperature, cell temperature, and weighted parasitic absorption. Efficiencies in excess of 35% appear feasible for a cell temperature of 300 K and a reasonable weighted parasitic absorption of 0.05.

For the two band gap TPV cell, efficiencies and corresponding band gaps have been calculated assuming equal short circuit current densities collected from each band gap. The two band gap efficiency is typically about 10% larger than that for a single band gap for fixed values of emitter temperature, cell temperature, and weighted parasitic absorption. This suggests that the route to high values of TPV efficiency likely will proceed by significant reductions in the parasitic absorption of single band gap cells rather than by the fabrication of multiple band gap cells.

4. THEORETICAL MODEL FOR INFERRING HIGH-TEMPERATURE TPV EFFICIENCY

4.1. INTRODUCTION

For a space-based TPV energy conversion system, it is necessary that the cell temperature be as high as possible in order to minimize the mass of the radiator, which is responsible for cooling the cells. Therefore, TPV properties at high temperatures should be known. However, the TPV test rig is able to operate only near room temperature.

In order to infer TPV efficiencies at elevated temperatures, it is necessary to determine η_{elec}, η_{use}, $\overline{A}_{par}$, and $\overline{A}_{ph}$ at elevated temperatures. Then η_{TPV} can be calculated according to

$$\eta_{TPV} = \frac{\eta_{elec}\eta_{use}}{1 + \dfrac{\overline{A}_{par}}{\overline{A}_{ph}}} \quad . \tag{4-1}$$

The procedure followed is described below.

4.2. η_{use}

The use factor η_{use} can be calculated from

$$\eta_{use} = \frac{\beta^3 + 2\beta^2 + 2\beta}{\beta^3 + 3\beta^2 + 6\beta + 6} \quad , \tag{4-2}$$

where $\beta = E_g/(k_B T_E)$, with E_g being the energy gap and T_E the emitter temperature. Since E_g decreases with increasing temperature, it is necessary to know $E_g(T)$. The temperature dependence of the band gap can be expressed approximately by a universal function of the form (Ref. 4-1)

$$E_g(T) = E_g(0) - \frac{\alpha T^2}{(T + \gamma)} \quad . \tag{4-3}$$

For GaAs (Ref. 4-1), $E_g(0) = 1.519$ eV, $\alpha = 5.405 \times 10^{-4}$ eV/K, and $\gamma = 204$ K. For Si (Ref. 4-1), $E_g(0) = 1.170$ eV, $\alpha = 4.73 \times 10^{-4}$ eV/K, and $\gamma = 636$ K. If E_g at 300 K is known, then $E_g(0)$ can be determined by

$$E_g(0) = E_g(T) + \frac{\alpha T^2}{(T + \gamma)} \quad . \tag{4-4}$$

For the InGaAs cells to be discussed, $E_g(0)$ was calculated from the known value of E_g (300 K) and Eq. 4-4, assuming that the parameters α and γ are the same for InGaAs as for GaAs. Then $E_g(T)$ was derived using Eq. 4-3. For indirect gap materials such as Si, it appears that the band gap is somewhat greater (for Si ~ 0.1 eV) than the actual band gap so far as $\overline{A}_{ph}$, η_{use}, and J_{ph} are concerned (Ref. 4-2). Therefore, for Si it was assumed that E_g (300 K) $= 1.12 + 0.1 = 1.22$ eV.

4.3. $\overline{A}_{ph}$

The weighted photoproduction absorption can be calculated using

$$\overline{A}_{ph} = \frac{e^{-\beta} \left(\beta^3 + 3\beta^2 + 6\beta + 6 \right)}{\pi^4/15} \quad . \tag{4-5}$$

4.4. $\overline{A}_{par}$

Because of the difficulty in inferring the temperature dependence of the weighted parasitic absorption $\overline{A}_{par}$, a fixed value will be chosen.

As discussed by Swanson (Refs. 4-2, 4-3), many factors contribute to $\overline{A}_{par}$ for Si p-i-n cells. Since fabrication of the InGaAs cells is even more complicated than that of the Si p-i-n, it is probably not feasible to calculate $\overline{A}_{par}$ from first principles. At least, it is necessary to minimize identifiable mechanisms, such as free carrier absorption, due to intraband transitions, that arises from the thick, heavily doped GaAs substrate upon which the InGaAs cells are grown.

Assuming that the InGaAs TPV cells have a back surface mirror which allows the below-band-gap energy photons two passes at the cell materials, the weighted free carrier absorption can be calcualted to be (Ref. 4-2)

$$\overline{A}_{fc} = \frac{\int_{0}^{\infty} P(\omega)A_{fc}(\omega)d\omega}{\int_{0}^{\infty} P(\omega)d\omega} \quad , \tag{4-6}$$

or

$$\overline{A}_{fc} = 5.5 \times 10^{-9} \left(\frac{m_e}{m^*}\right)^2 \frac{gWn}{\hat{n}\mu T_E^2} \quad , \tag{4-7}$$

in the limit of small $\overline{A}_{fc}$. In this equation, m_e is the free electron mass, m^* is the carrier conductivity effective mass, W is the layer thickness in cm, n is the free carrier concentration in cm^{-3}, $\hat{n}$ is the refractive index, and μ is the carrier mobility in $cm^2/(V-s)$.

For the InGaAs cells studied, the 350-μ-thick GaAs substrates were doped to a density of 2×10^{18} cm^{-3}. Therefore, in Eq. 4-7, the input parameters are taken to be n = 2×10^{18} cm^{-3} and W = 350×10^{-4} cm. If an n-type GaAs substrate is assumed, $m^* = 0.067$ and $\mu = 2.5 \times 10^3$ $cm^2/$ (V-s) at this doping level (Ref. 4-1). Between wavelengths of 1 and

10 μm, $\hat{n}$ = 3.3 for GaAs (Ref. 4-4). For ionized impurity scattering, g = 3.395, while for phonon scattering, g = 1.132. At room temperature and above, phonon scattering generally dominates so that g = 1.132. Assuming an emitter temperature of 2000 K, the weighted free carrier absorption then becomes $\overline{A}_{fc}$ = 2.9. Since this is not small, then Eq. 4-7 is not valid since it is true only when $\overline{A}_{fc}$ << 1. The above analysis indicates that the parasitic absorption due to free carrier absorption is not small.

The previous discussion suggests that the doping level of the GaAs substrate must be reduced to n ~ 10^{16} cm^{-3} where μ = 6 x 10^3 cm^2/(V-s). Then $\overline{A}_{fc}$ = 0.006, which is an extremely low value, and other parasitic mechanisms would probably dominate at this level. In the above discussion, an n-type GaAs substrate was assumed, since its mobility is 20 times higher than that of p-type, resulting in 20 times smaller $\overline{A}_{fc}$.

The free carrier absorption due to the active junctions of the InGaAs cell should also be small. The total thickness of these regions (i.e., p-n junctions, window layer, cap layer, etc.) is approximately 3 μm and the typical doping density is n = 10^{18} cm^{-3} (Ref. 4-5), where μ = 10^3 cm^2/V-s. Then $\overline{A}_{fc}$ = 0.032, which is quite acceptable.

The temperature dependence of the free carrier absorption will be primarily due to the temperature dependence of the free carrier density n and mobility μ. Since the intrinsic carrier density of GaAs at 500°C is n_i ~ 10^{15} cm^{-3} (Ref. 4-1), at the temperatures considered here, the carrier density due to the dopants (extrinsic carrier density) is always greater than the intrinsic carrier density and so the carrier density will remain essentially unchanged with temperature. The mobility due to phonon scattering varies at $T^{-1.0}$ for n-type GaAs (Ref. 4-1). Therefore, between 300 and 600 K, the mobility is expected to decrease according to

$$\frac{\mu(600\ K)}{\mu(300\ K)} = \frac{(600\ K)^{-1}}{(300\ K)^{-1}} = 0.5 \quad .$$

This will increase $\overline{A}_{fc}$ by a factor of 2. Therefore, it is reasonable to assume that $\overline{A}_{fc}$ will remain essentially unchanged (within a factor of 2 or so) as the cell temperature is increased from 300 to 600 K.

Other known contributions to parasitic absorption should also be minimized. GaAs has some optical phonon modes at an energy of 0.035 eV = 35 μm which are expected to cause negligible parasitic absorption. GaAs has a splitting of ~0.3 eV (Ref. 4-6) between valence bands, which could result in considerable parasitic absorption due to interband transitions at ~4 μm. This suggests that the majority of the cell should be n-type, so there are few holes to absorb at this wavelength. However, even for the p-type regions of the cell, the parasitic absorption should not be significant because for p-type GaAs, the absorption coefficient $\alpha < 30$ cm^{-1} for photon energies of 0.2 eV < hν < E_g (Ref. 4-6). In this energy range, 1 μm of p-type material will absorb $1 - e^{-\alpha W} \sim 0.003$ or only ~0.3% of the incident radiation. Note that this absorption mechanism has a weak temperature dependence.

The final absorption mechanism to be considered is absorption in the metal that makes up the electrical contacts and in any back surface mirror, which is necessary for a low-parasitic-absorption, high-efficiency TPV cell. A back surface mirror was not present on the cells studied under this contract. The infrared absorptivity of freshly vacuum deposited silver or gold is approximately 0.01 for a 1 to 30 μm range in wavelength. The absorptivity should remain rather constant with increasing temperature as long as the reflecting material (silver or gold) does not react with the material to which it is bonded.

The conclusion drawn from the preceding discussion is that the parasitic absorption due to the variety of causes cited above will be relatively temperature independent for TPV cell temperatures between 300 and 600 K. Therefore, in the TPV model, the analyses are performed assuming a temperature-independent value for $\overline{A}_{par}$.

4.5. η_{elec}

The electrical efficiency factor η_{elec} can be calculated using

$$\eta_{elec} = \frac{J_{mp} V_{mp}}{J_{ph} V_g} \quad , \tag{4-8}$$

where J_{mp} and V_{mp} are the current density and voltage at the maximum power point, respectively, J_{ph} is the photogenerated current, and $V_g = E_g/q$ is the band gap voltage. J_{ph} can be determined using

$$J_{ph} = 1.011 \times 10^{-8} T_E^3 \left[e^{-\beta} \left(\beta^2 + 2\beta + 2 \right) \right] \quad , \tag{4-9}$$

where J_{ph} has the units of A/cm^2 and T_E is in degrees K. If zero series resistance and infinite shunt resistance are assumed, the illuminated J vs V characteristic for an ideal p-n junction cell is

$$J = J_{ph} - J_o \left[\exp \left(\frac{qV}{A_o k_B T} \right) - 1 \right] \quad , \tag{4-10}$$

where J_o is the saturation current density and A_o is the diode ideality factor. The dark J vs V characteristic is given by

$$J = J_o \left[\exp \left(\frac{qV}{A_o k_B T} \right) - 1 \right] \quad . \tag{4-11}$$

Generally, the diode ideality factor A_o is between 1 and 2 (Ref. 4-7). When electrical transport is dominated by injection and diffusion of the carriers in the quasi-neutral regions of the p-n junction, then $A_o = 1$. If the recombination and generation transport mechanism in the depeletion layer dominates, then $A_o = 2$. Thus, the value of A_o can indicate the dominant transport mechanism.

In order to determine the temperature dependence of r_{elec}, the dark I vs V characteristics were measured as a function of temperature for currents up to 10 A, the limit of the experimental apparatus. For some of the cells investigated, the dark I vs V curves saturated at higher currents, indicative of finite series resistance effects (Ref. 4-7). Therefore, the dark I vs V curve was least squares fit to Eq. 4-11 for the largest values of I where series resistance effects were not influencing the I vs V curve. Values of J_o (using the measured cell area) and A_o were derived from the least squares fit results for every temperature at which there was a dark I vs V measurement.

The value of η_{elec} at a given temperature was then calculated as follows. At the cell temperature T, the band gap $E_g(T)$ was calculated using Eq. 4-3. The J_{ph} was determined from Eq. 4-9. Using this calculated value of J_{ph} and the values of J_o and A_o derived from the measured dark I vs V curve at the cell temperature T, the maximum power output per cm^2, $P_{mp} = J_{mp}V_{mp}$, was determined from Eq. 4-10 by varying V until $J \cdot V$ was maximized. Knowing J_{mp} and V_{mp}, η_{elec} was calculated using Eq. 4-8.

4.6. η_{TPV}

The computer program for calculating the temperature dependence of η_{TPV} has essentially been described above and will be summarized here. The inputs to the program are the room temperature band gap (whether the temperature dependence of the band gap is to follow GaAs or Si), the cell temperature, the emitter temperature, the values of J_o and A_o at the cell temperature, and the weighted parasitic absorption $\overline{A}_{par}$. The computer calculates the band gap at the input cell temperature and then finds η_{use}, $\overline{A}_{ph}$, and J_{ph}. Then the maximum power point values J_{mp} and V_{mp} are determined and η_{elec} is calculated. Finally, η_{TPV} is found using Eq. 4-1.

Other factors are also calculated. The fill factor FF is given by

$$FF = \frac{J_{mp}V_{mp}}{J_{ph}V_{oc}} \quad , \tag{4-12}$$

where V_{oc} is the open circuit voltage:

$$V_{oc} = \frac{A_o kT}{q} \ln\left(\frac{J_{ph}}{J_o} + 1\right) \quad . \tag{4-13}$$

The power absorbed P_{abs} by the TPV cell per cm^2 is given by

$$P_{abs} = \frac{P_{mp}}{\eta_{TPV}} \quad . \tag{4-14}$$

The power incident P_{inc} on the TPV cell per cm^2 is determined using Planck's blackbody radiation law:

$$P_{inc} = \sigma T_E^4 \quad , \tag{4-15}$$

where $\sigma = 5.67 \times 10^{-12}$ W/(cm^2-K^4). The power per cm^2 rejected as heat P_{heat} is given by

$$P_{heat} = P_{abs} - P_{mp} \quad . \tag{4-16}$$

The power per cm^2 reflected by the TPV cell back to the emitter is calculated using

$$P_{ref} = P_{inc} - P_{abs} \quad . \tag{4-17}$$

The power that must be supplied by the external source of power is equal to the power absorbed P_{abs}.

All the above powers are generated by the computer code. A typical printout is shown in Table 4-1 for InGaAs cell 706455 at two different cell temperatures.

TABLE 4-1
TYPICAL TPV EFFICIENCY PROGRAM COMPUTER PRINTOUT

Type of TPV Cell: InGaAs 706455a
Energy Gap at 300K (eV) = 1.2
Temperature Dependence of Energy Band Gap to Follow GaAs
Cell Temperature (K) = 301
Weighted Parasitic Absorption = .05
Dark Current J0 (Amps/cm^2) = 1.184E-07
Diode Ideality Factor = 2.26
Ratio of (Illuminated Area)/(Total Cell Area) = 1
Concentration (in Times) of Incident Emitter Radiation = 1
Energy Gap in eV at Cell Temperature = 1.199548

TE	PINC	PABS	PREF	PHEAT	NTPV	NOPT	NELEC	NUSE	APH	FF	JMP	JPH	PMAX	VMP	VOC
(K)	(W/cm^2)	(W/cm^2)	(W/cm^2)	(W/cm^2)							(A/cm^2)	(A/cm^2)	(W/cm^2)	(V)	(V)
1500	28.70	1.89	26.81	1.67	.11936	.21514	.55479	.88453	.01607	.76386	0.3138	0.3394	0.2259	0.7199	0.8716
1600	37.16	2.75	34.41	2.29	.16714	.28591	.58460	.87658	.02420	.77075	0.6085	0.6557	0.4600	0.7560	0.9102
1700	47.36	3.99	43.36	3.13	.21658	.35435	.61122	.86862	.03445	.77653	1.0972	1.1788	0.8646	0.7880	0.9446
1800	59.52	5.75	53.77	4.23	.26434	.41618	.63517	.86068	.04681	.78144	1.8614	1.9948	1.5205	0.8169	0.9754
1900	73.89	8.20	65.69	5.67	.30828	.46934	.65685	.85274	.06121	.78567	2.9994	3.2080	2.5286	0.8430	1.0032
2000	90.72	11.54	79.18	7.53	.34740	.51346	.67658	.84483	.07748	.78937	4.6264	4.9393	4.0101	0.8668	1.0285
2100	110.27	16.01	94.26	9.90	.38147	.54918	.69462	.83694	.09542	.79262	6.8726	7.3254	6.1061	0.8885	1.0516
2200	132.82	21.85	110.97	12.88	.41077	.57757	.71121	.82908	.11482	.79551	9.8803	10.5176	8.9763	0.9085	1.0728
2300	158.67	29.37	129.30	16.57	.43577	.59980	.72652	.82124	.13543	.79809	13.8063	14.6792	12.7977	0.9269	1.0924
2400	188.12	38.87	149.25	21.11	.45699	.61697	.74070	.81345	.15701	.80042	18.8168	19.9846	17.7631	0.9440	1.1105
2500	221.48	50.70	170.79	26.62	.47496	.63002	.75389	.80569	.17932	.80253	25.0848	26.6165	24.0790	0.9599	1.1273

Type of TPV Cell: InGaAs 706456f
Energy Gap at 300K (eV) = 1.2
Temperature Dependence of Energy Band Gap to Follow GaAs
Cell Temperature (K) = 466
Weighted Parasitic Absorption = .05
Dark Current J0 (Amps/cm^2) = .0002096
Diode Ideality Factor = 1.87
Ratio of (Illuminated Area)/(Total Cell Area) = 1
Concentration (in Times) of Incident Emitter Radiation = 1
Energy Gap in eV at Cell Temperature = 1.121335

TE	PINC	PABS	PREF	PHEAT	NTPV	NOPT	NELEC	NUSE	APH	FF	JMP	JPH	PMAX	VMP	VOC
(K)	(W/cm^2)	(W/cm^2)	(W/cm^2)	(W/cm^2)							(A/cm^2)	(A/cm^2)	(W/cm^2)	(V)	(V)
1500	28.70	2.29	26.42	2.08	.09200	.28917	.31814	.87621	.02463	.64560	0.4719	0.5512	0.2104	0.4459	0.5913
1600	37.16	3.40	33.76	2.97	.12724	.36191	.35159	.86770	.03578	.66128	0.8896	1.0265	0.4331	0.4868	0.6380
1700	47.36	5.02	42.33	4.20	.16290	.42674	.38174	.85920	.04934	.67404	1.5625	1.7863	0.8183	0.5237	0.6796
1800	59.52	7.32	52.20	5.88	.19694	.48146	.40904	.85072	.06519	.68464	2.5884	2.9374	1.4418	0.5570	0.7170
1900	73.89	10.50	63.39	8.11	.22821	.52596	.43389	.84226	.08314	.69358	4.0820	4.6043	2.3973	0.5873	0.7507
2000	90.72	14.81	75.91	11.02	.25626	.56121	.45662	.83383	.10293	.70124	6.1746	6.9280	3.7962	0.6148	0.7814
2100	110.27	20.52	89.75	14.75	.28105	.58860	.47748	.82543	.12427	.70788	9.0087	10.0645	5.7667	0.6401	0.8094
2200	132.82	27.92	104.90	19.47	.30277	.60954	.49672	.81707	.14686	.71370	12.7406	14.1819	8.4533	0.6635	0.8352
2300	158.67	37.34	121.33	25.33	.32173	.62529	.51453	.80876	.17041	.71885	17.5375	19.4589	12.0147	0.6851	0.8589
2400	188.12	49.14	138.97	32.52	.33824	.63689	.53108	.80049	.19466	.72343	23.5716	26.0828	16.6223	0.7052	0.8809
2500	221.48	63.70	157.79	41.24	.35259	.64519	.54649	.79227	.21933	.72755	31.0265	34.2470	22.4589	0.7239	0.9014

5. EXPERIMENTAL APPARATUS FOR HIGH-TEMPERATURE MEASUREMENTS

5.1. INTRODUCTION

In order to infer the expected TPV performance of various cells at
high temperatures, it was necessary to measure their high-temperature
dark and illuminated current (I) versus voltage (V) characteristics.
From the dark I vs V characteristics, values for the temperature depen-
dence of the saturation current density J_o and diode ideality factor A_o
can be determined. From the illuminated I vs V characteristics, the
variation of the short circuit current with cell temperature can be cor-
related with the variation of the band gap with temperature. At higher
temperatures, the band gap decreases, which increases the short circuit
current.

5.2. EXPERIMENTAL REQUIREMENTS

The high-temperature apparatus had to satisfy a number of
requirements:

1. Cell headers should be compatible with the TPV rig.

2. Cell temperature should be easily variable from 300 to 550 K.

3. Cell headers should be easily interchangeable.

4. Cell headers should allow cells of various sizes to be tested.

5. The apparatus should allow both dark and illuminated I vs V
   characteristics to be obtained.

6. Cell temperature should be stable (less than ±1 K variation) over the course of a measurement.

7. Because of the large quantity of data accumulated, data acquisition should be computer controlled.

All these requirements were taken into account in the design and operation of the high-temperature apparatus.

5.3. EXPERIMENTAL APPARATUS

The high-temperature rig is shown schematically in Fig. 5-1. The cell is soldered to the top of the cell header, which is then placed in the depression in the main body. The size of the protruding "nub" of the cell header and the mating depression in the main body are identical to those used in the TPV rig. The top plate of the outer body is screwed down until contact is made with the top of the cell. For dark I vs V characteristics, the cover plate is placed over the opening in the top plate. For illuminated I vs V characteristics, the cover plate is removed. Top plates are made with different sizes of openings and cell headers are fabricated with different diameters to account for the different cell sizes encountered.

Except for the insulating MACOR base, all the components of the apparatus are machined from high-conductivity OFHC copper to minimize series resistance effects due to the sample holder. This also allows the thermocouple, which is sunk into the thermocouple well, to accurately measure the cell temperature. The entire assembly is situated on a thermostatically controlled hot plate to allow temperatures up to 550 K to be attained. Temperature fluctuations in the hot plate causing temperature fluctuations in the cell temperature are minimized because of the poor thermal diffusivity of the insulating MACOR base.
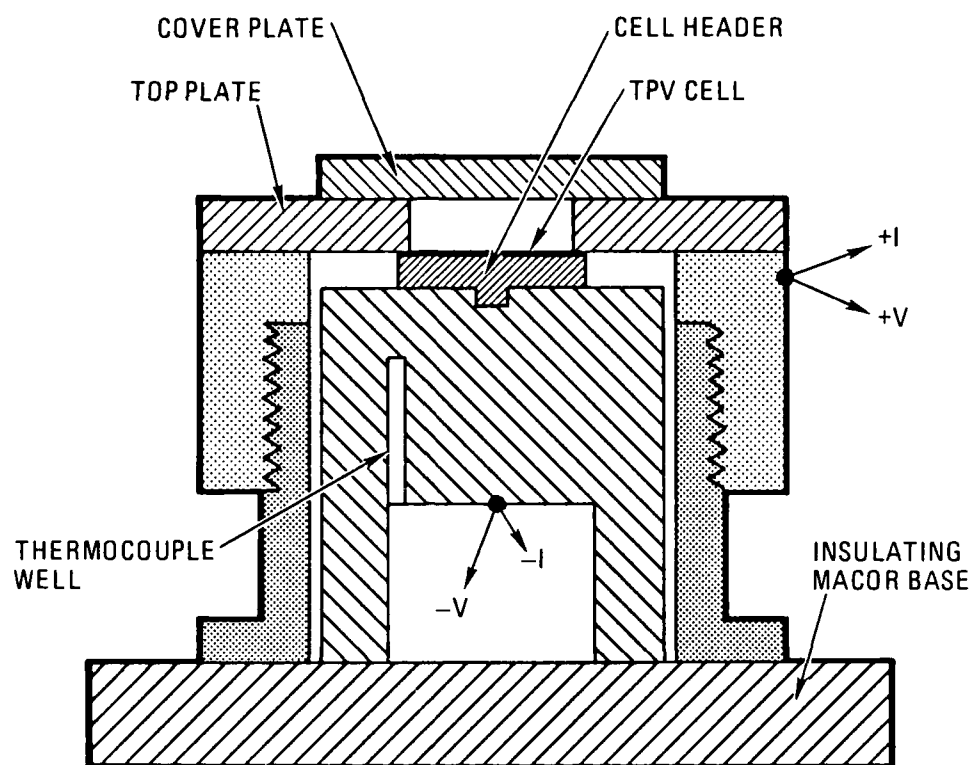
Fig. 5-1.   Test apparatus used for high-temperature TPV measurements

A schematic of the entire assembly used to obtain the high-temperature data is shown in Fig. 5-2. For the dark I vs V measurements, a constant current is driven through the cell either by the Keithley 220 for $I < 0.1$ A or by the Keithley 228 for 0.1 A $< I < 10$ A. The voltage is measured using the Keithley 195, and all the I and V data are collected by the IBM PC computer. For the illuminated I vs V measurements, 4.60 A were sent through an Optronic Laboratories Model 100C, 1000-W tungsten halogen (high-intensity standard) lamp which produced a color temperature of 2100 K. The current was sunk and measured by the Keithley 228 in the active load mode, while the voltage was measured by the Keithley 195. Again, the I vs V data were collected by computer. The computer code used to obtain these data was written and optimized during the course of the numerous measurements.
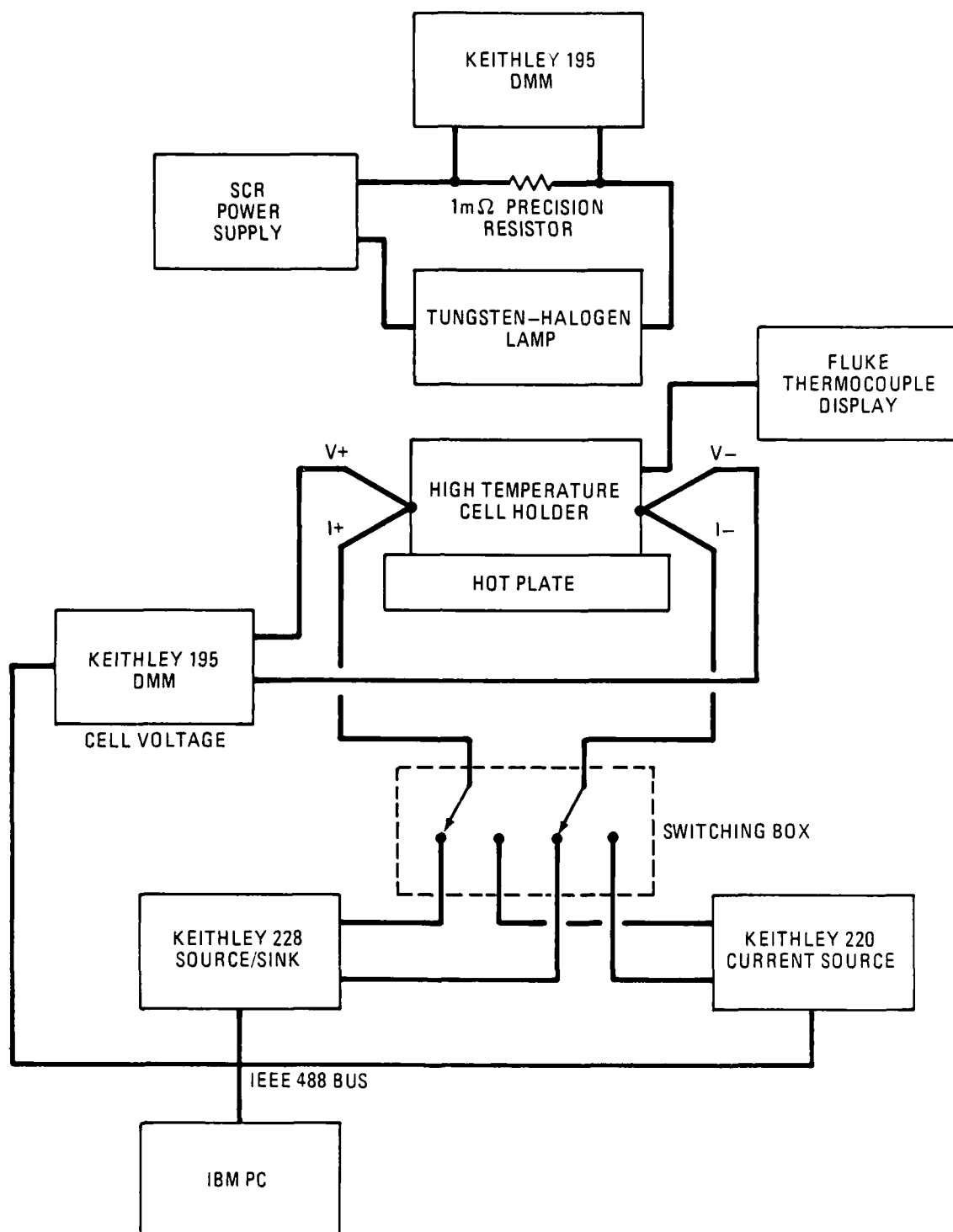
Fig. 5-2. Block diagram of equipment used to obtain high-temperature TPV data

6. EXPERIMENTAL DATA OBTAINED USING HIGH-TEMPERATURE APPARATUS

6.1. INTRODUCTION

The dark and illuminated I vs V characteristics of a number of different types of cells were investigated as a function of temperature. Typically, the temperature range over which data were obtained was from 300 to ~550 K, the upper limit of the hot plate on which the cell apparatus was mounted. In some cases, the upper temperature limit was low owing to cell failure. While some of the cells may have failed because of inherent problems, it is believed that most of the failures arose from differences in differential thermal expansion. If the top section of the apparatus was screwed on so that it made very tight contact with the top part of the cell, then there would have been little room for expansion as the cell warmed. In particular, this may have caused problems near the melting temperature (~200°C) of the solder used to attach the cell to the header. Generally, if the cell survived to the maximum temperature, additional I vs V characteristics were taken after cooling the cell to room temperature to check for reproducibility.

The current and voltage ranges explored for the dark I vs V experiments were as broad as possible in order to observe the temperature dependence of the transport mechanisms (for example, through the behavior of A_o with temperature) as well as series and shunt resistance effects. The minimum current in these experiments was that necessary to achieve approximately 0.001-V drop across the cell. The maximum current was typically the upper limit of the Keithley 228 voltage/current source, namely 10 A.

6.2. EXPERIMENTAL DATA

This section presents the high-temperature dark and illuminated I vs V characteristics obtained on the InGaAs, GaAs, and Si cells. For the dark measurements, the data are plotted as $\log_{10}$ (I) vs V, while for the illuminated measurements, the data are plotted as I vs V. Associated with each of the dark I vs V plots are the values for saturation current density J_o and diode ideality factor A_o at each temperature, derived by fitting the data to the equation

$$\frac{I}{\text{Cell Area}} = J = J_o \left[\exp\left(\frac{qV}{A_o kT}\right) - 1\right] \quad . \tag{6-1}$$

The current region over which the least squares fit was performed is also noted. For each of the illuminated I vs V data sets, there are tabulations of the short circuit current I_{sc}, open circuit voltage V_{oc}, current at maximum power point I_{mp}, voltage at maximum power point V_{mp}, maximum power P_{mp}, and fill factor FF. The incident power density from the 2100 K color temperature lamp was not determined. The primary goal of the illuminated I vs V experiments was to examine the relative temperature dependence of the above factors and, in particular, the short circuit current, which is a function of the temperature dependence of the band gap.

A list of all the cells studied in detail is given in Table 6-1. Each set of data is discussed below.

6.2.1. InGaAs Cell 706455

This cell exhibited a fairly low shunt resistance of ~30 Ω, causing the flat part of the dark I vs V curve between 0.2 and 0.6 V, and appreciable series resistance for I > 1 A, which resulted in the bending of the curve (Fig. 6-1, Table 6-2*). Both the series and shunt resistances

---

*Figures and tables are located at the end of this section.

changed in a complicated fashion with temperature. The before (706455a) and after (706457a) thermal cycling dark I vs V curves at room temperature (Fig. 6-2) suggest a desired increase in shunt resistance and decrease in series resistance, for unknown reasons. The effect of the shunt resistance and its complicated temperature dependence is evident in the illuminated I vs V curves (Fig. 6-3). From these data, I_{sc} is seen to increase by 37% between 301 and 466 K (Table 6-3). The theory previously discussed predicts an increase of 36% in I_{sc}, which is in close agreement.

6.2.2. InGaAs Cell 706463

This cell exhibited fairly high shunt and reasonably low series resistance, although the 130°C data showed an erratic behavior for I > 1 A (Fig. 6-4, Table 6-4). The illuminated I vs V data (Fig. 6-5) behaved in a reasonable and monotonic manner. Both the data and theory yield an increase in I_{sc} between 299 and 405 K of 22% (Table 6-5).

6.2.3. InGaAs Cell 706472

This cell showed negligible series resistance effects (Fig. 6-6, Table 6-6), but some complicated temperature dependence in the low-current dark I vs V characteristics is evident. The before (706472b) and after (706472t) thermal cycling room temperature dark I vs V curves (Fig. 6-7) are in good agreement for low and high currents but exhibit significant disagreement for intermediate currents. This leads to the large disparity in V_{oc} between the before (706472c) and after (706472u) illuminated I vs V data (Fig. 6-8), although the I_{sc} values are essentially identical. The data give an I_{sc} which increases by 26% between 307 and 452 K (Fig. 6-9, Table 6-7), whereas theory predicts a somewhat larger increase of 32%.

6.2.4. GaAs Cell 706481

The dark I vs V data indicate low shunt resistance and negligible series resistance effects, except possibly at high currents above 190°C (Fig 6-10, Table 6-8). This sample underwent thermal cycling from room temperature (706481a, 706481b) to high temperature (706481s, 706481t) to room temperature (706481u, 706481v) and back to high temperature (706481w, 706481x) (Figs. 6-11, 6-12). Except for the high current part of set 706481u, the data are extremely reproducible, in contrast to most of the InGaAs data collected. The illuminated I vs V curves behave in a reasonable, monotonic fashion (Fig. 6-13). The data show that I_{sc} increases by 57% between 299 and 513 K (Table 6-9), while theory predicts 54%, which is in excellent agreement.

6.2.5. GaAs Cell 706482

The dark I vs V data were extremely well behaved (Fig. 6-14, Table 6-10), with no series resistance effects evident and no appreciable shunt resistance. Both the dark and the illuminated I vs V curves before (706482a, 706482b) and after (706482u, 706482v) thermal cycling essentially lay on top of one another (Figs. 6-15, 6-16). The illuminated I vs V curves showed the expected temperature dependence (Fig. 6-17). Between 301 and 501 K, I_{sc} increased by 51%, close to the theoretically predicted increase of 54% (Table 6-11).

6.2.6. Si Cell 706480

This cell exhibited considerable series resistance effects in the dark I vs V characteristics for $I > 0.5$ A (Fig. 6-18, Table 6-12), leading to the decrease in slope at high currents. The monotonic dark I vs V data resulted in reasonable illuminated I vs V data (Fig. 6-19). Between 302 and 425 K, I_{sc} increased by 24% (Table 6-13), somewhat above the theoretically predicted increase of 15%.

6.2.7. Si Cell 706452

The dark I vs V data (Fig. 6-20, Table 6-14) indicate rather appre-
ciable series resistance effects for $I > 1$ A and essentially negligible
shunt resistance effects. The data behave in an expected monotonic
fashion. The dark I vs V data obtained before (706425b) and after
(706453k) heating are almost identical (Fig. 6-21). No illuminated
data were collected for this cell.

6.2.8. Si Cell 706458

The temperature dependence of these dark I vs V curves was reason-
able and monotonic (Fig. 6-22, Table 6-15), although appreciable series
resistance was evident for $I > 1$ A. The dark and illuminated data col-
lected before (706458a, 706458b) and after (706458s, 706458t) heating
(Figs. 6-23, 6-24) were extremely reproducible. No anomalous behavior
is evident in the illuminated I vs V curves (Fig. 6-25). Between 308
and 474 K, I_{sc} increased by 34% (Table 6-16), whereas the theoretical
expectation was 22%.

6.3. EXPERIMENTAL DATA ANALYSIS

Based on the previously discussed I vs V characteristics taken as a
function of temperature, a number of general conclusions can be formed.
The InGaAs cells appeared to be the least reproducible cells in terms of
their dark and illuminated I vs V characteristics before and after heat-
ing. In one case, the changes were appreciable over the entire current
range, while in another case, changes were evident over a fairly limited
range. In contrast, the Si and GaAs cells showed essentially no changes
with thermal cycling. The reason for the irreproducibility of the
InGaAs results upon thermal cycling is unclear but may arise from the
more complicated construction of the InGaAs cells compared with either
the GaAs or Si cells. In addition, the fabrication of InGaAs cells is
still in its infancy compared with the more mature technologies of GaAs
and Si cell syntheses. It is surmised that the cause of the complicated

temperature dependence of the I vs V curves for the InGaAs cells is the same as that associated with the irreproducible thermal cycling results. Again, the temperature dependence of the I vs V curves of the Si and GaAs cells was reasonable and monotonic.

Another unknown indirectly explored in this study is the temperature dependence of the band gap of the InGaAs cells, which leads to the temperature dependence of the photogenerated (short circuit) current. The assumptions concerning their temperature dependence were presented in Section 4.2. These assumptions were more or less substantiated by the measured temperature dependence of the short circuit current, which was in very good agreement with that predicted by the theoretical model. The values of the temperature dependence of I_{sc} for the GaAs cells were also close to those predicted by theory, while the values for the Si cells were somewhat in disagreement.

TABLE 6-1

CELLS WHOSE PROPERTIES WERE MEASURED AS A FUNCTION OF TEMPERATURE

Cell Type	Manufacturer	Manufacturer's Code	GA Code	300 K Band Gap (ev)	Temperature Range (K)	Cell Area (cm^2)
InGaAs n/p	Varian	30M 1802 #4	706455	1.20	300-469	0.49
InGaAs n/p	Varian	30M 1802 #3	706463	1.20	298-405	0.49
InGaAs p/n	Varian	30M 1823 #4	706472	1.15	301-471	0.49
GaAs p/n	Applied Solar		706481	1.42	298-517	0.90
GaAs p/n	Applied Solar		706482	1.42	299-501	0.90
Si p-i-n	Swanson-Stanford		706480	1.12	301-446	0.28
Si n/p	Applied Solar		706452	1.12	299-490	1.49
Si n/p	Applied Solar		706458	1.12	299-474	1.49

Fig. 6-1.   Dark I vs V for InGaAs cell 706455 at various temperatures

TABLE 6-2
TEMPERATURE DEPENDENCE OF J_o AND A_o DERIVED FROM THE
DARK I VS V DATA OF InGaAs CELL 706455

T [K (°C)]	J_o (A/cm^2)	A_o	Fitting Regime
301 (28)	1.184×10^{-7}	2.26	$0.1\ A < I < 1\ A$
323 (50)	3.608×10^{-7}	2.17	
348 (75)	1.518×10^{-6}	2.12	
366 (93)	1.737×10^{-6}	1.95	
386 (113)	8.804×10^{-6}	2.02	
405 (132)	2.824×10^{-5}	2.04	
425 (152)	3.794×10^{-5}	1.89	
445 (172)	4.878×10^{-5}	1.76	
466 (193)	2.096×10^{-4}	1.87	
300 (27)	2.406×10^{-10}	1.60	
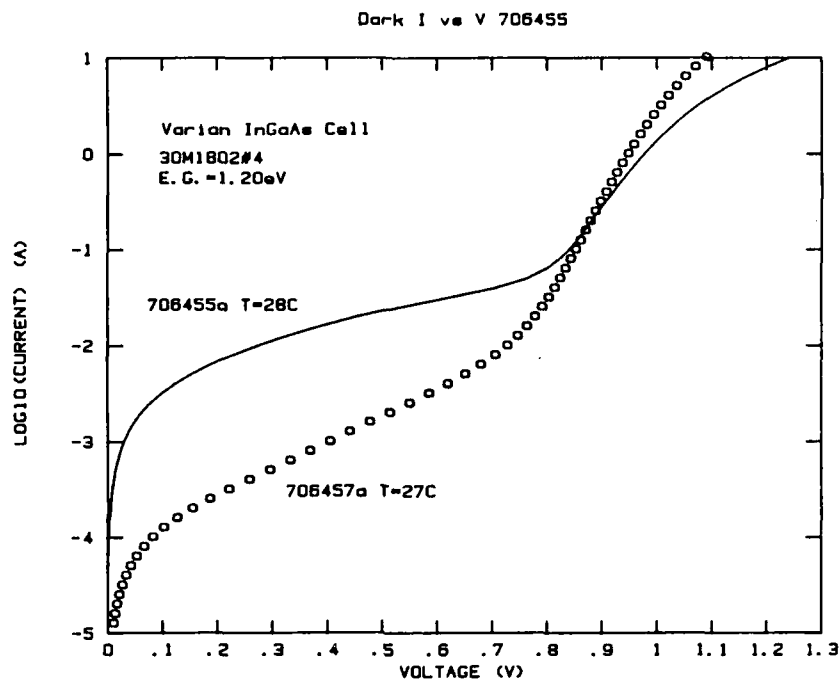
Fig. 6-2. Dark I vs V for InGaAs cell 706455 taken before (706455a) and after (706457a) heating
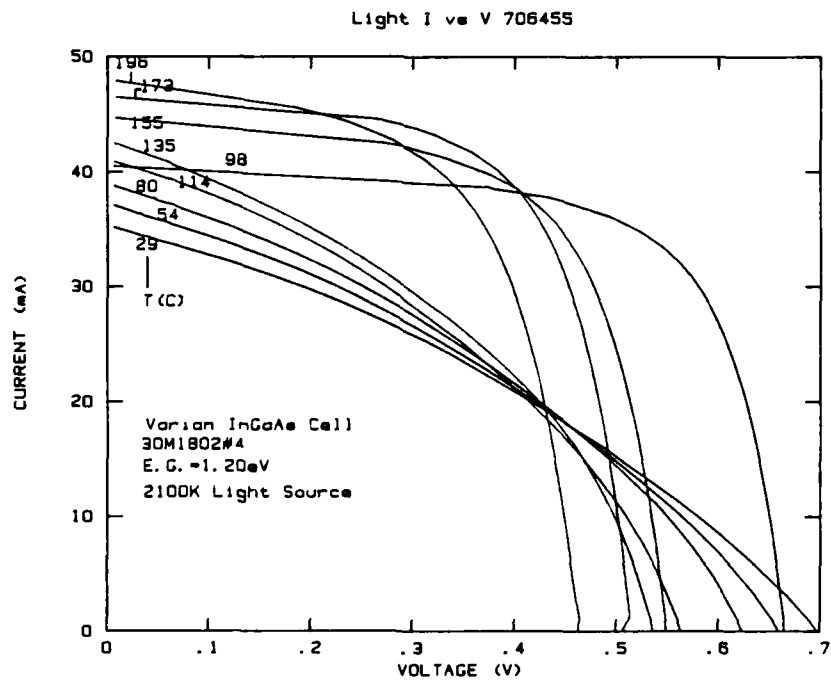
Fig. 6-3. Illuminated I vs V for InGaAs cell 706455 at various temperatures

TABLE 6-3

TEMPERATURE DEPENDENCE OF PARAMETERS DERIVED FROM THE ILLUMINATED
I VS V DATA OF InGaAs CELL 706455

T [K (°C)]	I_{sc} (mA)	V_{oc} (V)	I_{mp} (mA)	V_{mp} (V)	P_{mp} (mW)	FF
302 (29)	35.2	0.696	20.6	0.4055	8.35	0.341
328 (54)	37.1	0.659	21.7	0.3915	8.50	0.348
353 (80)	38.8	0.623	23.8	0.3651	8.69	0.360
371 (98)	40.5	0.665	33.5	0.5442	18.2	0.817
387 (114)	40.9	0.563	25.0	0.3508	8.77	0.381
408 (135)	42.5	0.536	25.7	0.3565	9.16	0.402
428 (155)	44.7	0.549	36.9	0.4242	15.6	0.636
446 (173)	46.5	0.507	38.7	0.3995	15.5	0.656
469 (196)	47.9	0.464	38.1	0.3476	13.2	0.594

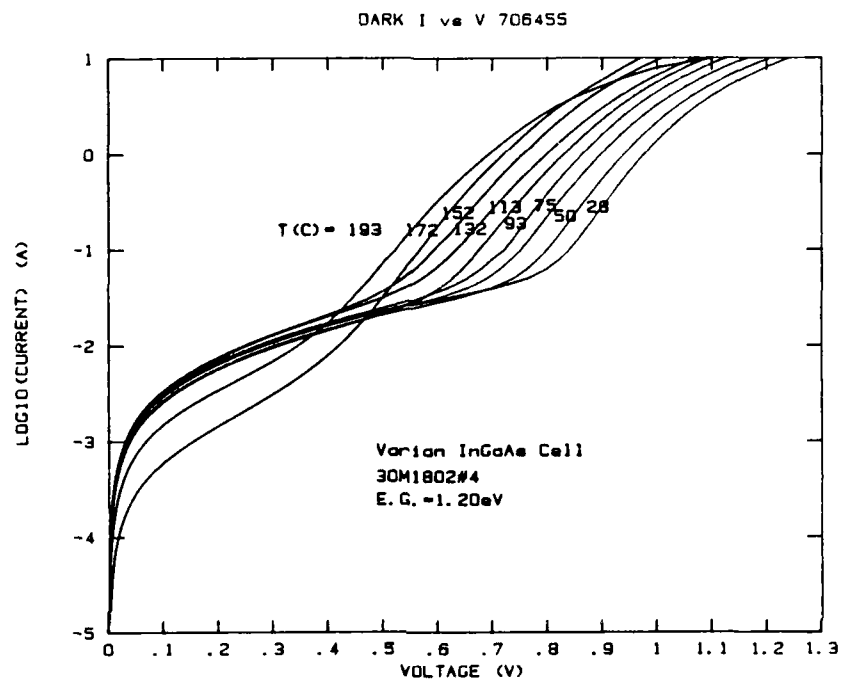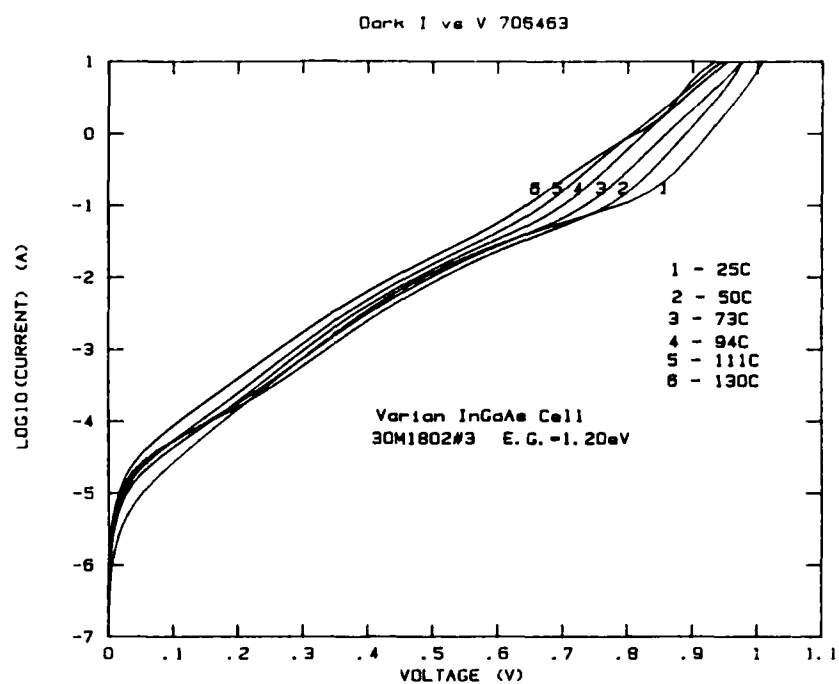Fig. 6-4. Dark I vs V for InGaAs cell 706463 at various temperatures

Fig. 6-5. Illuminated I vs V for InGaAs cell 706463 at various
temperatures

TABLE 6-4

TEMPERATURE DEPENDENCE OF J_o AND A_o DERIVED FROM THE
DARK I VS V DATA OF InGaAs CELL 706463

T [K (°C)]	J_o (A/cm^2)	A_o	Fitting Regime
298 (25)	6.786×10^{-11}	1.49	0.3 A < I < 10 A
323 (50)	7.024×10^{-10}	1.47	
346 (73)	9.094×10^{-8}	1.71	
367 (94)	4.841×10^{-7}	1.71	
384 (111)	2.835×10^{-6}	1.81	
403 (130)	3.978×10^{-6}	1.76	

TABLE 6-5

TEMPERATURE DEPENDENCE OF PARAMETERS DERIVED FROM THE ILLUMINATED
I VS V DATA OF InGaAs CELL 706463

T [K (°C)]	I_{sc} (mA)	V_{oc} (V)	I_{mp} (mA)	V_{mp} (V)	P_{mp} (mW)	FF
299 (27)	32.1	0.654	27.2	0.4662	12.68	0.604
324 (51)	33.7	0.640	29.3	0.4422	12.96	0.601
347 (74)	35.5	0.623	29.5	0.4478	13.21	0.597
368 (95)	37.1	0.602	30.9	0.4307	13.30	0.595
385 (112)	38.4	0.583	31.3	0.4192	13.12	0.586
405 (132)	39.2	0.554	32.0	0.3890	12.45	0.573

DARK I vs V 706472

9 8 7 6 5 4 3 2 1

1 - 33C
2 - 46C
3 - 67C
4 - 87C
5 - 112C
6 - 135C
7 - 155C
8 - 179C
9 - 198C

Varian InGaAs Cell
30M1823#4
E.G. - 1.15 eV

Fig. 6-6.   Dark I vs V for InGaAs cell 706472 at various temperatures

DArk I vs V 706472

Varian InGaAs Cell
30M1823#4
E.G. -1.15eV

o 706472t T=28C
— 706472b T=33C
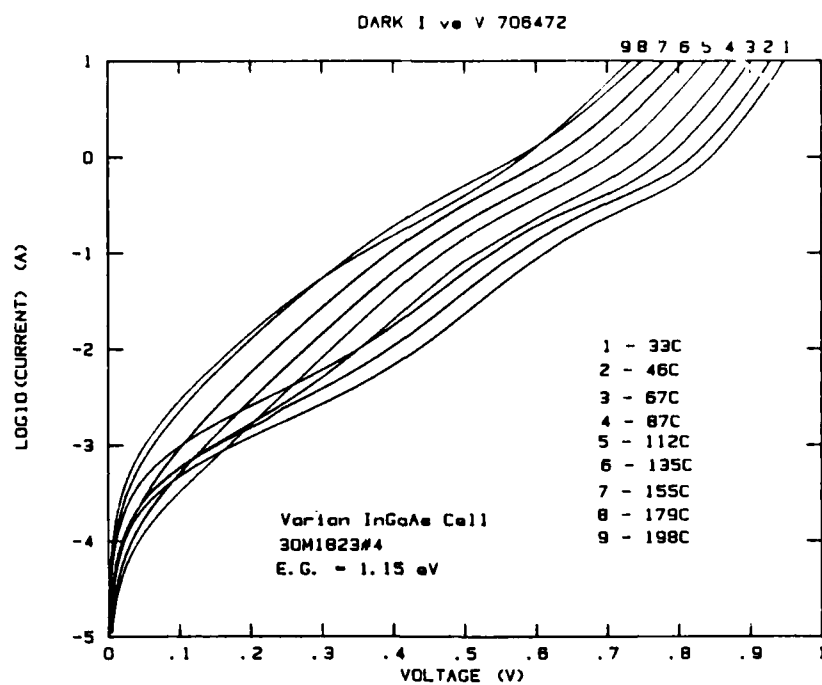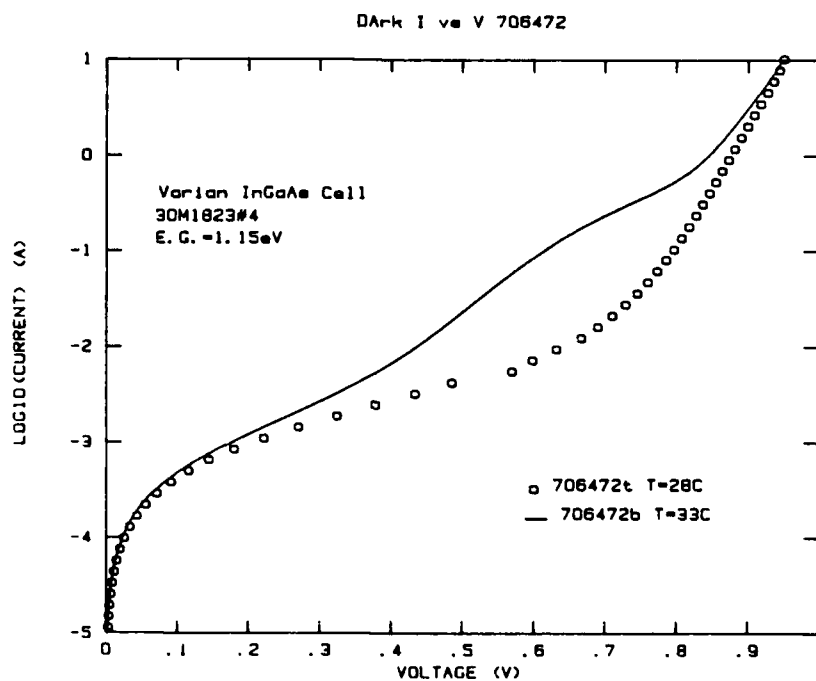
Fig. 6-7.   Dark I vs V for InGaAs cell 706472 taken before
(706472b) and after (706472t) heating

6-15

TABLE 6-6

TEMPERATURE DEPENDENCE OF J_0 AND A_0 DERIVED FROM THE
DARK I VS V DATA OF InGaAs CELL 706472

T [K (°C)]	J_0 (A/cm^2)	A_0	Fitting Regime
306 (33)	8.961×10^{-9}	1.67	1 A < I < 10 A
319 (46)	4.508×10^{-8}	1.70	
340 (67)	2.284×10^{-7}	1.69	
360 (87)	1.194×10^{-6}	1.70	
385 (112)	7.641×10^{-6}	1.71	
408 (135)	3.578×10^{-5}	1.74	
428 (155)	1.669×10^{-4}	1.81	
452 (179)	7.390×10^{-4}	1.89	
471 (198)	2.231×10^{-4}	1.58	
301 (28)	3.406×10^{-12}	1.25	

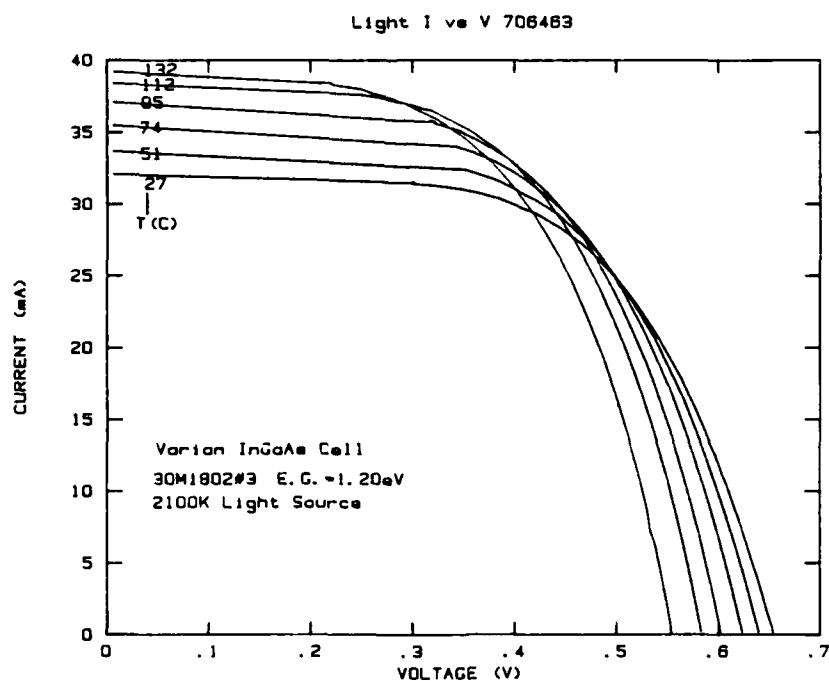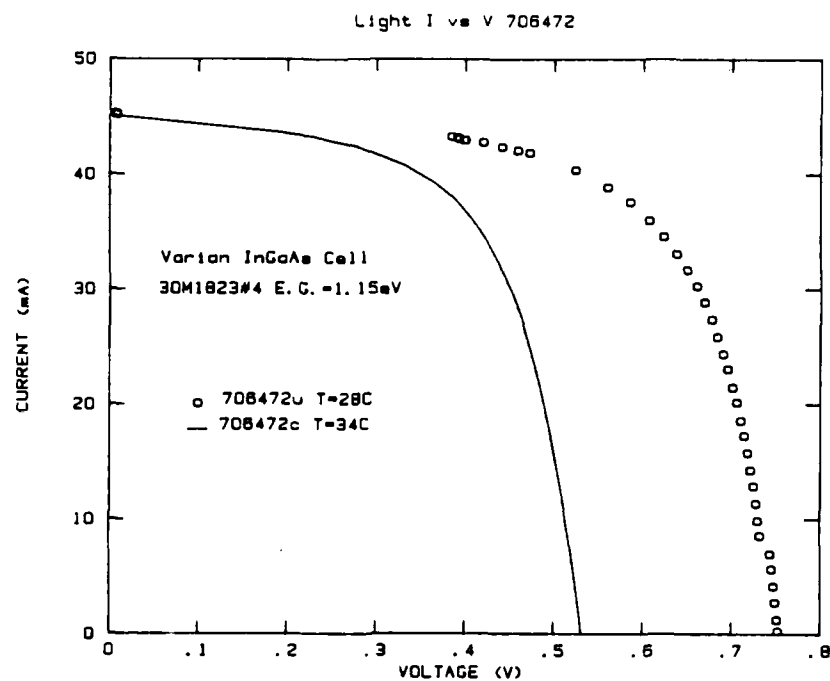Fig. 6-8. Illuminated I vs V for InGaAs cell 706472 taken before (706472c) and after (706472u) heating

Fig. 6-9. Illuminated I vs V for InGaAs cell 706472 at various temperatures

6-17

TABLE 6-7
TEMPERATURE DEPENDENCE OF PARAMETERS DERIVED FROM THE ILLUMINATED
I VS V DATA OF InGaAs CELL 706472

T [K (°C)]	I_{sc} (mA)	V_{oc} (V)	I_{mp} (mA)	V_{mp} (V)	P_{mp} (mW)	FF
307 (34)	45.1	0.5312	36.4	0.4041	14.7	0.614
321 (48)	45.8	0.4956	35.6	0.3765	13.4	0.590
341 (68)	48.1	0.4806	40.4	0.3602	14.6	0.632
361 (88)	49.6	0.4489	43.1	0.3272	14.1	0.633
385 (112)	51.4	0.4082	43.0	0.3042	13.1	0.623
408 (135)	53.4	0.3742	43.3	0.2756	11.9	0.596
429 (155)	55.3	0.3388	44.7	0.2380	10.6	0.568
452 (179)	57.1	0.2963	44.7	0.1973	8.82	0.521
471 (198)	57.9	0.2306	36.1	0.1430	5.16	0.387
301 (28)	45.2	0.7525	37.5	0.5858	22.0	0.647

Fig. 6-10. Dark I vs V for GaAs cell 706481 at various temperatures

TABLE 6-8

TEMPERATURE DEPENDENCE OF J_o AND A_o DERIVED FROM THE
DARK I VS V DATA OF GaAs CELL 706481

T [K (°C)]	J_o (A/cm^2)	A_o	Fitting Regime
298 (25)	5.508×10^{-20}	0.97	0.1 A < I < 10 A
322 (49)	1.743×10^{-17}	1.00	
348 (75)	2.163×10^{-15}	0.99	
378 (103)	1.145×10^{-13}	1.01	
396 (123)	1.311×10^{-12}	1.01	
420 (147)	2.054×10^{-11}	1.01	
441 (168)	1.740×10^{-10}	1.02	
462 (189)	2.477×10^{-9}	1.06	0.1 A < I < 3 A
482 (209)	9.037×10^{-9}	1.02	
510 (237)	4.645×10^{-8}	1.01	
298 (25)	2.725×10^{-18}	1.05	
517 (244)	4.921×10^{-7}	1.15	
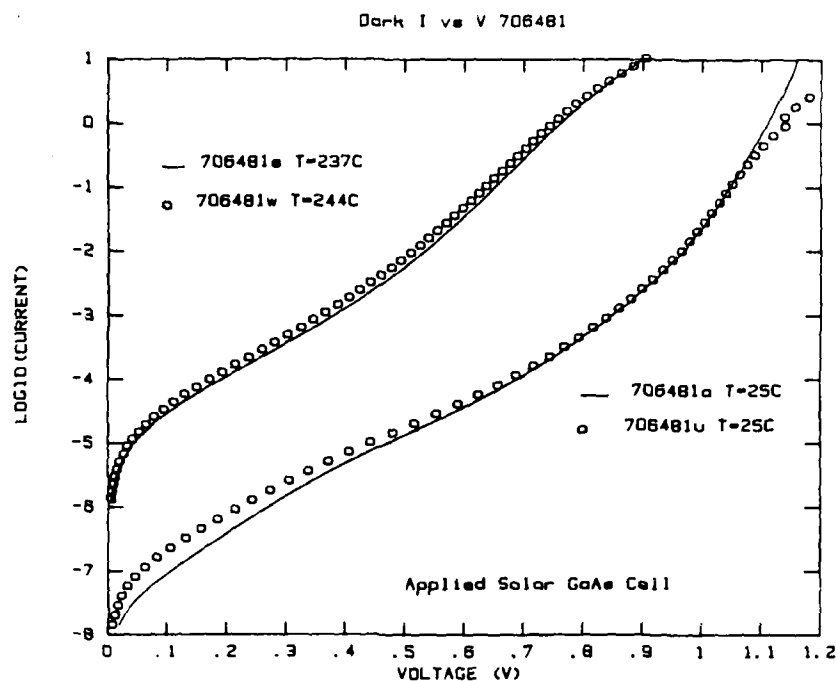
Dark I vs V 706481

Fig. 6-11. Dark I vs V for GaAs cell 706481 taken at low (706481a), then high (706481s), then low (706481u), then high (706481w) temperature

Light I vs V 706481
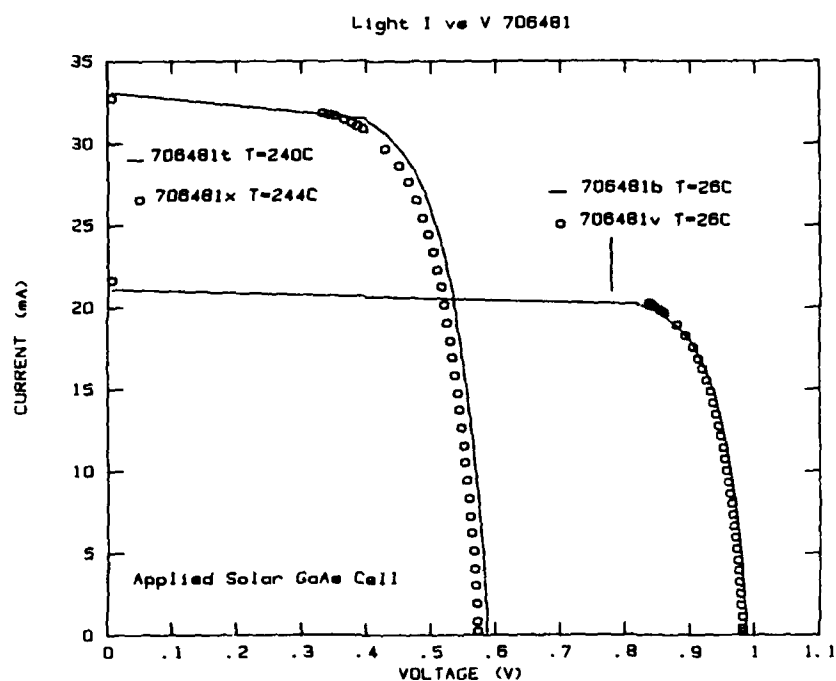
Fig. 6-12. Illuminated I vs V for GaAs cell 706481 taken at low (706481b), then high (706481t), then low (706481v), then high (706481x) temperature

6-21

Light I vs V 706481

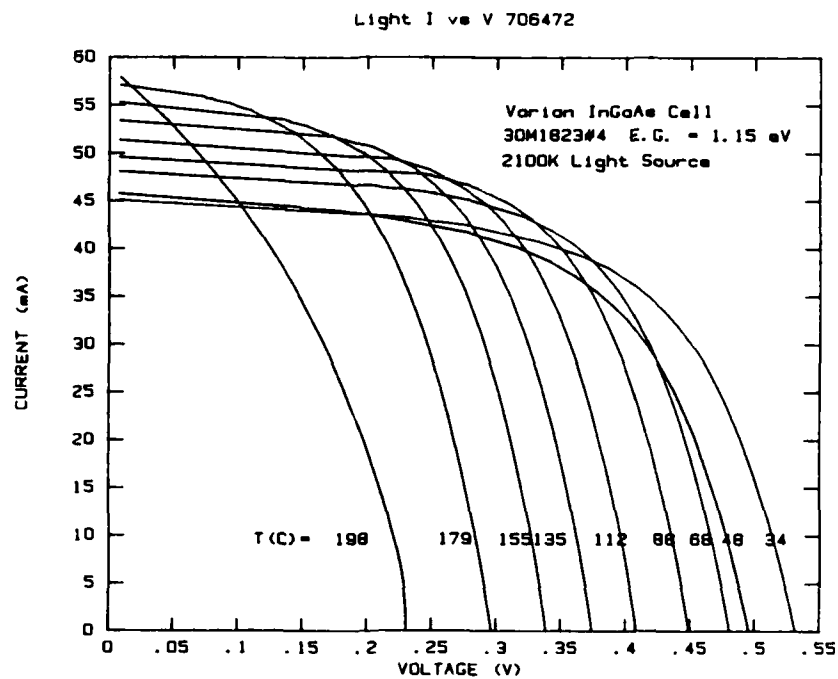Fig. 6-13. Illuminated I vs V for GaAs cell 706481 at various temperatures

Dark I vs V 706482

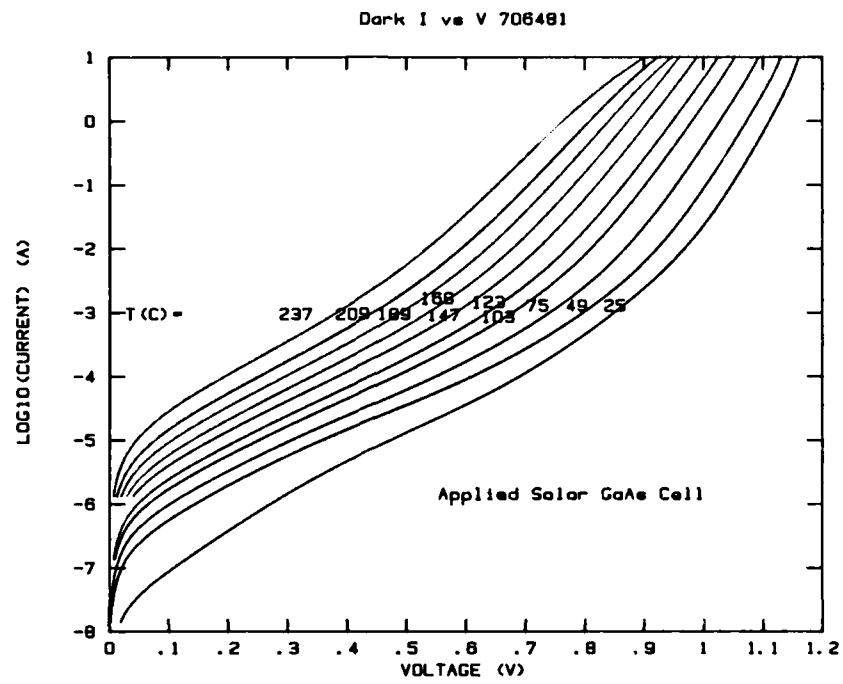Fig. 6-14. Dark I vs V for GaAs cell 706482 at various temperatures

TABLE 6-9

TEMPERATURE DEPENDENCE OF PARAMETERS DERIVED FROM THE ILLUMINATED
I VS V DATA OF GaAs CELL 706481

T [K (°C)]	I_{sc} (mA)	V_{oc} (V)	I_{mp} (mA)	V_{mp} (V)	P_{mp} (mW)	FF
299 (26)	21.1	0.9888	19.6	0.8528	16.7	0.800
324 (51)	22.5	0.9428	20.9	0.8068	16.9	0.797
348 (75)	23.8	0.8963	21.9	0.7681	16.8	0.788
375 (102)	25.4	0.8458	23.3	0.7162	16.7	0.777
398 (125)	26.5	0.8062	24.3	0.6736	16.4	0.768
422 (149)	27.8	0.7603	24.7	0.6433	15.9	0.752
441 (168)	28.9	0.7219	25.7	0.6025	15.5	0.743
464 (191)	30.3	0.6798	27.4	0.5454	14.9	0.723
481 (208)	31.0	0.6528	27.5	0.5292	14.6	0.721
513 (240)	33.1	0.5878	28.4	0.4727	13.4	0.689
299 (26)	21.6	0.9828	20.2	0.8360	16.9	0.796
517 (244)	33.1	0.5735	28.6	0.4501	12.9	0.680

TABLE 6-10

TEMPERATURE DEPENDENCE OF J_o AND A_o DERIVED FROM THE
DARK I VS V DATA OF GaAs CELL 706482

T [K (°C)]	J_o (A/cm^2)	A_o	Fitting Regime
299 (26)	6.056×10^{-23}	0.83	0.3 A < I < 10 A
331 (58)	2.897×10^{-19}	0.85	
353 (80)	2.806×10^{-17}	0.86	
376 (103)	2.078×10^{-15}	0.88	
398 (125)	8.436×10^{-14}	0.90	
419 (146)	1.909×10^{-12}	0.91	
440 (167)	3.020×10^{-11}	0.93	
458 (185)	4.124×10^{-10}	0.96	
480 (207)	3.369×10^{-9}	0.97	
501 (228)	1.972×10^{-8}	0.97	
299 (26)	1.512×10^{-21}	0.89	
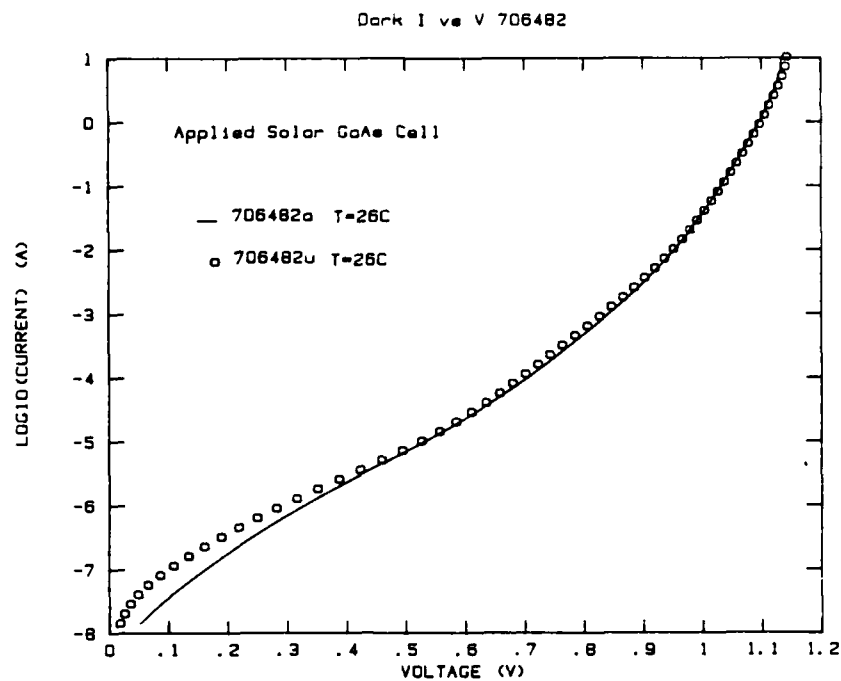
Fig. 6-15. Dark I vs V for GaAs cell 706482 taken before (706482a) and after (706482u) heating
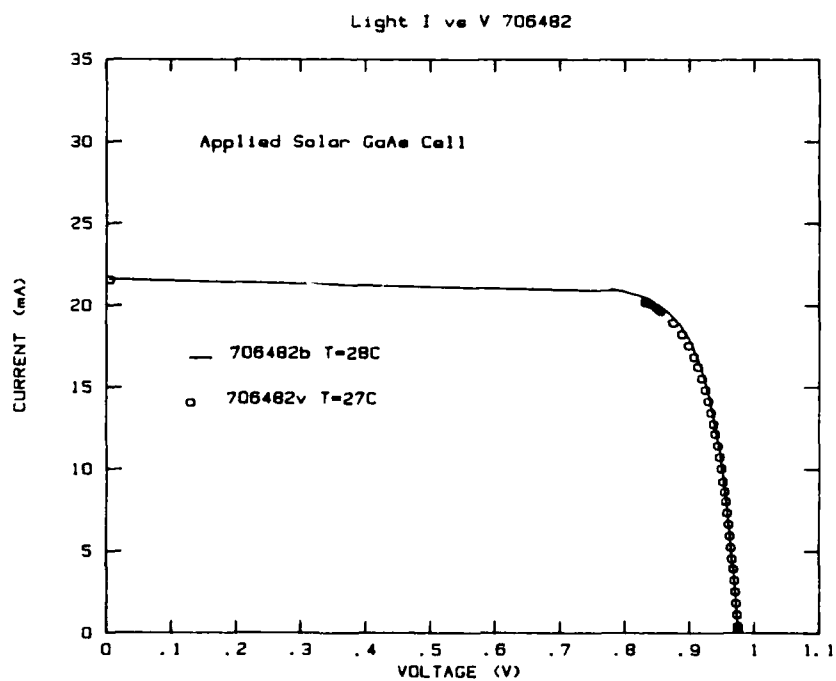
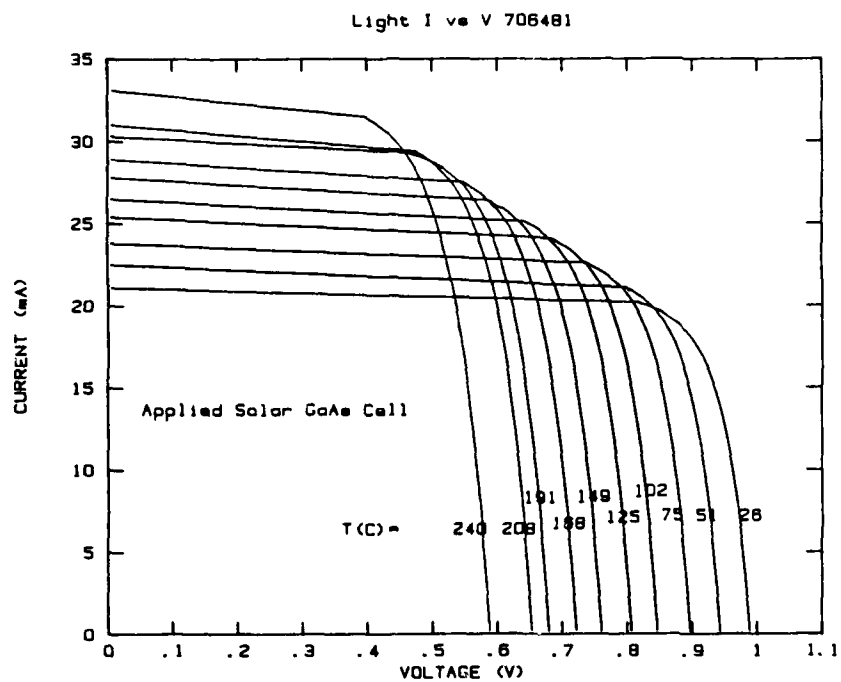Fig. 6-16. Illuminated I vs V for GaAs cell 706482 taken before (706482b) and after (706482v) heating

6-25
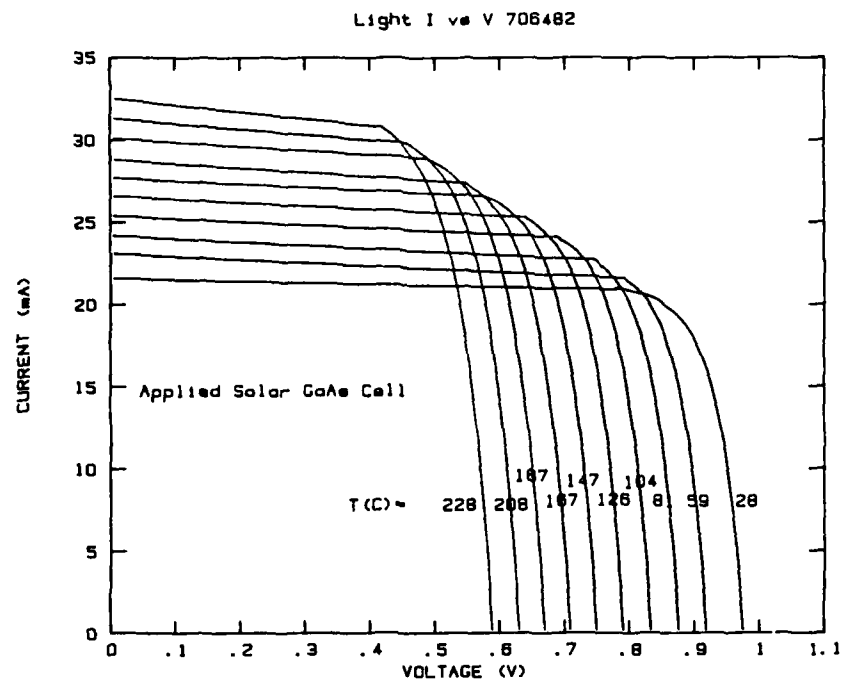
Fig. 6-17.   Illuminated I vs V for GaAs cell 706482 at various temperatures
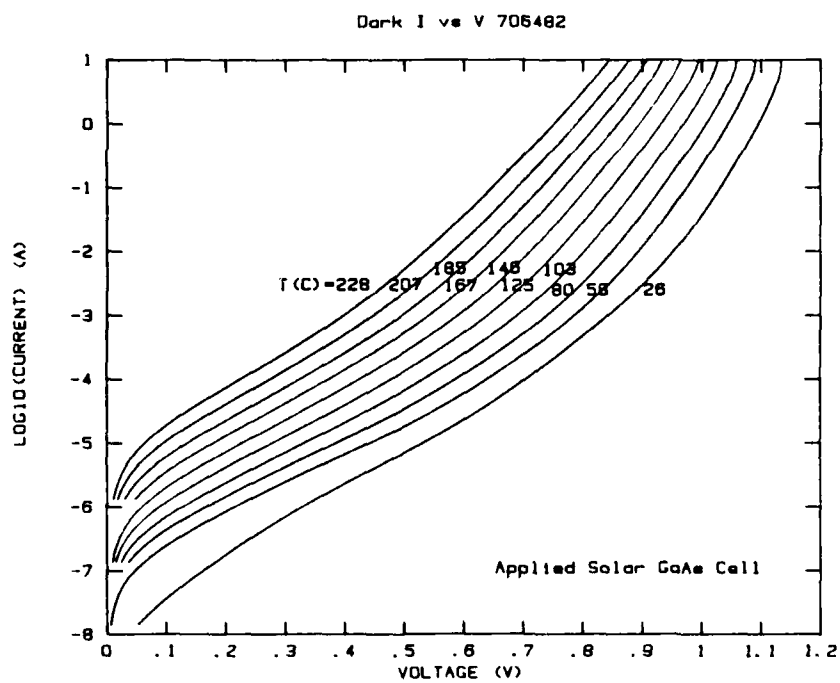

Fig. 6-18.   Dark I vs V for Si cell 706480 at various temperatures

6-26

TABLE 6-11

TEMPERATURE DEPENDENCE OF PARAMETERS DERIVED FROM THE ILLUMINATED
I VS V DATA OF GaAs CELL 706482

T [K (°C)]	I_{sc} (mA)	V_{oc} (V)	I_{mp} (mA)	V_{mp} (V)	P_{mp} (mW)	FF
301 (28)	21.6	0.9745	20.3	0.8418	17.1	0.812
332 (59)	23.1	0.9182	21.5	0.7949	17.1	0.806
354 (81)	24.2	0.8762	22.6	0.7481	16.9	0.797
377 (104)	25.4	0.8330	23.5	0.7112	16.7	0.789
399 (126)	26.6	0.7903	24.5	0.6673	16.3	0.775
420 (147)	27.7	0.7492	24.9	0.6361	15.8	0.761
440 (167)	28.8	0.7089	25.6	0.5977	15.3	0.749
460 (187)	30.1	0.6694	27.0	0.5489	14.8	0.735
481 (208)	31.3	0.6301	27.8	0.5126	14.2	0.720
501 (228)	32.5	0.5888	28.8	0.4677	13.5	0.705
300 (27)	21.5	0.9749	20.1	0.8365	16.8	0.802

TABLE 6-12
TEMPERATURE DEPENDENCE OF J_o AND A_o DERIVED FROM THE
DARK I VS V DATA OF Si CELL 706480

T [K (°C)]	J_o (A/cm^2)	A_o	Fitting Regime
301 (28)	1.728×10^{-9}	1.38	10^{-4} A < I < 0.1 A
326 (53)	1.640×10^{-8}	1.36	
355 (82)	1.727×10^{-7}	1.34	
377 (104)	8.135×10^{-7}	1.31	
403 (130)	4.377×10^{-6}	1.30	
425 (152)	1.514×10^{-5}	1.29	
446 (173)	4.409×10^{-5}	1.27	
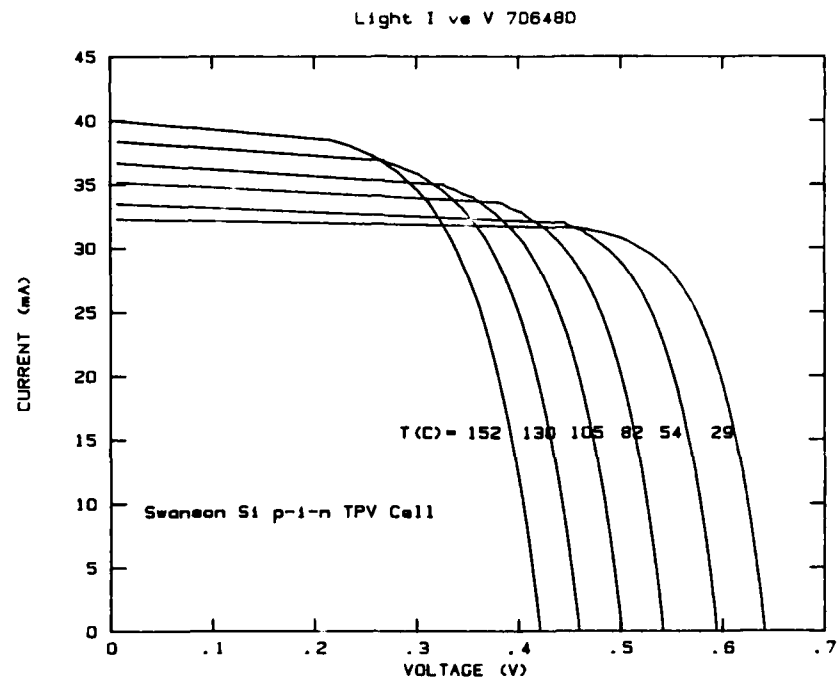
Fig. 6-19. Illuminated I vs V for Si cell 706480 at various temperatures

Fig. 6-20. Dark I vs V data for Si cell 706452 at various temperatures

TABLE 6-13

TEMPERATURE DEPENDENCE OF PARAMETERS DERIVED FROM THE ILLUMINATED
I VS V DATA OF Si CELL 706480

| T [K (°C)]	I_{sc} (mA)	V_{oc} (V)	I_{mp} (mA)	V_{mp} (V)	P_{mp} (mW)	FF
302 (29)	32.3	0.6409	29.5	0.5303	15.64	0.756
327 (54)	33.5	0.5938	29.8	0.4888	14.57	0.732
355 (82)	35.2	0.5415	31.5	0.4268	13.45	0.706
378 (105)	36.7	0.5006	31.5	0.3932	12.38	0.674
403 (130)	38.4	0.4590	33.2	0.3440	11.42	0.648
425 (152)	40.0	0.4209	33.5	0.3125	10.47	0.622

TABLE 6-14

TEMPERATURE DEPENDENCE OF J_o AND A_o DERIVED FROM THE
DARK I VS V DATA OF Si CELL 706452

T [K (°C)]	J_o (A/cm^2)	A_o	Fitting Regime
299 (26)	4.581×10^{-12}	1.10	$0.01 \text{ A} < \text{I} < 0.3 \text{ A}$
326 (53)	1.788×10^{-10}	1.11	
343 (70)	1.034×10^{-9}	1.09	
365 (92)	1.213×10^{-8}	1.08	
385 (112)	8.069×10^{-8}	1.08	
412 (139)	7.699×10^{-7}	1.08	
435 (162)	4.610×10^{-6}	1.07	
460 (187)	1.972×10^{-5}	1.05	
490 (217)	1.517×10^{-4}	1.07	
307 (34)	1.478×10^{-11}	1.10	
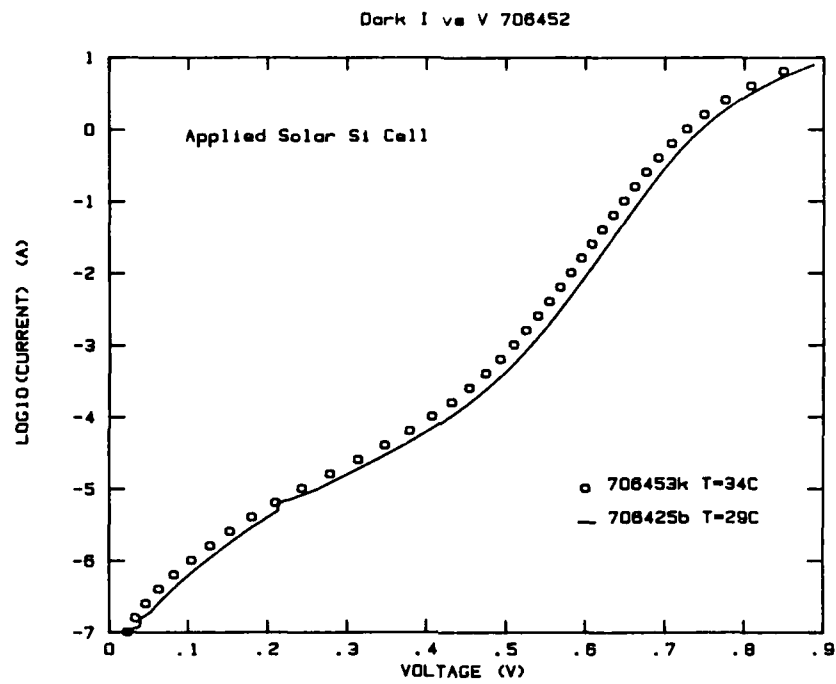
Fig. 6-21. Dark I vs V for Si cell 706452 taken before (706425b) and after (706453k) heating
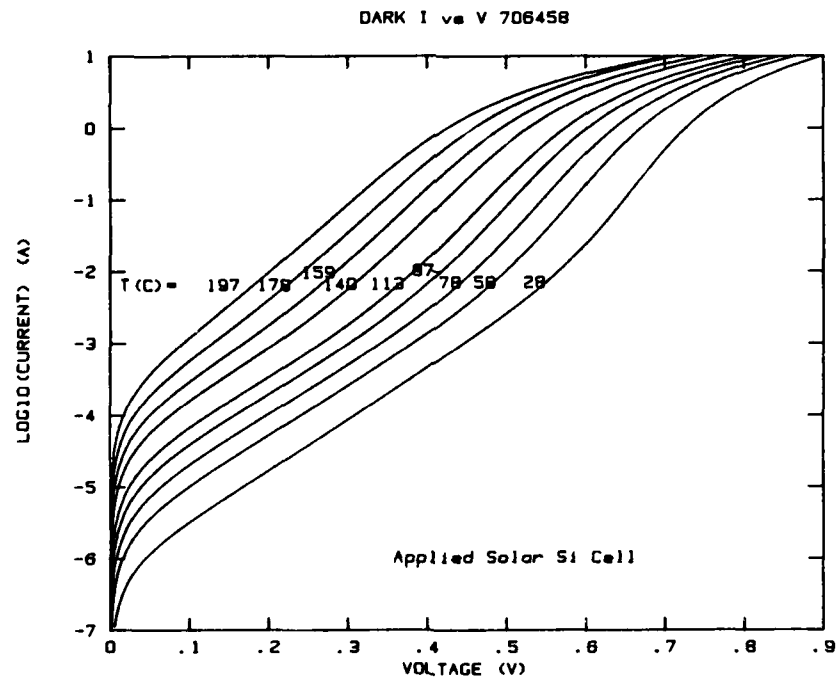
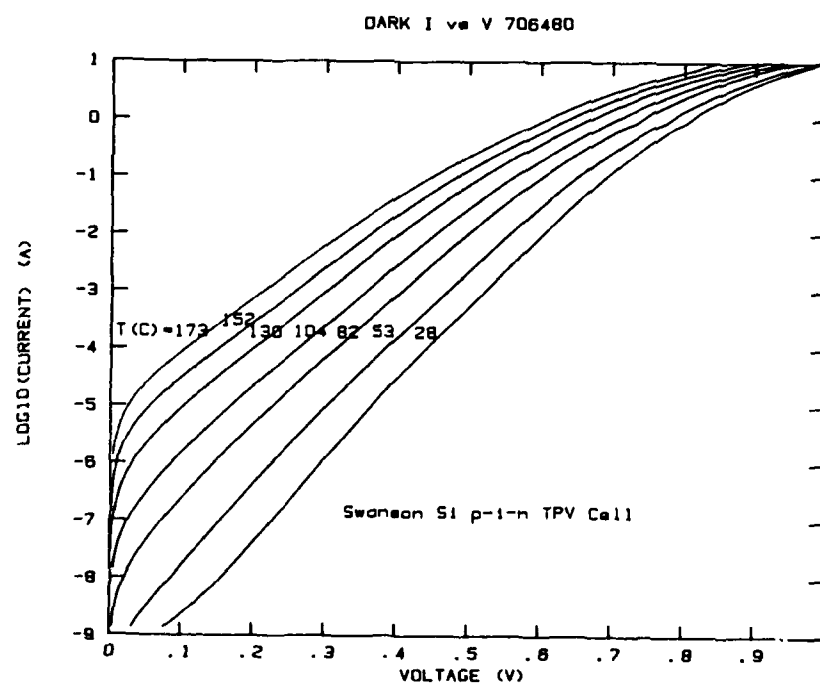Fig. 6-22. Dark I vs V for Si cell 706458 at various temperatures

6-32

TABLE 6-15

TEMPERATURE DEPENDENCE OF J_o AND A_o DERIVED FROM THE
DARK I VS V DATA OF Si CELL 706458

T [K (°C)]	J_o (A/cm^2)	A_o	Fitting Regime
301 (28)	1.328×10^{-10}	1.25	0.03 A < I < 0.6 A
331 (58)	3.415×10^{-9}	1.22	
351 (78)	2.003×10^{-8}	1.20	
370 (97)	1.024×10^{-7}	1.19	
386 (113)	3.755×10^{-7}	1.18	
413 (140)	2.646×10^{-6}	1.17	
432 (159)	9.213×10^{-6}	1.16	
451 (178)	3.093×10^{-5}	1.16	
470 (197)	9.542×10^{-5}	1.16	
299 (26)	1.456×10^{-10}	1.26	

6-33
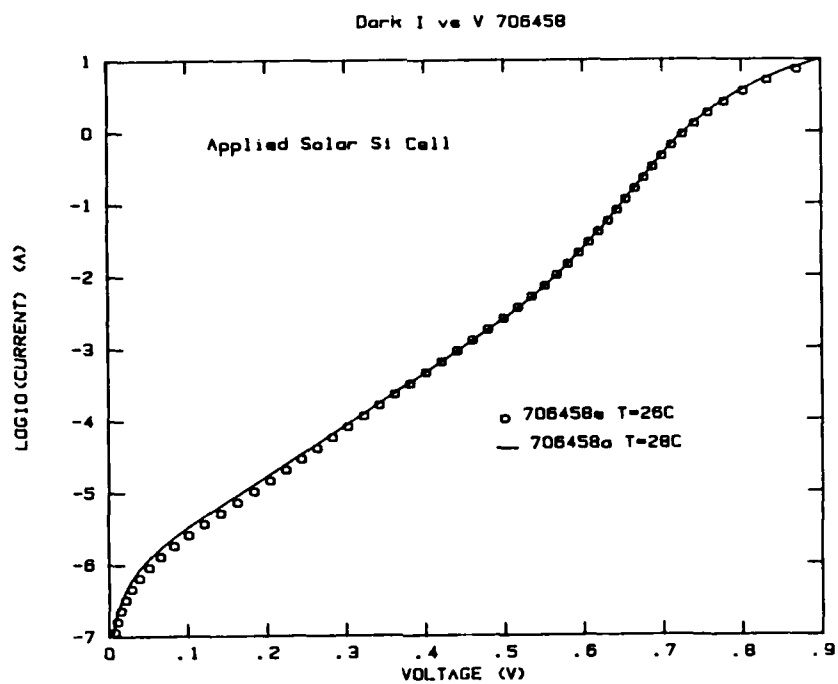
Dark I vs V 706458

Fig. 6-23. Dark I vs V for Si cell 706458 taken before (706458a) and after (706458s) heating

Light I vs V 706458
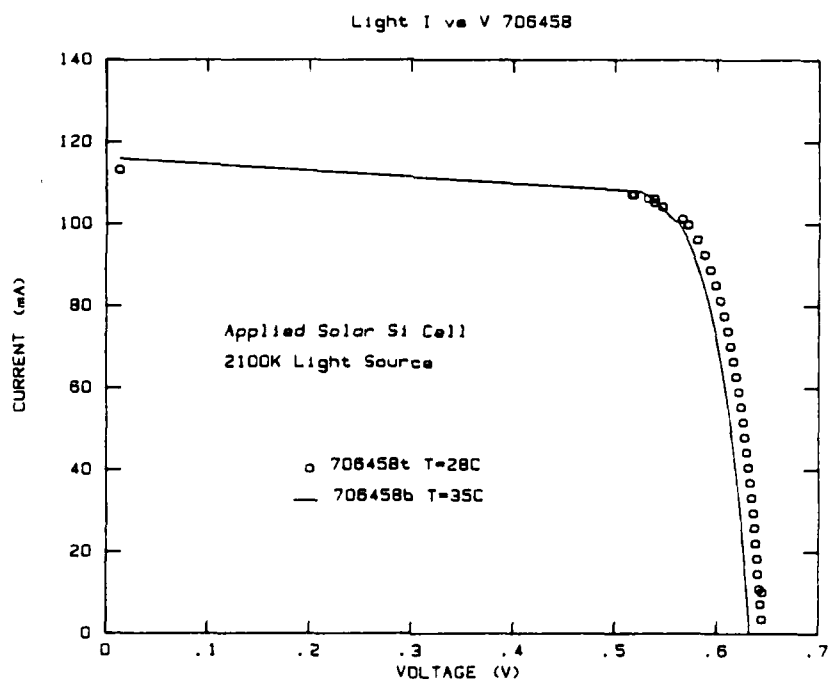
Fig. 6-24. Illuminated I vs V for Si cell 706458 taken before (706458b) and after (706458t) heating
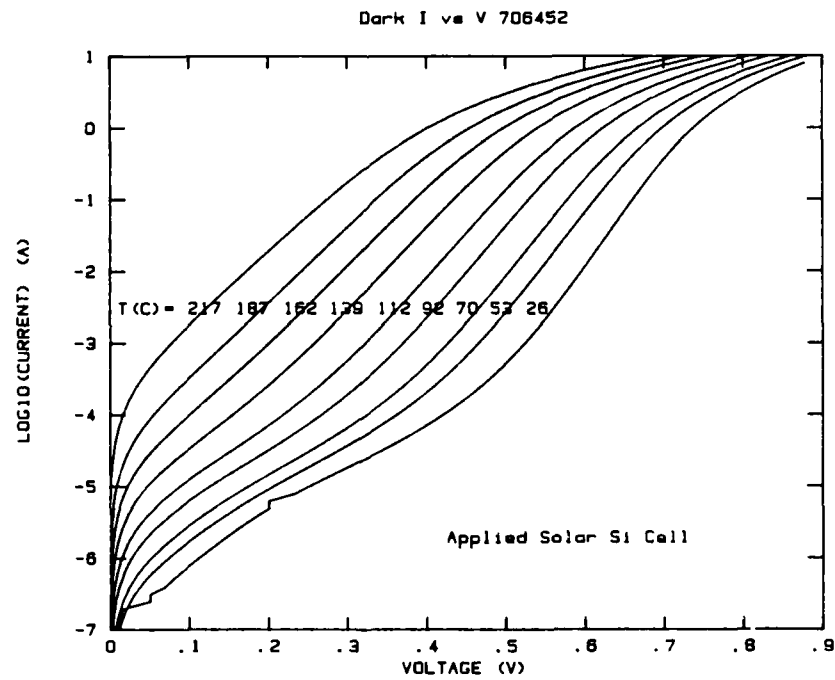
6-34
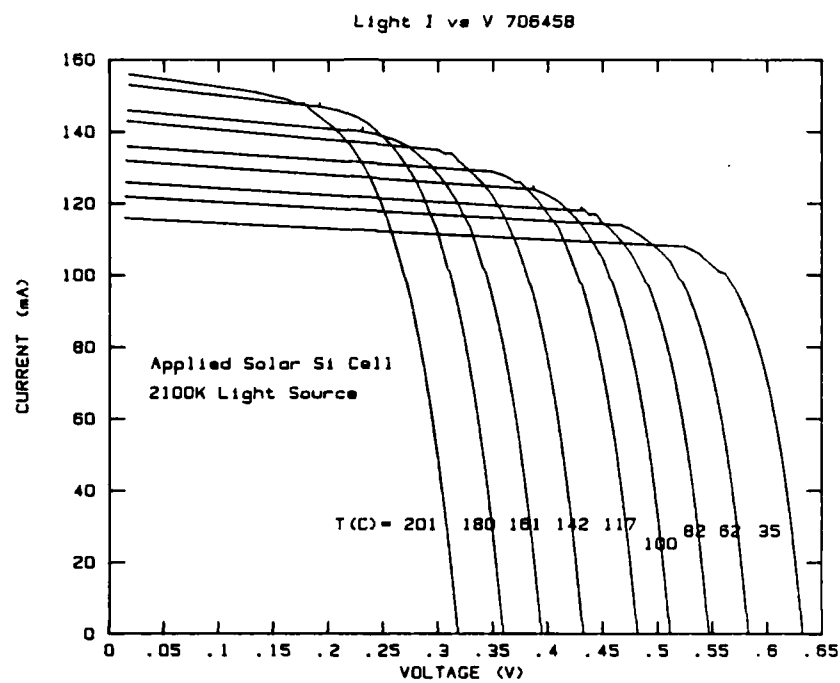
Fig. 6-25. Illuminated I vs V for Si cell 706458 at various temperatures

TABLE 6-16

TEMPERATURE DEPENDENCE OF PARAMETERS DERIVED FROM THE ILLUMINATED
I VS V DATA OF Si CELL 706458

T [K (°C)]	I_{sc} (mA)	V_{oc} (V)	I_{mp} (mA)	V_{mp} (V)	P_{mp} (mW)	FF
308 (35)	116	0.632	106	0.5376	56.99	0.777
335 (62)	122	0.583	111	0.4848	53.81	0.757
354 (82)	126	0.546	117	0.4437	51.91	0.755
373 (100)	132	0.511	120	0.4119	49.42	0.733
390 (117)	136	0.481	121	0.3898	47.17	0.721
415 (142)	143	0.432	126	0.3392	42.74	0.692
434 (161)	146	0.394	126	0.3052	38.45	0.668
453 (180)	153	0.359	132	0.2674	35.33	0.643
474 (201)	156	0.318	131	0.2304	30.19	0.609
301 (28)	113	0.645	101	0.5657	57.14	0.784

7. HIGH-TEMPERATURE TPV EFFICIENCY

Using the theoretical model previously discussed and the values of J_o and A_o derived from the measured dark I vs V characteristics, the expected temperature dependence of the TPV efficiency was calculated. The results of these calculations are plotted in Figs. 7-1 through 7-3 for emitter temperatures of 1700, 1900, and 2100 K. For each emitter temperature, the dependence of η_{TPV} on cell temperature for three InGaAs, one GaAs, and two Si cells is presented. For each plot, a weighted parasitic absorption of 5% is assumed, since it is probably a reasonable goal that can be attained.

What is most striking about these results is the apparent over-riding advantage of InGaAs cells with band gaps of 1.15 and 1.20 eV compared with GaAs and Si cells. Typically, the InGaAs cells have a TPV efficiency which is ~40% higher than that of Si cells. The GaAs cells approach the TPV efficiency of the InGaAs cells only at high emitter and cell temperatures. For example, for an emitter temperature of 2100 K, η_{TPV} for GaAs reaches the InGaAs value of η_{TPV} only for cell temperatures above ~550 K. For a lower emitter temperature of 1900 K, the crossover temperature appears to be close to 650 K.

The TPV efficiency decreases approximately linearly with increasing cell temperature. The rate of decrease is approximately the same for the InGaAs and the Si cells. In contrast, the rate of decrease is much smaller for the GaAs cells owing to the higher band gap and concomitant smaller increase in dark current with temperature. A summary of these results is presented in Table 7-1. From this compendium, it is also clear that $\Delta\eta_{TPV}/\Delta T_{CELL}$ increases significantly with increasing emitter temperature.

VARIABLE BAND GAP MATERIALS FOR THERMOPHOTOVOLTAIC
GENERATORS(U) GA TECHNOLOGIES INC SAN DIEGO CA
L D WOOLF ET AL SEP 85 GA-A18140 AFOSR-TR-85-1069

UNCLASSIFIED F49620-84-C-0105 F/G 10/2 NL

END
FILMED
DTIC
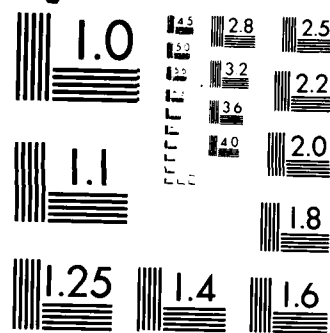
MICROCOPY RESOLUTION TEST CHART
NATIONAL BUREAU OF STANDARDS-1963-A
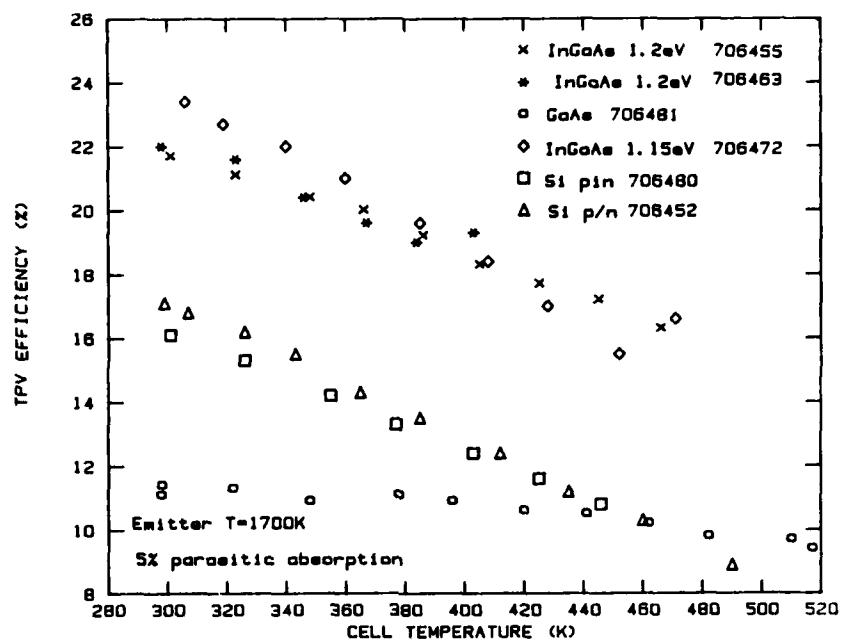
Fig. 7-1. Calculated TPV efficiency versus cell temperature
for an emitter temperature of 1700 K
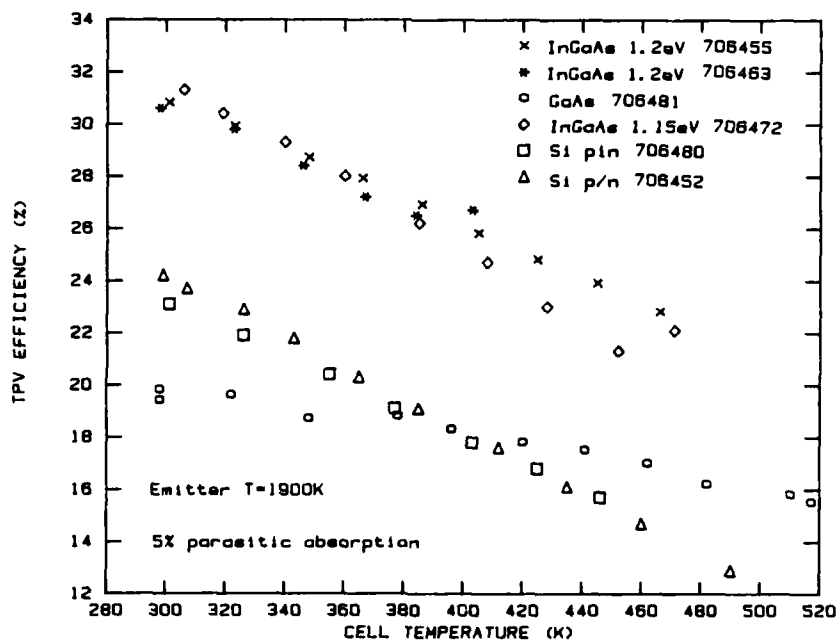
Fig. 7-2. Calculated TPV efficiency versus cell temperature
for an emitter temperature of 1900 K
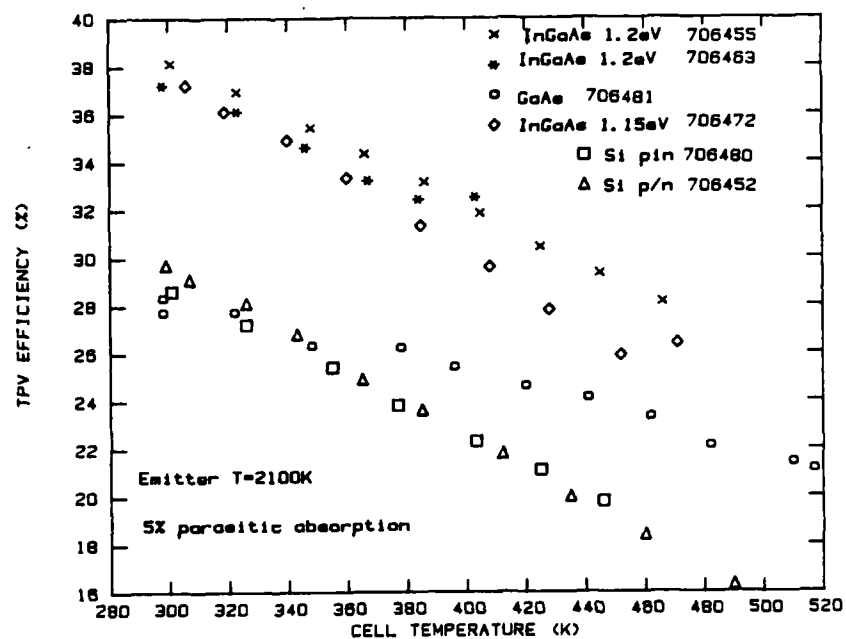
Fig. 7-3. Calculated TPV efficiency versus cell temperature
for an emitter temperature of 2100 K

TABLE 7-1
DECREASE IN TPV EFFICIENCY WITH INCREASING CELL
TEMPERATURE ASSUMING $\overline{A}_{par}$ = 0.05

Cell Type	GA Code	Emitter Temperature (K)	$\dfrac{\Delta \eta_{TPV}}{\Delta T_{CELL}}$ (%/K)
InGaAs	706455	2100	0.061
		1900	0.048
		1700	0.029
InGaAs	706463	2100	0.050
		1900	0.042
		1700	0.033
InGaAs	706472	2100	0.071
		1900	0.059
		1700	0.045
GaAs	706481	2100	0.032
		1900	0.018
		1700	0.008
Si	706480	2100	0.063
		1900	0.052
		1700	0.037
Si	706452	2100	0.071
		1900	0.059
		1700	0.044

The rate of increase of η_{TPV} with increasing emitter temperature is significantly greater for the higher band gap GaAs cell than for the InGaAs and Si cells. This difference arises primarily from the rapidly increasing value of $\overline{A}_{ph}$ for GaAs compared with InGaAs and Si.

It is also informative to examine the temperature dependence of the various power (or heat) flows that are important in the TPV energy conversion system. As discussed in Section 4.6, the external source of power must supply an amount equal to the power absorbed to keep the emitter temperature constant. Recall that

$$P_{inc} = P_{ref} + P_{abs} \quad , \tag{7-1}$$

$$P_{abs} = P_{out} + P_{heat} \quad , \tag{7-2}$$

and

$$\eta_{TPV} = \frac{P_{out}}{P_{abs}} \quad . \tag{7-3}$$

Using the dark I vs V characteristics of InGaAs cell 706455 as input to the TPV efficiency computer program, the cell temperature dependence of the above quantities was calculated, assuming $\overline{A}_{par} = 0.05$ and an emitter temperature of 2100 K (Fig. 7-4). The incident power of 110.3 W/cm^2 is that calculated by using the blackbody law with a blackbody temperature equal to 2100 K. With increasing cell temperature, η_{TPV}, P_{ref}, and P_{out} all decrease and P_{abs} and P_{heat} increase. Between 301 and 466 K, η_{TPV} decreases by 36%, while the power output decreases by only 6%. The reason that η_{TPV} decreases so much is that the power absorbed increases by 28% and the power rejected as heat increases by 49%. Thus, between 301 and 466 K, 28% more power must be supplied by the external source of power to keep the emitter at 2100 K, while the electrical power output decreases by 6%.
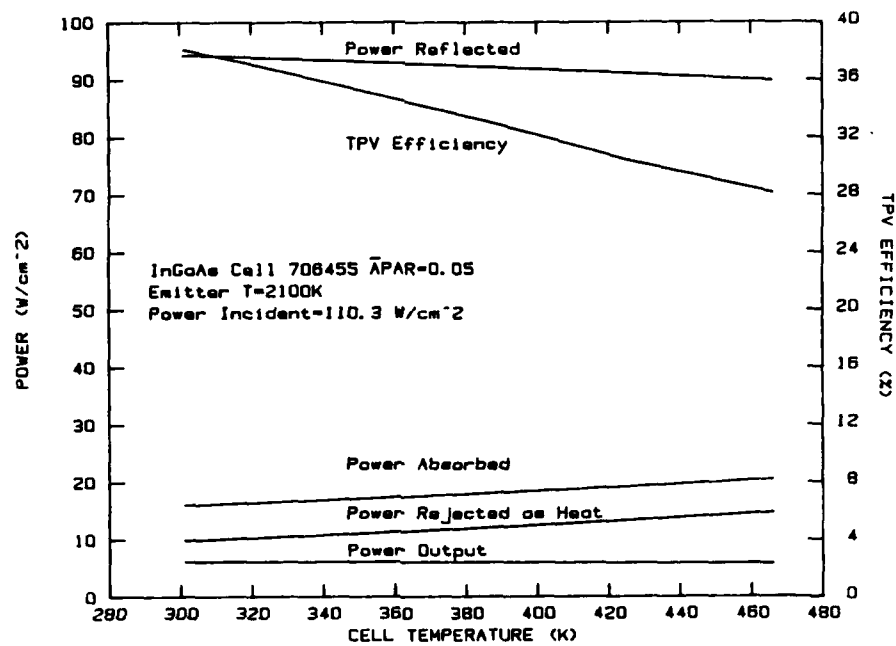
Fig. 7-4.   Power reflected, absorbed, output, and rejected as
            heat and TPV efficiency versus cell temperature
            for an emitter temperature of 2100 K

8. TPV EFFICIENCY MEASUREMENTS

TPV efficiency measurements were directly measured using the TPV test apparatus designed and built by Professor R. M. Swanson of Stanford University. Experiments were performed using the cells listed under GA in Table 8-1. Data obtained by Professor Swanson are also shown in the table.

The illuminated I vs V characteristics of these cells are displayed in Fig. 8-1. The larger value of I_{sc} for the lower band gap cell and the larger value of V_{oc} for the higher band gap cell are in accord with expectations. The increase in short circuit current that occurs when the emitter temperature is increased from 1900 to 2000 K is somewhat misleading in that the total incident power is greater at 2000 K than at 1900 K.

The TPV efficiency was calculated from the following equation:

$$\eta_{TPV} = \frac{P_{out}}{P_{abs}} = \frac{P_{out}}{P_{out} + P_{heat}} \quad , \tag{8-1}$$

where P_{out} is the power output generated by the cell at the maximum power point and P_{heat} is the power absorbed as heat by the cell and detected by the calorimeter part of the TPV test apparatus. The total power absorbed by the cell is then just the sum of the above two terms. The TPV efficiencies calculated in this way are listed in Table 8-1.

TABLE 8-1
RESULTS OF TPV EFFICIENCY MEASUREMENTS

Investigator	Cell Type	η_{elec} (%)	FF (%)	A_{par} (%)	η_{TPV} (%)	T_E (K)
Swanson (Stanford)	3 Si p-i-n TPV	23.0		15.0	3.5	1730
		31.0		16.0	6.8	2020
		29.0		14.0	10.0	2350
	5	48.9		25.8	7.2	1900
		51.2		24.8	10.4	2100
		49.1(a)		25.8	13.0	2300
	8	54.0(a)		9.5	26.2	?
	16	51.0		5.0(a)	28.0(a)	2300
	?	50.0		4.3(a)	30.0(a)	?
GA	InGaAs n/p E_g = 1.20 eV Varian No. 30M 1802 #4 GA No. 706455	53.5	76	68.0	2.0	1900
	InGaAs p/n E_g = 1.15 eV Varian No. 30M 1823 #2 GA No. 706428	55.0(a)	79	67.0	2.8	1900
		54.5	78	68.0	3.6	2000
Future Performance Estimates						
GA	1	53.5		5(b)	18.0	1900
	2	55.0		5(b)	21.8	1900
	InGaAs, $E_g \sim$ 0.9 eV	54.5		5(b)	25.1(b)	2000
		55.0		5	34.5	1900

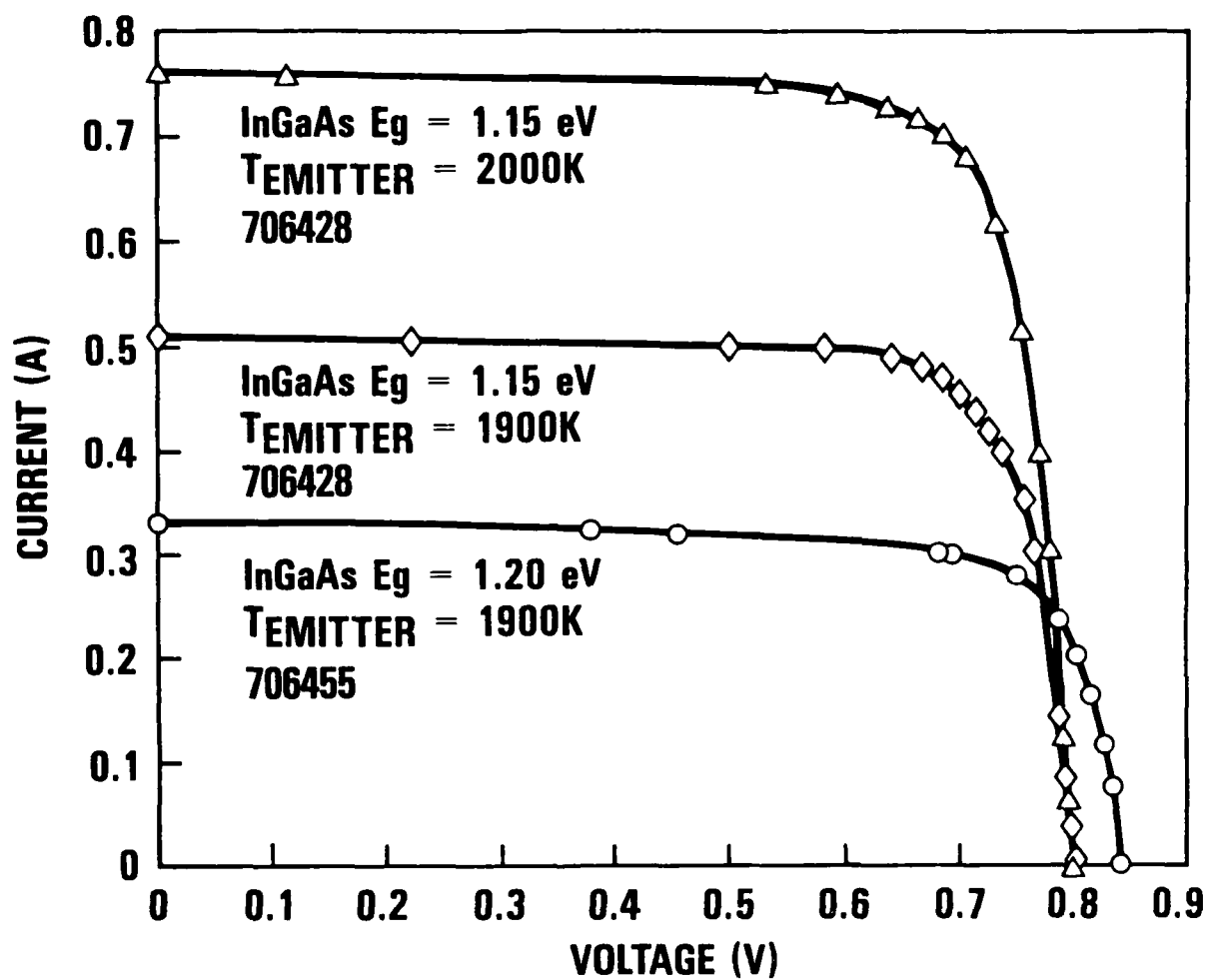(a) Optimum value obtained.
(b) Goal.

Fig. 8-1.   Illuminated I vs V data obtained in TPV test apparatus

With η_{TPV} known, the weighted parasitic absorption $\overline{A}_{par}$ was calculated. The ratio of $\overline{A}_{par}/A_{ph}$ can be calculated using

$$\frac{\overline{A}_{par}}{\overline{A}_{ph}} = \frac{\eta_{use}\eta_{elec}}{\eta_{TPV}} - 1 \quad , \tag{8-2}$$

where η_{elec} and η_{TPV} are measured and η_{use} is calculated from the previously developed theory. Using the fact that the fraction of incident power that is absorbed leads to electricity and heat generated in the cell, the total weighted absorptivity of the cell $\overline{A}$ was then calculated:

$$\overline{A} = \overline{A}_{par} + \overline{A}_{ph} = \frac{P_{heat} + P_{out}}{P_{inc}} \quad , \tag{8-3}$$

where P_{inc} is the total incident power. Since $P_{heat} + P_{out} = P_{abs}$ and P_{inc} are both known, Eqs. 8-2 and 8-3 are two equations in two unknowns which can be solved for $\overline{A}_{par}$ and $\overline{A}_{ph}$. The values of $\overline{A}_{par}$ derived in this way are shown in Table 8-1 along with the experimentally measured η_{elec} factors.

Comparing these results with Swanson's data for Si p-i-n TPV cells optimized for low parasitic absorption, it is apparent that $\overline{A}_{par}$ for the InGaAs cells is significantly higher than that for the Si cells. This high value is likely due to the absence of a high-quality mirror on the back surface of the cell as well as to free carrier absorption associated with the thick, heavily doped GaAs substrate on which the cells are grown. It should be stressed that these InGaAs cells are research concentrator cells that have been designed for use in concentrated sunlight and have not been fabricated for the purpose of achieving low parasitic absorption and high TPV efficiency.

The electrical efficiency factor η_{elec} for the InGaAs cells is comparable to the best values attained from the Si p-i-n TPV cells. The

closely related fill factor FF of the InGaAs cells was typically ~77%, which is quite high and indicative of the relatively low series and high shunt resistance of these cells in this range of interest. This indicates that the electrical properties of these cells at the high current levels expected in a realistic TPV system environment would be excellent.

If the parasitic absorption of the cells studied were reduced from ~68% to ~5%, typical of Swanson's best Si TPV cells, then keeping all other factors constant, the TPV efficiency would rise from 3.6% to 25% for InGaAs cell 706428 at T_E = 2000 K. Using an InGaAs optimized for an emitter temperature of 1900 K, i.e., E_g ~ 0.9 eV, would result in η_{TPV} = 34.5%. This assumes η_{elec} = 55.0%, as previously measured, $\overline{A}_{par}$ = 5%, and the values of $\overline{A}_{ph}$ = 17% and η_{use} = 81% calculated theoretically. This value of η_{TPV} is in close agreement with that calculated by the theoretical model of Section 3.

The experimental data discussed above were obtained using Professor Swanson's TPV rig when it was in his laboratory at Stanford University. After these experiments, it became clear that scheduling conflicts would inhibit performing further TPV efficiency experiments at that location. Therefore, the TPV apparatus was subsequently moved and installed at GA Technologies. After the move, some leaks were detected in the vacuum system and repaired. In addition, some minor modifications were made in the test apparatus itself. At the conclusion of this program, a complete calibration of the system had been performed and some preliminary tests had been made. However, these results are not discussed in this report.

9. MICROMETALLURGICAL ANALYSIS OF CELLS

To verify the expected composition of the InGaAs cells obtained from Varian, Inc., two InGaAs cells with different compositions were examined using SEM and EDAX. A schematic cross section of the structure of an InGaAs cell is shown in Fig. 9-1. The top side electrical contact primarily consists of a thick layer of Au lying on top of a Au/Pd alloy layer which makes ohmic electrical contact to a heavily doped InGaAs layer. An AlGaInAs window layer is present to reduce the surface recombination rate. The p-n junction lies below the window layer and is followed by a grading layer of InGaAs whose composition varies gradually to relieve the lattice mismatch (and minimize the dislocation density) between the InGaAs active layers and the GaAs substrate. Electrical contact to the bottom of the GaAs substrate is made using a Au/Ge alloy.

The results of the SEM and EDAX analyses are shown in Table 9-1 and Figs. 9-2 and 9-3. In the SEM photographs, it is easy to distinguish the top Au contact from the remainder of the cell. However, it is difficult to distinguish the subsequent layers from each other or from the GaAs substrate. The EDAX measurements indicate that the bulk of the top of these cells consists of Au, as expected. Region 5 of the $In_{0.25}Ga_{0.75}As$ cell (Fig. 9-2) and region 4 of the $In_{0.20}Ga_{0.80}As$ (Fig. 9-3) cell consist primarily of stoichiometric GaAs, with no In present, so these regions must be the GaAs substrate material.

Consider now just the $In_{0.25}Ga_{0.75}As$ sample. As noted above, regions 1 and 2 are primarily Au, with a considerable and anomalous amount of Pb present. The origin of the Pb is unknown, although it may be associated with the Pb/Sn solder used to attach the cells during the high-temperature I vs V measurements. If just the elements In, Ga, and As are considered, region 3 corresponds to a composition of $In_{0.10}Ga_{0.87}As$, while region 4 corresponds to $In_{0.24}Ga_{1.01}As$. The
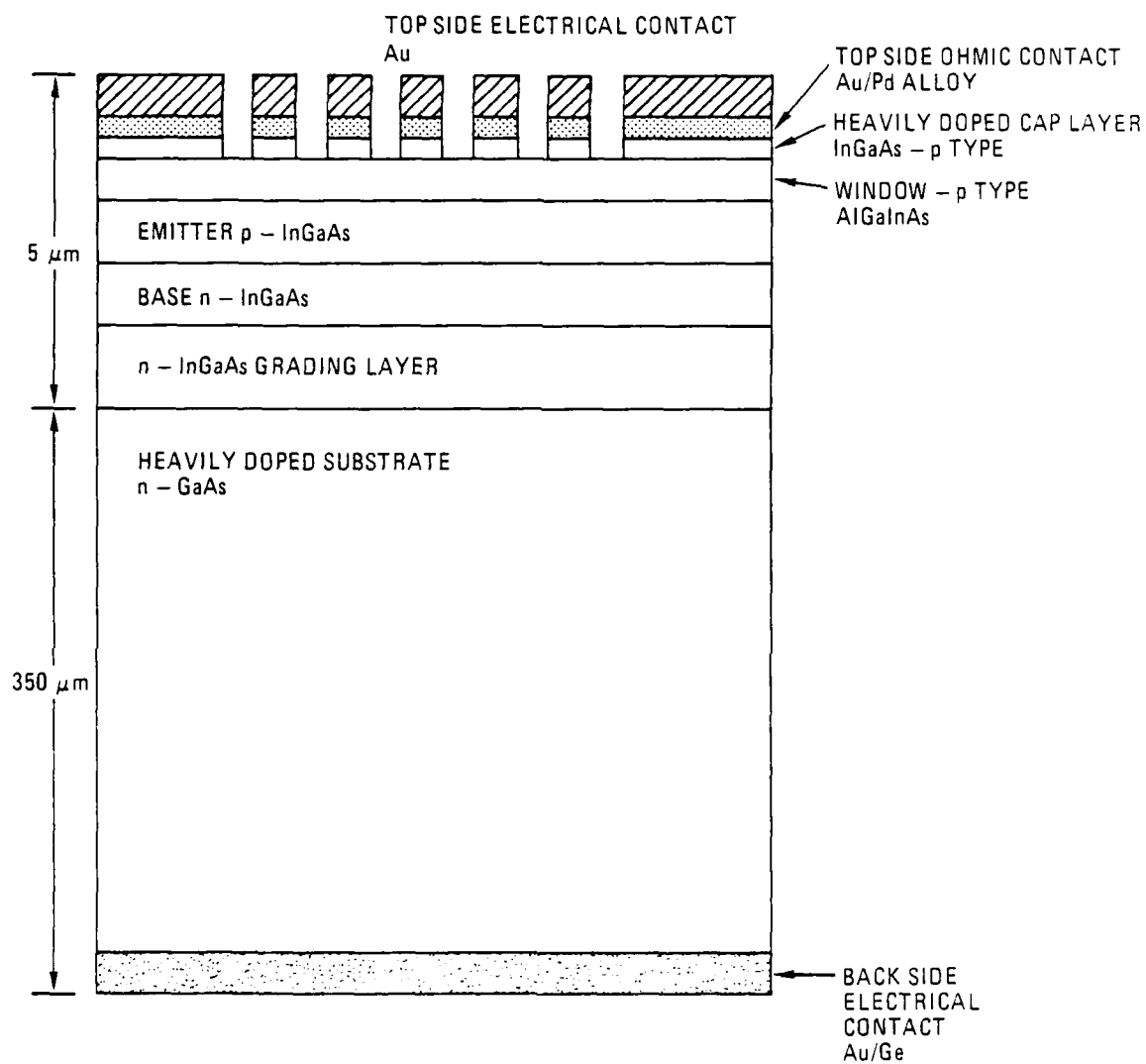
Fig. 9-1. Schematic cross section of a p/n InGaAs concentrator solar cell structure

TABLE 9-1
COMPOSITION OF InGaAs CELLS

	Cell Type								
	$In_{0.25}Ga_{0.75}As$ Varian No. 30M 1823 #4 $E_g = 1.15$ eV					$In_{0.20}Ga_{0.80}As$ Varian No. 30M 1802 #5 $E_g = 1.20$ eV			
	Atomic Percent in Region[a]					Atomic Percent in Region[b]			
Element	1	2	3	4	5	1	2	3	4
Ga	0.3	1.7	30.0	36.8	46.7	0	37.3	44.0	47.9
As	0	0	34.5	36.5	43.6	0	38.3	43.9	46.9
In	0.3	0.2	3.6	8.7	0	0	6.4	6.3	0
Al	1.5	1.0	5.9	4.9	5.6	1.9	6.4	1.4	1.4
Au	82	81.6	17.2	9.4[c]	3.3[c]	96.9	10.9[c]	3.9[c]	3.4[c]
Ag	1.8	1.2	5.3	2.0	0.7	0.4	0.3	0.2	0.4
Pb	14	14.3	3.3	0.8	0.1	0.8	0.1	0	0
Sn	0	0	0.2	0.9	0	0	0.3	0.3	0

[a] Regions are indicated in Fig. 9-2.

[b] Regions are indicated in Fig. 9-3.

[c] A thin Au coating was applied to the entire cross-sectional area to prevent electrical charging problems in the SEM. The Au in this region probably partially or completely results from this coating.

Fig. 9-2. SEM photograph of a cross section of the top 7 μm of $In_{0.25}Ga_{0.75}As$ cell 706472, Varian No. 30M 1823 #4
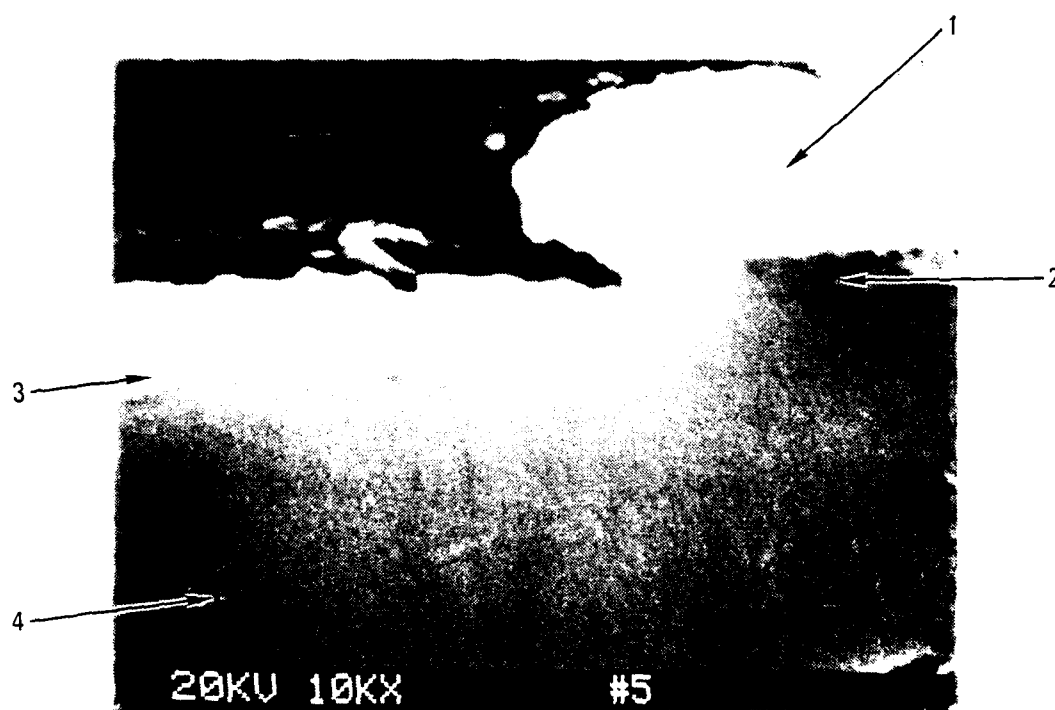
Fig. 9-3. SEM photograph of a cross section of the top 7 μm of $In_{0.20}Ga_{0.80}As$ cell, Varian No. 30M 1823 #4

9-4

region 4 composition is very close to the expected nominal composition of the p-n active layers of $In_{0.25}Ga_{0.75}As$. The presence of 5% Al in regions 3, 4, and 5 is unexpected but may be due to diffusion of Al into the bulk from the AlGaInAs window layer.

The $In_{0.20}Ga_{0.80}As$ cell studied seems to have fewer impurities present than the sample just discussed. Again, if just In, Ga, and As are considered, region 3 corresponds to a composition of $In_{0.17}Ga_{0.97}As$, while region 4 corresponds to $In_{0.14}GaAs$, in close agreement with the nominal composition. The relatively high proportion of Al in region 2 may be due to the proximity of region 2 to the AlGaInAs window layer.

10. ANALYSIS OF InGaAs CELLS FOR TPV SPACE POWER PRODUCTION

This section applies the data previously discussed in this report
to a typical space prime power system. By this means, one can weigh the
merits of TPV power conversion systems compared with those of space
prime power systems using thermoelectrics or thermionics.

10.1. BACKGROUND

In 1983 a study of a space prime power system utilizing TPV power
conversion was completed for NASA (Ref. 10-1). This study used a modi-
fied version of the SP-100 reactor, a TPV power conversion system, and
an aluminum heat pipe radiator. The nominal power output of the SP-100
reactor was 1100 kW(t).

The study discussed in detail the modification necessary to change
the SP-100 reactor from the reference thermoelectric configuration to a
TPV configuration. This change was primarily pointed toward increasing
the reactor operating temperature capability from the reference 1400 to
2100 K. A conceptual sketch of the modified SP-100 reactor with a TPV
power conversion system is shown in Fig. 10-1. The power output of this
system using TPV power conversion was estimated to be 184 kW(e).

Table 10-1 lists the mass of each of the major system components
for the modified SP-100 system with TPV power conversion. The total
mass was estimated to be 1742 kg, which would result in a system spe-
cific mass (α) of 9.43 kg/kW. This system specific mass compares with
projected goals for α in the range of 20 to 25 kg/kW for both thermo-
electric and thermionic systems.

The TPV power conversion system used in the Ref. 10-1 study sug-
gested the use of a variable band gap photovoltaic cell containing AlSb,
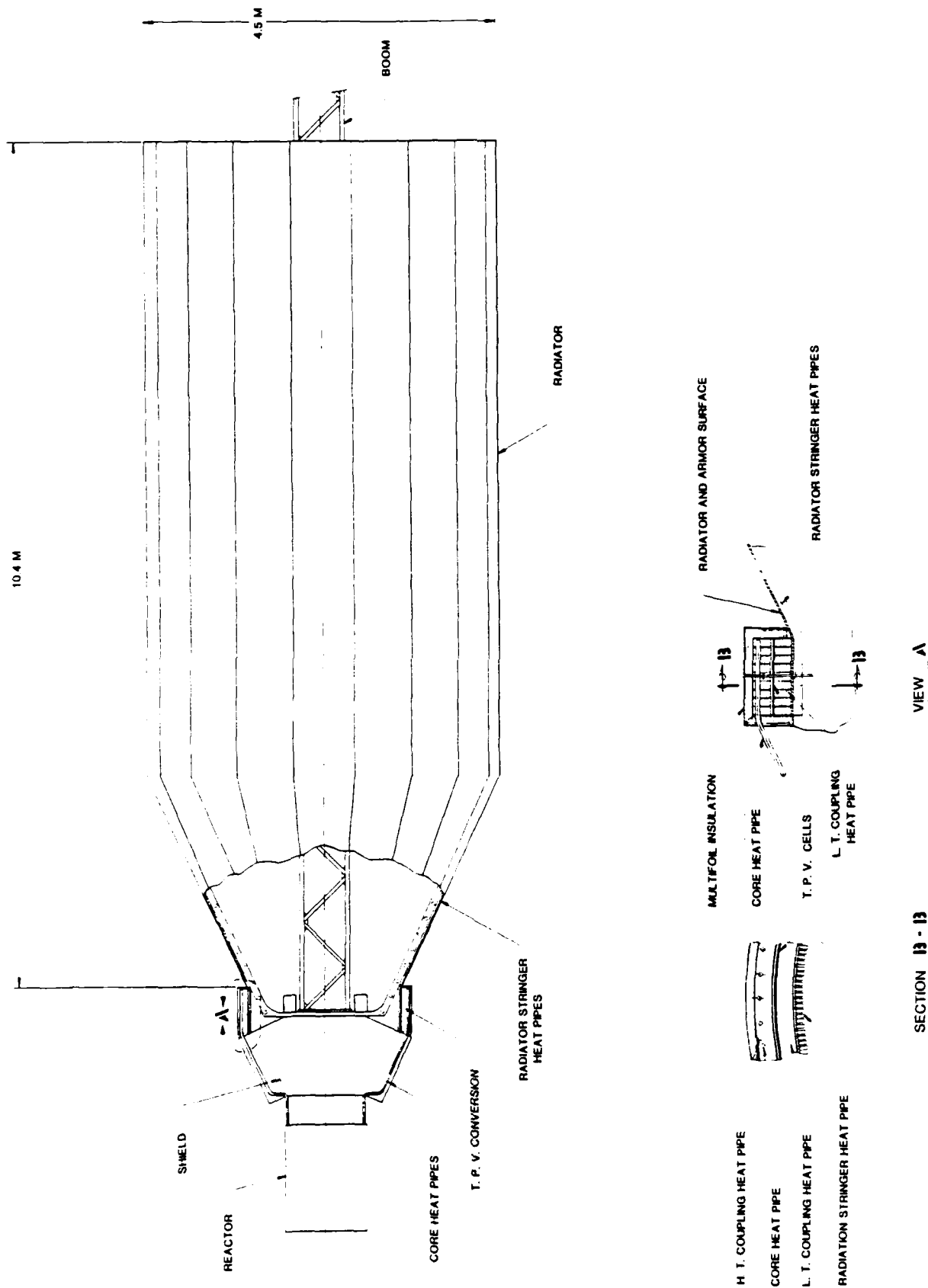
Fig. 10-1. 184-kW(e) TPV space reactor concept

TABLE 10-1
TPV POWER SYSTEM MASS

Reactor power, kW(t)	1100
Power output, kW(e)	184.7
Reactor mass, kg	400
Radiator and TPV cell mass, kg	759
Shield mass, kg	380
High-temperature coupling heat pipe mass, kg	45
Structure mass, kg	158
Total mass, kg	1742[a]

[a] $\alpha = \dfrac{1742}{184.7} = 9.43 \ \dfrac{kg}{kW}$.

GaSb, and InAs. Since no such cell or cell data were known to exist at that time, the calculations of conversion efficiency were based on estimated values for the cell parameters. During the present program, as discussed in Section 7 of this report, data have been obtained on cells which are applicable to this system. Therefore, comparison can now be made between the previous specific mass estimate made using estimated cell parameters and the specific mass estimate based on data from actual photovoltaic cells.

10.2. ESTIMATE OF SYSTEM SPECIFIC MASS

The information on component mass presented in Ref. 10-1 was used as the basis for estimating the system specific mass (α) for TPV systems using TPV cells constructed with properties similar to those tested in this program. These cells would, of course, have to be optimized for TPV applications.

The reactor power of the system was held constant at 1100 kW(t). This allowed both the reactor and shield masses to remain the same as shown in Table 10-1. The radiator mass was then adjusted to compensate for changes in area required to accommodate the necessary changes in both rejected heat and radiator surface temperature. The change in rejected heat is a linear effect, while the change in surface temperature is inversely proportional to the fourth power of the absolute temperature.

In this study the radiator was assumed to be made of aluminum as was the case in the Ref. 10-1 study. This means that the maximum radiator temperature is limited by strength considerations to about 625 K or a cell temperature of about 675 K. The cell operating temperature is likely to be limited to a somewhat lower value, 600 to 650 K, for the GaAs and InGaAs cells and even lower, 450 K, for the Si cells. These cell temperature limitations are a result of either material diffusion within the cell or, as in the case of Si, attack of the metallic

electric contacts and are based on information previously reported in Ref. 10-1.

Figures 10-2 through 10-4 present the estimated system specific mass as a function of TPV cell temperature for emitter temperatures of 2100, 1900, and 1700 K, respectively. In all cases the study assumed that the weighted parasitic absorption is 5% and that there is a 50 K temperature drop between the cell temperature and the radiator surface temperature. The four cells used as a basis for the study are listed in Table 10-2.

In Fig. 10-2, it can be seen that the InGaAs reaches a minimum specific mass of about 9.94 kg/kW at about 595 K. The higher band gap GaAs cell reaches nearly the same minimum, but at about a 100 K higher temperature. The lower band gap InGaAs cell reaches its minimum of just under 13 kg/kW at about 550 K, while the Si cell reaches its minimum of about 20 kg/kW at about 500 K. Since the Si cell temperature was limited to 450 K, the minimum attainable specific mass would be about 22 kg/kW.

The temperature at which the specific mass is a minimum is dependent on the negative slope of the efficiency versus cell temperature curve. Since the GaAs cell has the lowest slope of the cells tested, it always optimizes at a higher cell temperature.

The minimum of 9.94 kg/kW for the 1.2-eV InGaAs cell compares favorably with the predicted value of 9.43 kg/kW estimated in the Ref. 10-1 study for the same emitter temperature. The estimated specific mass for all of the systems is at or below the projections for other space prime power systems.

Figures   and 10-4 show the specific mass relationship at lower emitter temperatures. As expected, the specific mass increases as the emitter temperature decreases. At temperatures below 1900 K, the system

Fig. 10-2. Specific mass versus cell temperature for 2100 K
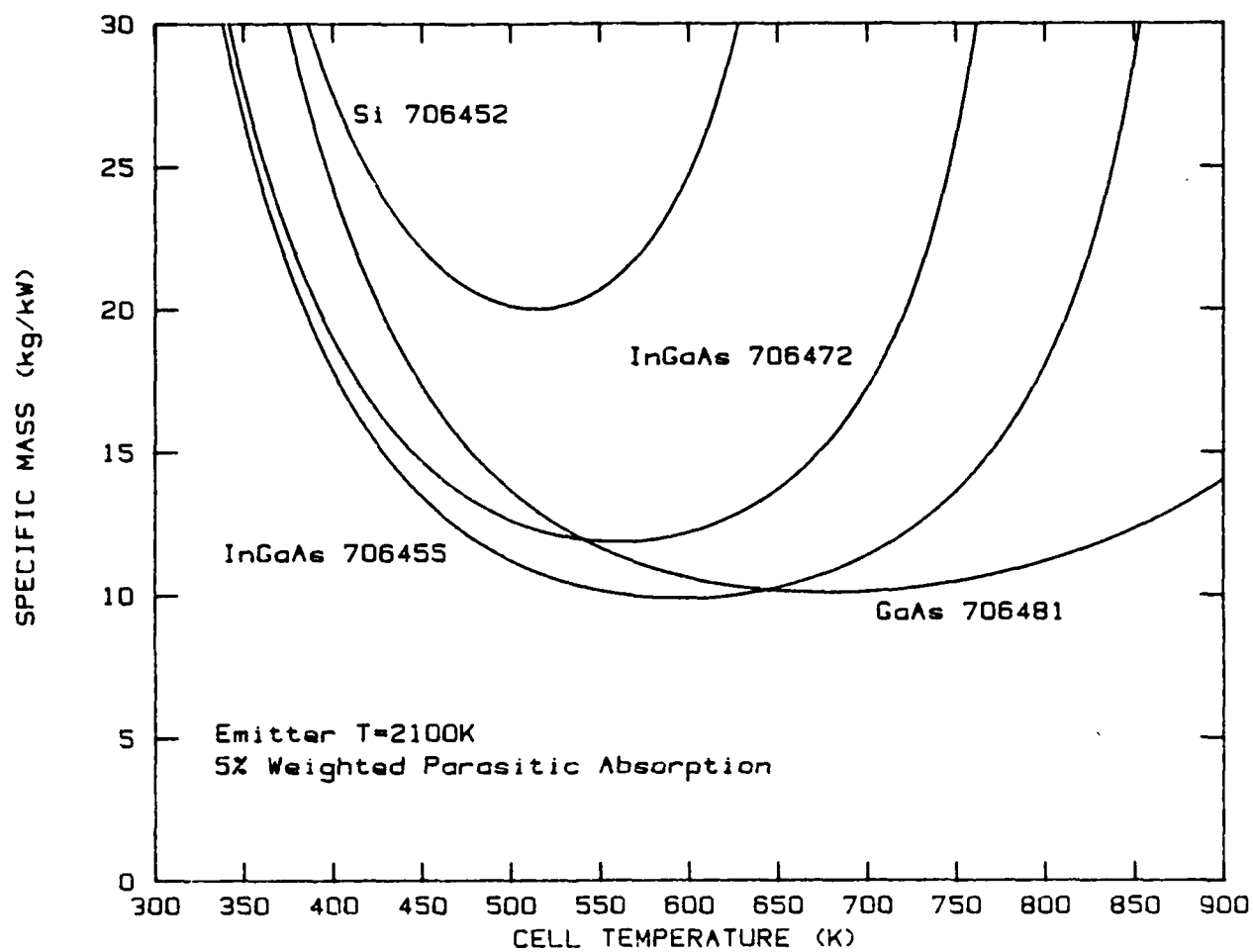emitter temperature
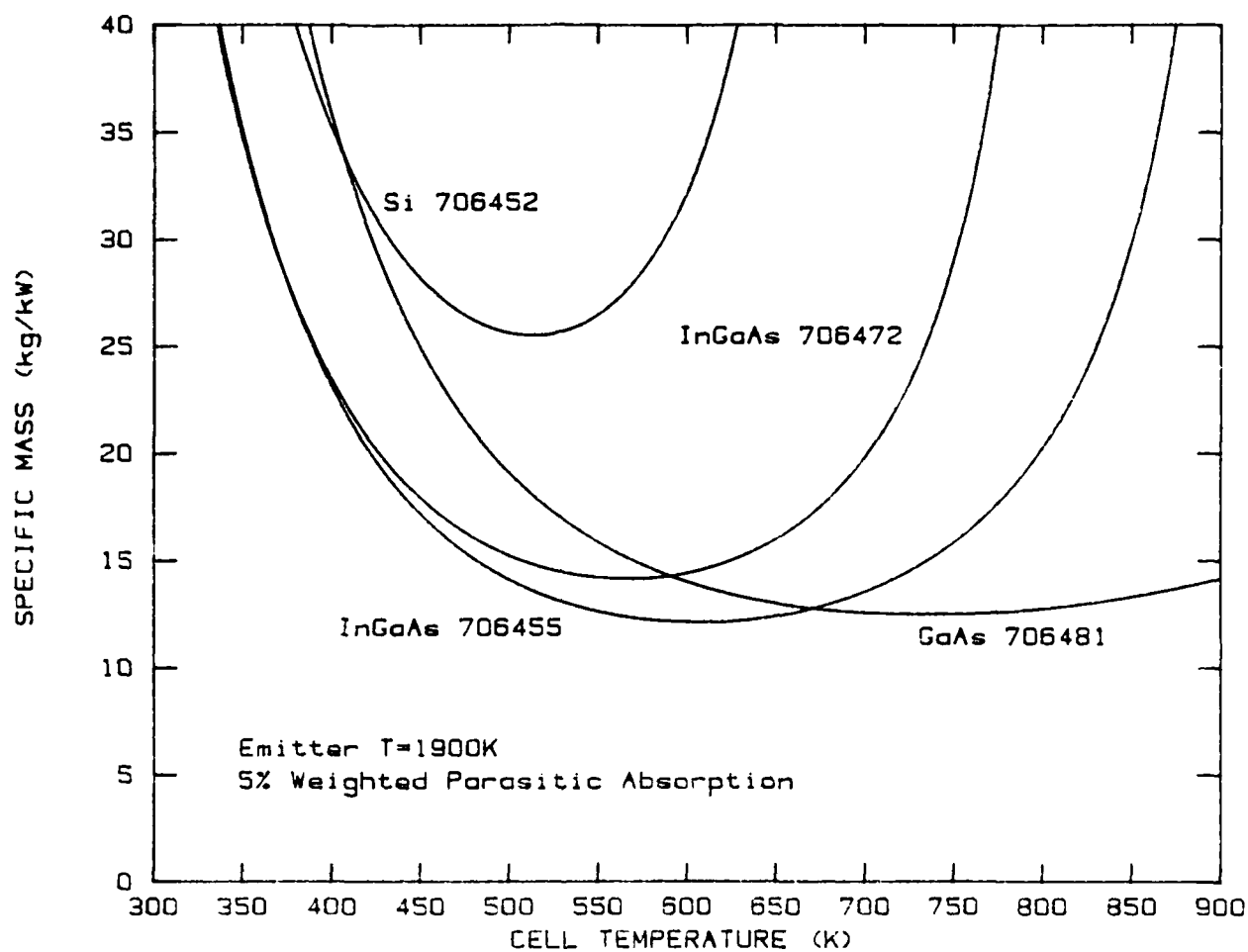
Fig. 10-3. Specific mass versus cell temperature for 1900 K
emitter temperature
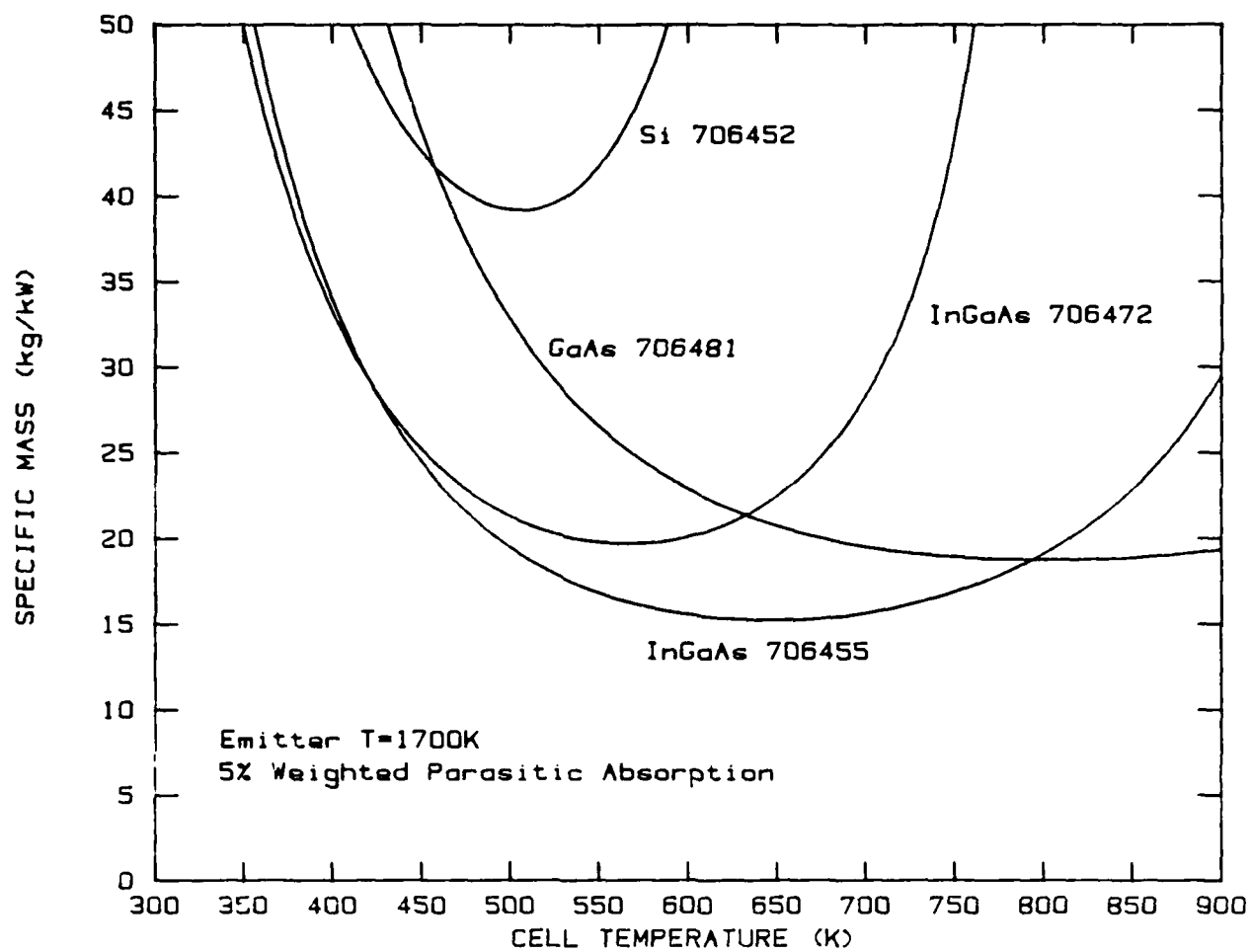
Fig. 10-4. Specific mass versus cell temperature for 1700 K
emitter temperature

TABLE 10-2
SYSTEM SPECIFIC MASS STUDY CELLS

Cell Number	Material	Band Gap (300 K) (eV)
706481	GaAs	1.4
706455	InGaAs	1.2
706472	InGaAs	1.15
706452	Si	1.1

using Si cells no longer appears to be competitive in specific mass with
other space prime power systems.

The InGaAs and GaAs systems appear to remain at system specific
masses which are lower than those of other space prime power systems
until emitter temperatures below 1700 K. The 1.2-eV band gap InGaAs
cell appears to provide the best system specific mass at lower emitter
temperatures. While the GaAs cell provides a low specific mass, it
tends to reach its minimum at cell temperatures above the 650 K
materials limit.

11. RECOMMENDATIONS FOR CONTINUED WORK

The TPV efficiencies for the InGaAs cells studied during this program would approach 40% at room temperature if the weighted parasitic absorption could be reduced to a value near 5%. Therefore, the development of low parasitic absorption TPV cells with an optimum band gap that depends on the emitter temperature, cell temperature, and magnitude of the weighted parasitic absorption is of primary importance. As previously discussed, low parasitic absorption can probably be achieved by significantly reducing the free carrier absorption that currently arises from the thick, heavily doped GaAs substrate and by the development of a highly reflecting back surface mirror. The design and fabrication of TPV cells with these properties should be the focus of the next phase of research.

It would also be useful to devise a more direct method for measuring the TPV efficiency than the one used by Swanson (and GA Technologies, see Section 8), since numerous calibrations must be performed before the TPV efficiency can be inferred. In addition, since in a space power environment, the TPV cells would be at a high temperature to minimize the radiator mass, a TPV efficiency measurement apparatus should be designed and fabricated for use at high cell temperatures. Tungsten oxide forms when the tungsten emitter is heated to high temperatures ($\sim 2000°C$) in the current vacuum system ($\sim 5 \times 10^{-7}$ torr) of the TPV efficiency apparatus. It subsequently is deposited on the silvered chamber surrounding the emitter, on the pyrometer sight glass, and on the TPV cell. To reduce these problems, the measurements should be performed in an ultra-high-vacuum environment ($\leq 10^{-9}$ torr).

Further work should involve the investigation of emitter materials such as tungsten, graphite, ZrC (Ref. 11-1), and selective emitters such as Yb_2O_3 and Er_2O_3 (Refs. 11-2, 11-3, 11-4). A high emissivity of the

emitter for energies above the band gap and a high absorptivity in the below-band-gap regime are prerequisites for high TPV efficiency. A low vapor pressure for the emitter is required for extended operation of a TPV system since the deposition of vaporized material on the TPV cell surface will significantly degrade the performance.

Finally, life testing of the TPV cells will be necessary. Since the cells will be heated to temperatures as high as 500 to 600 K in a space power system for periods as long as approximately 5 to 10 years, it is necessary to know any failure mechanisms which may occur in the cell material in this environment. Thus, microscopic examination and property measurements should be performed on TPV cells that have been subjected to a fixed high temperature for a known length of time.

12. CONCLUSIONS

1. The specific mass of a nuclear-TPV energy conversion system is
    superior to that of space prime power systems based on thermoelec-
    trics or thermionics if an emitter temperature greater than ~1700 K
    and a weighted parasitic absorption of ~5% can be attained. A sys-
    tem based on InGaAs TPV cells with a band gap of 1.2 eV has a lower
    specific mass than one using GaAs or Si cells. For an emitter tem-
    perature of 2100 K and a weighted parasitic absorption of 5% for an
    InGaAs cell with E_g = 1.2 eV, the specific mass attained a value of
    9.94 kg/kW at a cell temperature of 595 K.

2. For a given weighted parasitic absorption of 5%, InGaAs cells have
    significantly higher TPV efficiencies than GaAs or Si cells. TPV
    efficiencies approaching 40% at 300 K and 26% at 500 K appear feasi-
    ble for InGaAs cells with E_g = 1.2 eV.

3. A theoretical model for determining the optimum efficiency of single
    and multiple band gap cells in TPV energy conversion was developed.
    This theory will provide useful guidance in choosing the appropriate
    band gap cell for a given TPV energy conversion system. For a given
    emitter temperature, cell temperature, and weighted parasitic
    absorption, there is an optimum band gap for maximum TPV efficiency
    which can be attained using the InGaAs system. The preferred route
    to high TPV efficiencies is through a decrease in the weighted
    parasitic absorption rather than by using multiple band gaps.

13. REFERENCES

1-1. Bass, J. C., _et al._, "Nuclear-Thermophotovoltaic Energy Conversion," NASA Report CR-167988 (GA-A16653), December 1983.

2-1. Ludowise, M. J., et al., "High-Efficiency (21.4%) $Ga_{0.75}In_{0.25}As/$ GaAs (E_g = 1.15 eV) Concentrator Solar Cells and the Influence of Lattice Mismatch on Performance," Appl. Phys. Lett. 43, 468 (1983).

2-2. Lewis, C. R., C. W. Ford, and J. G. Werthen, "Magnesium Doping of Efficient GaAs and $Ga_{0.75}In_{0.25}As$ Solar Cells Grown by Metalorganic Chemical Vapor Deposition," Appl. Phys. Lett. 45, 896 (1984).

2-3. Dietze, W. T., M. J. Ludowise, and P. E. Gregory, "$Ga_{0.80}In_{0.20}As$ 1.20-eV High Quantum Efficiency Junction for Multijunction Solar Cells," Appl. Phys. Lett. 41, 985 (1982).

2-4. Werthen, J. G., et al., "18.7% Efficient (1-sun, AMO) Large-Area GaAs Solar Cells," Appl. Phys. Lett. 46, 776 (1985).

3-1. Henry, C. H., "Limiting Efficiencies of Ideal Single and Multiple Energy Gap Terrestrial Solar Cells," J. Appl. Phys. 51, 4494 (1980).

3-2. Bennett, A., and L. C. Olsen, "Analysis of Multiple-Cell Concentrator/Photovoltaic Systems," 13th IEEE Photovoltaic Specialists Conference, 1978, p. 868.

3-3. Moon. R. L., et al., "Multigap Solar Cell Requirements and the Performance of AlGaAs and Si Cells in Concentrated Sunlight," 13th IEEE Photovoltaic Specialists Conference, 1978, p. 859.

3-4. Mitchell, K. W., "High Efficiency Concentrator Cells," 15th IEEE Photovoltaic Specialists Conference, 1981, p. 142.

3-5. Wysocki, J. J., and P. Rappaport, "Effect of Temperature on Photovoltaic Solar Energy Conversion," J. Appl. Phys. 31, 571 (1960).

3-6. Gokcen, N. A., and J. J. Loferski, "Efficiency of Tandem Solar Cell Systems as a Function of Temperature and Solar Energy Concentration Ratio," Solar Energy Materials 1, 271 (1979).

3-7. Wedlock, B. D., "Thermo-Photo-Voltaic Energy Conversion," Proc. IEEE 51, 694 (1963).

3-8. Bracewell, R. N., and R. M. Swanson, "Silicon Photovoltaic Cells in TPV Conversion," EPRI Report ER-633, 1978.

3-9. Swanson, R. M., "Silicon Photovoltaic Cells in TPV Conversion," EPRI Report ER-1272, 1979.

3-10. Fahrenbruch, A. L., and R. H. Bube, Fundamentals of Solar Cells, Academic Press, New York, 1983, pp. 526-530.

3-11. Swanson, R. M., "A Proposed Thermophotovoltaic Solar Energy Conversion System," Proc. IEEE 67, 446 (1979).

3-12. Swanson, R. M., "Silicon Photovoltaic Cells in Thermophotovoltaic Energy Conversion," Proc. IEEE Int. Elec. Dev. Mtg., 1973, p. 70.

3-13. Swanson, R. M., "Recent Developments in Thermophotovoltaic Conversion," Proc. IEEE Int. Elec. Dev. Mtg., 1980, p. 186.

3-14. Vera, E. S., et al., "Performance of Ultra High Efficiency Thin Germanium P-N Junction Solar Cells Intended for Solar Thermophotovoltaic Application," Proceedings of the 3rd European Communities Photovoltaic Solar Energy Conference, 1980, p. 911.

3-15. Vera, E. S., J. J. Loferski, and M. Spitzer, "Theoretical Limit Efficiency of Two Junction Tandem Silicon-Germanium Solar Cells Intended for Thermophotovoltaic Application," 15th IEEE Photovoltaic Specialists Conference, 1981, p. 1.

3-16. Wurfel, P., and W. Ruppel, "Upper Limit of Thermophotovoltaic Solar-Energy Conversion," IEEE Trans. Elec. Dev. ED-27, 745 (1980).

3-17. Yeargen, J. R., R. G. Cook, and F. W. Sexton, "Thermophotovoltaic Systems for Electrical Energy Conversion," 12th IEEE Photovoltaic Specialists Conference, 1976, p. 807.

3-18. Edenburn, M. W., "Analytical Evaluation of a Solar Thermophotovoltaic (TPV) Converter," Solar Energy 24, 367 (1980).

3-19. Bell, R. L., "Concentration Ratio and Efficiency in Thermophotovoltaics," Solar Energy 23, 203 (1979).

4-1. Sze, S. M., _Physics of Semiconductor Devices_, John Wiley, New York, 1981.

4-2. Bracewell, R. N., and R. M. Swanson, "Silicon Photovoltaic Cells in TPV Conversion," EPRI Report ER-633, February 1978.

4-3. Swanson, R. M., "Silicon Photovoltaic Cells in TPV Conversion," EPRI Report ER-1272, December 1979.

4-4. Seraphin, B. O., and H. E. Bennett, "Optical Constants," Ch. 12 in _Semiconductors and Semimetals_, Vol. 3, R. K. Willardson and A. C. Beer (eds.), Academic Press, New York, 1967.

4-5. Lewis, C. R., C. W. Ford, and J. G. Werthen, "Magnesium Doping of Efficient GaAs and $Ga_{0.75}In_{0.25}As$ Solar Cells Grown by Metalorganic Chemical Vapor Deposition," _Appl. Phys. Lett._ 45, 895 (1984).

4-6. Braunstein, R., and E. O. Kane, "The Valence Band Structure of the III-V Compounds," _J. Phys. Chem. Solids_ 23, 1423 (1962).

4-7. Fahrenbruch, A. L., and R. H. Bube, _Fundamentals of Solar Cells: Photovoltaic Solar Energy Conversion_, Academic Press, New York, 1983.

10-1. Bass, J. C., _et al._, "Nuclear-Thermophotovoltaic Energy Conversion," NASA Report CR-167988 (GA-A16653), December 1983.

11-1. Bass, J. C., _et al._, "Nuclear-Thermophotovoltaic Energy Conversion," NASA Report CR-167988 (GA-A16653), December 1983.

11-2. Guazzoni, G. E., "High-Temperature Spectral Emittance of Oxides of Erbium, Samarium, Neodymium and Ytterbium," _Appl. Spectros._ 26, 60 (1972).

11-3. Kittl, E., M. D. Lammert, and R. J. Schwartz, "Performance of Germanium PIN-Photovoltaic Cells at High Incident Radiation Intensity," _Proceedings of the 11th IEEE Photovoltaic Specialists Conference_, 1975, p. 424.

11-4. Kittl, E., and G. Guazzoni, "Design Analysis of TPV-Generator System," _25th Annual Proceedings, Power Sources Symposium_, May 1972, Atlantic City, New Jersey.

14. LIST OF WRITTEN PUBLICATIONS IN TECHNICAL JOURNALS

1. Woolf, L. D., "Optimum Efficiency of Single and Multiple Band Gap Cells in Thermophotovoltaic Energy Conversion," submitted to Solar Cells, September 1985.

2. Woolf, L. D., N. B. Elsner, and J. C. Bass, "Performance of InGaAs Cells in Thermophotovoltaic Energy Conversion," to be submitted to Solar Cells.

15. LIST OF PROFESSIONAL PERSONNEL ASSOCIATED WITH THE RESEARCH EFFORT

Dr. Lawrence D. Woolf   - Senior Scientist/Principal Investigator

Mr. John C. Bass   - Senior Staff Engineer

Mr. Norbert B. Elsner   - Principal Investigator/Technical Consultant

Dr. Richard M. Swanson   - Technical Consultant

Dr. Ting L. Chu   - Technical Consultant

Dr. Park H. Miller, Jr.   - Technical Consultant

16. PAPERS PRESENTED AT CONFERENCES

1. Woolf, L. D., "Optimum Efficiency of Single and Multiple Band Gap Cells in Thermophotovoltaic Energy Conversion," to be submitted as a post-deadline paper to the 18th IEEE Photovoltaic Specialists Conference, Las Vegas, Nevada, October 21-25, 1985.

2. Woolf, L. D., J. C. Bass, and N. B. Elsner, "Theoretical and Experimental Investigation of Variable Band Gap Cells in Thermophotovoltaic Energy Conversion," to be submitted to the 32nd International Power Sources Symposium, Cherry Hill, New Jersey, June 9-12, 1986.

17. PATENT DISCLOSURES

1. Woolf, L. D., and J. C. Bass, "Direct Band Gap Solar Cell with Back Surface Reflector," in process.

END

FILMED

1-86

DTIC